ISTANBUL TECHNICAL UNIVERSITY ★ INSTITUTE OF SCIENCE AND TECHNOLOGY

ELECTROCHEMICAL COPOLYMERIZATION OF 3,4-PROPYLENEDIOXYTHIOPHENE AND N-PHENYLSULFONYL PYRROLE AND DETECTION OF DOPAMINE IN PRESENCE OF ASCORBIC ACID

M.Sc. Thesis by
Fatma Gül GÜLER

Department : Chemistry

Programme : Chemistry

JUNE 2011

ISTANBUL TECHNICAL UNIVERSITY ★ INSTITUTE OF SCIENCE AND TECHNOLOGY

ELECTROCHEMICAL COPOLYMERIZATION OF 3,4-PROPYLENEDIOXYTHIOPHENE AND N-PHENYLSULFONYL PYRROLE AND DETECTION OF DOPAMINE IN PRESENCE OF ASCORBIC ACID

M.Sc. Thesis by
Fatma Gül GÜLER
509081244

Date of submission : 06 May 2011
Date of defence examination: 06 June 2011

Supervisor (Chairman) : Prof. Dr. A. Sezai SARAC (ITU)
Members of the Examining Committee : Prof. Dr. Gözen BEREKET(ESOGU)
Assoc. Prof. Dr. Orhan GÜNEY(ITU)

JUNE 2011

İSTANBUL TEKNİK ÜNİVERSİTESİ ★ FEN BİLİMLERİ ENSTİTÜSÜ

3,4-PROPİLENDİOKSİTİYOFEN VE N-FENİLSULFONİL PİROLÜN ELEKTROKİMYASAL KOPOLİMERİZASYONU VE ASKORBİK ASİT VARLIĞINDA DOPAMİN TAYİNİ

YÜKSEK LİSANS TEZİ

Fatma Gül GÜLER
(509081244)

Tezin Enstitüye Verildiği Tarih : 06 Mayıs 2011
Tezin Savunulduğu Tarih : 06 Haziran 2011

Tez Danışmanı : Prof. Dr. A. Sezai SARAÇ (İTÜ)
Diğer Jüri Üyeleri : Prof. Dr. Gözen BEREKET(ESOGÜ)
Doç. Dr. Orhan GÜNEY(İTÜ)

Haziran 2011

FOREWORD

Firstly, I would like to thank my advisor, Prof. Dr. A. Sezai SARAC, for his encouragement, incomparable advices, guidance and discussions in my studies and I have had to learn across broad disciplines, to develop as a scientist.

I would like to offer the most grateful and special thanks to Prof.Dr. Gözen BEREKET for her support and help.

I would like to thank to my family, especially my mother Guler ILGINER and my aunt Nuray ILGINER for precious critics against some of my opinions, respect to my decisions and being always with me at every stage of my life.

My personal thanks goes to Murat SARI for his full support, patience, understanding and being always with me during these two years.

I wish to express my special thanks to all Electropol-Nanotech Group members for all their help. Damla ECEVIT, Timucin BALKAN, N.Ugur KAYA, Suat CETINER, with all of you, it has really been a great pleasure.

Also I would like to thank my old friend Elif UCKARDES for her full support.

June 2011 Fatma Gül GÜLER

Chemist

TABLE OF CONTENTS

Page

TABLE OF CONTENTS ..... **vii**
ABBREVIATIONS ..... **ix**
LIST OF TABLES ..... **xi**
LIST OF FIGURES ..... **xiii**
SUMMARY ..... **xvii**
ÖZET ..... **xix**
1. INTRODUCTION **1**
2. THEORETICAL PART **3**
2.1 Conductive Polymers 3
2.1.1 Electronic conduction in conjugated polymers 4
2.1.2 Synthesis of conducting polymers 8
2.1.3 Applications of conducting polymers 9
2.2 Poly(3,4-alkylenedioxythiophene)s Derivatives 10
2.2.1 Poly (3,4-Propylenedioxythiophene) [Poly(ProDOT)] 12
2.3 N-Phenylsulfonyl Pyrrole (PSP) 13
2.4 Dopamine ($C_8H_{11}NO_2$) and Ascorbic Acid ($C_6H_8O_6$) 14
2.5 Electrochemical Techniques Used in the Synthesis of Conductive Polymers . 17
2.5.1 Chronoamperometry 17
2.5.2 Chronopotentiometry 18
2.5.3 Cyclic voltammetry 18
2.6 Factors Affecting the Electropolymerization 21
2.7 Electrochemical Impedance Spectroscopy (EIS) 24
2.8 Equivalent Circuit Modelling (ECM) 28
2.8.1 Equivalent circuit elements 30
2.9 Carbon Fiber Micro Electrodes 35
2.10 Biosensors 36
2.10.1 Electrochemical biosensors 37
2.10.2 Dopamine sensors 39
2.11 Characterizations 40
2.11.1 Attenuated total reflection Fourier transform infrared spectroscopy (FTIR-ATR) 40
2.11.2 Scanning electron microscopy (SEM) 41
2.11.3 Atomic force microscopy (AFM) 42
3. EXPRIMENTAL **45**
3.1 Chemicals 45
3.2 Electrocopolymerizations 45
3.3 Electrode Preperations 45
3.4 Electrochemical Impedance Spectroscopy (EIS) and Equivalent Circuit Modelling (ECM) 46
3.5 Fourier Transform Infrared-Attenuated Total Reflectance (FTIR-ATR) 47
3.6 Scanning Electron Microscopy (SEM) 47

3.7 Atomic Force Microscopy (AFM) 47
4. RESULTS AND DISCUSSION..... 49
4.1 The Experimental Details of Electrochemical Copolymerization of 3,4-Propylene dioxythiophene (ProDOT) and N-Phenylsulfonyl Pyrrole (PSP) on SCFME in Different Mole Fractions of PSP 49
4.2 Electrocopolymerization of ProDOT and PSP 49
4.3 Ex-situ FTIR-ATR Measurements of Poly(ProDOT-co-PSP) and Poly(ProDOT)..... 55
4.4 Morphological Analyses of Poly(ProDOT-co-PSP) Films via SEM and AFM..... 57
4.5 EIS Investigation of Poly(ProDOT) and Poly(ProDOT-co-PSP) on SCFME 61
4.6 Equivalent Circuit Modelling of Poly(ProDOT) and Poly(ProDOT-co-PSP) on SCFME 64
4.7 Sensor Behaviours of Poly(ProDOT) and Poly(ProDOT-co-PSP) Microelectrodes..... 67
4.7.1 Electrochemical behaviour of Dopamine and Ascorbic acid at the Poly(ProDOT) and Poly(ProDOT-co-PSP) microelectrodes 68
4.7.2 Determination of concentration of Dopamine by CV (Calibration Curve)..... 69
5. CONCLUSIONS..... 73
REFERENCES..... 75
CURRICULUM VITAE..... 87

ABBREVIATIONS

AA	**:** Ascorbic Acid
AC	**:** Alternating Current
ACN	**:** Acetonitrile
AFM	**:** Atomic Force Microscopy
CA	**:** Chronoamperometry
CF	**:** Carbon Fiber
CP	**:** Conducting Polymer
CPE	**:** Constant Phase Element
CV	**:** Cyclic Voltammetry
$\mathbf{C_{DL}}$	**:** Double Layer Capacitance
$\mathbf{C_{LF}}$	**:** Low Frequency Capacitance
DA	**:** Dopamine
DC	**:** Direct Current
DMF	: Dimethylformamide
DMSO	**:** Dimethylsulfoxide
ECM	: Equivalent Circuit Modelling
EDOT	**:** 3,4-Ethylenedioxythiophene
EPR	**:** Electro Paramagnetic Resonance
ESR	**:** Electro Spin Resonance
FTIR-ATR	**:** Foruier Transform Infrared-Attenuated Total Reflection
HOMO	**:** Highest Occupied Molecular Orbital
LUMO	**:** Lowest Occupied Molecular Orbital
MMA	**:** Methyl methacrylate
$\mathbf{NaClO_4}$	**:** Sodium Perchlorate
PAN	: Polyacrylonitrile
PC	**:** Propylenecarbonate
PEDOT	**:** Poly(3,4-Ethylenedioxythiophene)
PPy	**:** Polypyrrole
ProDOT	**:** 3,4-Proylenedioxythiophene
PProDOT	**:** Poly(3,4-Proylenedioxythiophene)
PSP	**: N-**Phenylsulfonyl pyrrole
PTh	**:** Polythiophene
R	**:** Alkyl group
SCFME	: Single Carbon Fiber Micro Electrode
SEM	**:** Scanning Electron Microscope

LIST OF TABLES

Page

Table 2.1: Electrical elements and their impedance response. 28
Table 2.2: Circuit elements used in the models. 30
Table 4.1: Comparison of thickness of copolymer coated SCFME, ΔQ, C_{LF} and phase angle of copolymer films. 53
Table 4.2: FTIR-ATR assignments of Poly(ProDOT-co-PSP)s and Poly(ProDOT). 57
Table 4.3: Mole fraction dependence of parameters calculated from the equivalent 66

LIST OF FIGURES

Page

Figure 2.1: Molecular structures of several conjugated polymers. 4
Figure 2.2: Band theory of conjugated polymers. 4
Figure 2.3: *n*-and *p*-doping process in polymers. 5
Figure 2.4: Possible structures of polythiophene showing the non-degenerate (a) and quinoid (b) configurations; a polaron defect (c) and a bipolaron defect (d). 7
Figure 2.5: Electrochemical polymerization mechanism of EDOT. 9
Figure 2.6: Poly(3,4-alkylenedioxythiophene)s (PXDOTs). 11
Figure 2.7: Poly(3,4-Propylenedioxythiophene). 12
Figure 2.8: N-phenylsulfonyl pyrrole (PSP). 13
Figure 2.9: Structure of Dopamine. 14
Figure 2.10: Structure of Ascorbic Acid. 15
Figure 2.11: Mechanism of the electrocatalytic oxidation of AA by DA. 16
Figure 2.12: Voltage vs time excitation signals used in voltammetry and corresponding current responses: cyclic voltammentry potential (a), corresponding current response (b). 19
Figure 2.13: A typical cyclic voltammogram for an reversible process. 20
Figure 2.14: A typical cyclic voltammogram for an irreversible process. 21
Figure 2.15: Relationship between current and voltage in impedance measurements. 25
Figure 2.16: Nyquist plot of the impedance of a simple electrode reaction. 26
Figure 2.17: Bode plot for a simple electrochemical system (impedance – solid line, phase angle - dotted line). 27
Figure 2.18: Electrical Circuit (Randles Circuit). 28
Figure 2.19: Scheme of the electrical double layer, IHP: Inner Helmholtz Plane, OHP: Outer Helmholtz Plane. 33
Figure 2.20: SEM image of single carbon fiber microelectrode (SCFME). 36
Figure 2.21: The ECE mechanism for DA oxidation. 39
Figure 2.22: Infrared spectrum bands for general subtitutions. 40
Figure 2.23: A multiple reflection ATR system. 41
Figure 2.24: Schematic diagram of scanning electron microscopy. 42
Figure 2.25: Schematic diagram of atomic force microscope. 43
Figure 3.1: A geometry of one compartment-3 electrode cell. 46
Figure 4.1: Cyclic voltammogram of electrogrowth of 10 mM ProDOT and 5 mM PSP in 0.1 M $NaClO_4$/ACN at 30mV.s^{-1}, 10 cycle on SCFME. Inset: CV of monomer free of Poly(ProDOT-co-PSP) film in 0.1 M $NaClO_4$/ACN at different scan rates between 15 and 200 mV.s^{-1} 50
Figure 4.2: Cyclic voltammogram of electrogrowth of 10 mM ProDOT and 10 mM PSP in 0.1 M $NaClO_4$/ACN at 30mV.s^{-1}, 10 cycle on SCFME. Inset: CV of monomer free of Poly(ProDOT-co-PSP) film in 0.1 M $NaClO_4$/ACN at different scan rates between 15 and 200 mV.s^{-1} 51

Figure 4.3: Cyclic voltammogram of electrogrowth of 10 mM ProDOT and 20 mM PSP in 0.1 M $NaClO_4$/ACN at 30mV.s^{-1}, 10 cycle on SCFME. Inset: CV of monomer free of Poly(ProDOT-co-PSP) film in 0.1 M $NaClO_4$/ACN at different scan rates between 15 and 200 mV.s^{-1}. 51
Figure 4.4: Mechanism of electrochemical copolymer formation of ProDOT and PSP on SCFME. 52
Figure 4.5: Plot of oxidation potential and peak current obtained from CV for different mole fraction of Poly(ProDOT-co-PSP)..... 53
Figure 4.6: Plots of anodic and cathodic peak current density vs. square root of scan rates for the copolymer films in monomer free solution (in 0.1M $NaClO_4$ / ACN)..... 54
Figure 4.7: Plots of anodic and cathodic peak current density vs. scan rates for the copolymer films in monomer free solution(in 0.1M $NaClO_4$ / ACN.).. 55
Figure 4.8: Chemical structure of random Poly(ProDOT-co-PSP). 55
Figure 4.9: Ex-Situ FTIR-ATR spectrum of Poly(ProDOT-co-PSP) and Poly(ProDOT) films on ITO-PET. 56
Figure 4.10: SEM image of the copolymer coated SCFME of X_{PSP} = 0.33..... 58
Figure 4.11: SEM image of the copolymer coated SCFME of X_{PSP} = 0.50..... 58
Figure 4.12: SEM image of the copolymer coated SCFME of X_{PSP} = 0.66..... 59
Figure 4.13: AFM image of Poly(ProDOT-co-PSP) coated ITO-PET. 60
Figure 4.14: AFM topography image of Poly(ProDOT-co-PSP) coated ITO-PET.. 60
Figure 4.15: SEM image of Poly(ProDOT-co-PSP) coated ITO-PET. 61
Figure 4.16: Nyquist plots of Poly(ProDOT) and different mole fractions of Poly(ProDOT-co-PSP) electrografted on SCFMEs; correlated with the calculated data from the equivalent circuit model; (R(W(CR)(QR))(CR)). 62
Figure 4.17: Bode Magnitude plots of Poly(ProDOT) and different mole fractions of Poly(ProDOT-co-PSP) electrografted on SCFMEs; correlated with the calculated data from the equivalent circuit model; (R(W(CR)(QR))(CR)). 62
Figure 4.18: Bode Phase plots of Poly(ProDOT) and different mole fractions of Poly(ProDOT-co-PSP) electrografted on SCFMEs; correlated with the calculated data from the equivalent circuit model; (R(W(CR)(QR))(CR)). 63
Figure 4.19: Graph of thicknesses of copolymer coated SCFMEs obtained from SEM, low frequency capacitances and total charges (ΔQ) which were applied during the electropolymerization vs. mole fractions of Poly(ProDOT-co-PSP). 64
Figure 4.20: The equivalent circuit model of Poly(ProDOT), X_{PSP} = 0.33, X_{PSP} = 0.50 and X_{PSP} = 0.66 coating on a single carbon fiber electrode. (R_s=solution and pore resistance and W=Warburg impedance, Z_W; R_a and C_a are the resistance and the adsorption capacitance; R_{ct}= charge transfer resistance; CPE is used for modelling the double layer capacitance, C_{dl}; R_f and C_f are film resistance and film capacitance of coated copolymer film on carbon fiber microelectrode). 65
Figure 4.21: Charge transfer (R_{ct}) and film (R_f) resistances; double layer (C_{dl}) and film (C_f) capacitances obtained rom ECM for Poly(ProDOT), X_{PSP} = 0.33, X_{PSP} = 0.50 and X_{PSP} = 0.66. 67

Figure 4.22: Cyclic voltammograms of DA at the Poly(ProDOT) and Poly(ProDOT-co-PSP) microelectrodes in a buffer solution at scan rate 50mV/s. 68
Figure 4.23: Cyclic voltammograms of DA and AA at the Poly(ProDOT) and Poly(ProDOT-co-PSP) microelectrodes in a buffer solution at scan rate 50mV/s. 69
Figure 4.24: CV of Poly(ProDOT-co-PSP) modified SCFME in buffer solution containing 100µM AA different concentration of DA. 70
Figure 4.25: Changes in anodic peak current density by dopamine concentration for Poly(ProDOT-co-PSP) modified SCFME in 10^{-4} M to 10^{-11} M dopamine-containing buffer solution. 71

ELECTROCHEMICAL COPOLYMERIZATION OF 3,4-PROPYLENE DIOXYTHIOPHENE AND N-PHENYLSULFONYL PYRROLE AND DETECTION OF DOPAMINE IN PRESENCE OF ASCORBIC ACID

SUMMARY

The preparation, characterization and application of electrochemically active conducting polymers are challenging research activity in electrochemistry. Electrochemical polymerization represents a widely employed route for the synthesis of some important classes of conjugated polymers.

Carbon fiber micro electrode shows superior performance in electrochemical studies due to its micron size cylindrical structure. It has a disposable character having a new surface area at each uses compared to Pt or Au electrodes.

In this study, 3,4-Proylenedioxythiophene (ProDOT) and N-phenylsulfonyl pyrrole (PSP) electrocopolymerized in various mole fractions with a cyclic voltammetry (CV), their characterizations were performed by CV, electrochemical impedance spectroscopy (EIS), scanning electron microcopy (SEM), attenuated total reflection Fourier transform infrared spectroscopy (FTIR-ATR) and sensor behaviors against dopamine were investigated.

Electropolymerization process was performed on the single carbon fiber microelectrodes (SCFME) by CV at a scan rate of 30 mV/s at (-0.8 – 1.5)V for the monomers using 10 cycles in 0.1M sodium perchlorate / acetonitrile ($NaClO_4$/ACN).

For spectroscopic characterization of Poly(ProDOT-co-PSP) films, the same mole fractions of the copolymers were also prepared by cyclic voltammetry on ITO-PET with the same conditions of random Poly(ProDOT-co-PSP) films formation on SCFME. FTIR-ATR, SEM and EIS measurements indicate that the inclusion of PSP into the copolymer structure.

EIS measurements were performed at open circuit potential range of 0.01Hz-100kHz (applicationof amplitude of 10 mV) for Poly(ProDOT) and Poly(ProDOT-co-PSP) The copolymers are also exhibiting different impedance data from that of Poly(ProDOT) which shown an ideal capacitive line (Bode phase angles close to 90^0) by the application of electrochemical impedance spectroscopic measurements.

The electrochemical parameters of the Poly(ProDOT-co-PSP) / Electrolyte system were evaluated by employing ZSimpWin (version 3.10) software from Princeton Applied Research. Variation of the electrolyte and pore resistance (Rs), the adsorption capacitance and resistance (C_a and R_a), double-layer capacitance and charge-transfer resistance (C_{dl} and R_{ct}), Warburg impedance (W), resitance and capacitance of the copolymer film on SCMFE (R_f and C_f) in different initial mole fractions of Poly(ProDOT-co-PSP) film were investigated via equivalent circuit model, (R(W(CR)(QR))(CR)).

Morphology of coatings for different mole fractions were studied for Poly(ProDOT-co-PSP) films on SCFMEs. The differences at film thicknesses were obtained due to an increase of PSP in the feed.

The SCFME/Poly(ProDOT) and SCFME/Poly(ProDOT-co-PSP) electrodes were used as a sensor against dopamine. The influence of the presence of ascorbic acid on the dopamine signal was analyzed by cyclic voltammetry. SCFME/Poly(ProDOT-co-PSP) electrode sensor displaying a good current response to different dopamine concentrations with a detection limit of 1 nM in dopamine.

3,4-PROPİLENDİOKSİTİYOFEN VE N-FENİLSULFONİL PİROLÜN ELEKTROKİMYASAL KOPOLİMERİZASYONU VE ASKORBİK ASİT VARLIĞINDA DOPAMİN TAYİNİ

ÖZET

Elektroaktif konjuge polimerlerin sentezi, karakterizasyonu ve uygulama alanları günümüzde çok çalışılan en popüler elektrokimya konularıdır. Elektrokimyasal polimerizasyon iletken polimerlerin sentezinde ve karakterizasyonunda kullanılan en önemli yöntemdir.

Karbon fiber mikro elektrotların mikron boyutunda ve silindirik yapıda olması, altın ve platindeki gibi yüzey temizleme işlemi gerektirmeden tek kullanımlık olarak hazırlanması açısından elektrokimyasal polimerizasyon işlemlerinde tercih edilmektedir. Ayrıca birçok durumda metal elektrotlara nazaran daha verimli sonuçlar saptanmıştır.

Bu çalışmada, farklı mol farksiyonlarındaki 3,4-Propilendioksitiyofen (ProDOT) ve N-Fenilsülfonil pirol (PSP), döngülü voltametri (DV) ile elektrokimyasal olarak kopolimerleştirilmiştir. Bu filmlerin karakterizasyonu döngülü voltametri, elektrokimyasal empedans spektroskopisi (EES), taramalı elektron mikroskobu (SEM), hafifletilmiş toplam yansıtma - Fourier dönüşümlü kızılötesi spektroskopisi (FTIR-ATR) ile gerçekleştirilmiş ve dopamine karşı sensör davranışı incelenmiştir.

Elektrokimyasal proses, tek karbon fiber mikro elektrot (TKFME) üzerinde döngülü voltametri ile, 30 mV/s tarama hızında, (-0,8 - 1,5)V potansiyel aralığında, 0,1M $NaClO_4$/ACN elektrolit çözeltisinde 10 döngü uygulanarak gerçekleştirilmiştir.

Poli(ProDOT-ko-PSP) filmlerinin spektroskopik karakterizasyonu için aynı mol oranlarında, aynı şartlar altında döngülü voltametri ile İTO-PET üzerinde de elektrokolimerizasyonlar gerçekletirildi. FTIR-ATR, EES ve SEM ölçümlerinin sonuçlarına göre, PSP'nin kopolimer yapısına girişi belirgin şekilde gözlenmiştir.

Elektrokimyasal empedans ölçümleri farklı mol fraksiyonlarına (X_{PSP}) sahip Poli(ProDOT-ko-PSP) kopolimerleri için 100kHz-10mHz aralığında açık devre potansiyelinde ve monomer içermeyen elektrolit ortamında 10mV potansiyelde ölçülmüştür. X_{PSP}=0,66 olduğu durumda en düşük, düşük- frekans kapasitans değeri (C_{LF}) elektrokimyasal empedans spektroskopisi ile elde edilmiştir.

Poli(ProDOT-ko-PSP) / Elektrolit sisteminde elektrokimyasal parametreler Princeton Applied Research için uygulanan ZSimpWin (versiyon 3.10) yazılımında gerçekleştirilmiştir. Poli(ProDOT-ko-PSP) filmlerinin çözelti dirençlerinin çeşitliliği, çift tabaka kapasitans, film resistansı, yük transfer resistansı, Warburg difüzyon sabiti ve sabit faz elementi, film kapasitans ve resistansı farklı mol fraksiyonlarındaki kopolimer filmler için bir eşdeğer devre modeli (R(W(CR)(QR))(CR)) üzerinde incelenmiştir.

Farklı mol fraksiyonlarına sahip Poli(ProDOT-ko-PSP) film kaplamalarının morfolojileri SEM görüntüleri ile analiz edilmiştir. SEM görüntülerinde, kopolimer yapısında PSP oranının artmasıyla TKFME üzerindeki film kalınlıklarının belirgin bir şekilde azaldığı görülmüştür.

TKFME/Poli(ProDOT) ve TKFME/Poli(ProDOT-ko-PSP) elektrotları dopamine karşı sensör olarak test edilmiştir. Askorbik asidin varlığında dopamine ait pikin tayin edilebildigi gösterilmiştir. TKFME/Poli(ProDOT-ko-PSP) sensörü inilebilcek en düşük değer 1nM ile farklı dopamin konsantrasyonlarında çok iyi sonuç vermiştir.

1. INTRODUCTION

Conductive polymers have been electrochemically preferred because of their physical or chemical properties such as volume, color, stored charge or porosity and used for a number of applications such as electrochromic displays [1], smart windows [2], solar cells [3], supercapacitors [4] and biosensors [5].

3,4-alkylenedioxythiophene based polymers exhibit low oxidation potential, high and quite stable conductivities, a high degree of optical transparency as a conductor, and the ability to be rapidly switched between conducting doped and insulating neutral states. Substitution at the 3- and 4- positions of thiophene prevents the occurrence of α-β and β-β coupling during electropolymerization, yielding more ordered polymers with longer conjugation lengths. The synthesis of 3,4-disubstituted polythiophenes was carried out stabilizing the oxidized form, providing solubility, processibility [6].

Films of conjugated polymers are generally synthesized on a support electrode surface by electropolymerization (anodic oxidation) of the corresponding monomer in the presence of an electrolyte solution. Carbon fibers have highly accessible surface area, low resistivity and high stability which consist of stacked hexagonal carbon layers, forming small co-herent units (crystallites) of only a few micrometers in the stacking direction [7]. Electropolymerization on carbon fiber microelectrode (CFME) can improve the interfacial properties between the carbon fiber and polymeric matrix. Generally electrocoating of conjugated polymers on carbon fiber easily allows the characterization of the deposited films by spectroscopic, morphological and electrochemical techniques. Conducting polymers which were coated electrochemically on CFMEs were studied in detail and reported [8].

Electrochemical impedance spectroscopy (EIS) is a powerful technique to study charge transfer, ion diffusion and capacitance of conducting polymer modified electrodes [9]. EIS has been used to develop equivalent electric circuits to describe the electrochemical properties of films of conducting polymers in organic solution [10]. EIS has also provided information concerning corrosion protection by inhibitors [11].

The copolymers from different monomers or comonomers have been synthesized by both electrochemical and chemical oxidative polymerizations to efficiently modify the structure and to improve the properties of the conducting polymers [12]. The electrochemical polymerization allows obtaining materials with controlled properties without suffering the experimental disadvantages [13].

Dopamine (DA) is one of the most important catecholamine neurotransmitters in the mammalian central nervous system. Abnormalities in DA concentrations have been linked with several neurological disorders. Consequently, it is not surprising that the measurement of DA has been the focus of much recent research work. In particular, there has been much interest in the development of electrochemical sensors. This is because DA is electroactive and thus the oxidation of DA can be followed using electrochemical techniques. Electrochemical sensors are usually inexpensive to manufacture, highly sensitive and easy to employ. Furthermore, the electrodes used in the sensing can be miniaturised and conveniently placed in the living organism for real time analysis. This is not possible with non-electrochemical techniques.

In this thesis, the electrochemical random copolymerization of ProDOT (3,4-Propylenedioxythiophene) and PSP (N-Phenylsulfonyl pyrrole) (used as self-dopant) on different working electrodes were reported. The electrochemical and morphological properties of Poly(ProDOT) and copolymer films were characterized by FTIR-ATR (Foruier Transform Infrared-Attenuated Total Reflection), EIS (Electrochemical Impedance Spectroscopy), SEM (Scanning Electron Microscope) and AFM (Atomic Force Microscopy). The electrochemical impedance data was fitted to an equivalent circuit in order to identify differences between the conductivities of Poly(ProDOT) and copolymers. The electrochemical response of the Poly(ProDOT) and copolymer modified electrodes toward ascorbic acid (AA) and dopamine (DA) was investigated by cyclic voltammetry (CV). Briefly, the effect of PSP mole fractions on the electrochemical and morphologic properties of resulting copolymers using alternative characterization techniques was shown with this thesis.

2. THEORETICAL PART

2.1 Conductive Polymers

Traditionally polymers have been associated with insulating properties in the electronic industry and are applied as insulators of metallic conductors or photoresists. Since the discovery in 1977 of the doping of polyacetylene (PA), which resulted in increasing the conductivity of polyacetylene by eleven orders of magnitude [14-15], many academic and industrial research laboratories initiated projects in the field of conducting polymers. The importance of the field of semiconducting polymers was recently stressed by awarding the 2000 Nobel prize in chemistry to the discoverers Heeger, Shirakawa and MacDiarmid. The three winners established that polymer plastics can be made to conduct electricity if alternating single and double bonds link their carbon atoms, and electrons are either removed through oxidation or introduced through reduction. Normally the electrons in the bonds remain localized and cannot carry an electric current, but when the team "doped" the material with strong electron acceptors such as iodine, the polymer began to conduct nearly as well as a semimetal. Although polyacetylene exhibits a very high conductivity in the doped form, the material is not stable against oxygen or humidity and is intractable. For these reasons, much work has been devoted to synthesizing soluble and stable polyacetylenes [16-17]. Unfortunately, these substituted derivatives exhibit electrical conductivities that are much lower than of the parent polyacetylene. The discovery of polyacetylene led to the search for new structures that could lead to new and improved polymer properties. Since then, more polymers with conjugated π electrons were found to undergo transition from insulator to conductor after doping with weak oxidants or reducing agents and developed for their specific physical or chemical properties and implemented in a variety of applications as novel materials in rechargeable batteries, electrochromic display devices, sensors, electromagnetic interference shielding and corrosion protection. New classes of conducting polymers include polythiophene, polyfuran, polypyrrole, poly(p-phenylene), poly(p-phenylenevinylene), polyfluorene and

polyaniline (Figure 2.1). Although none have exhibited higher conductivity than polyacetylene, these polymers have been useful in designing new structures that are stable and soluble in some cases.

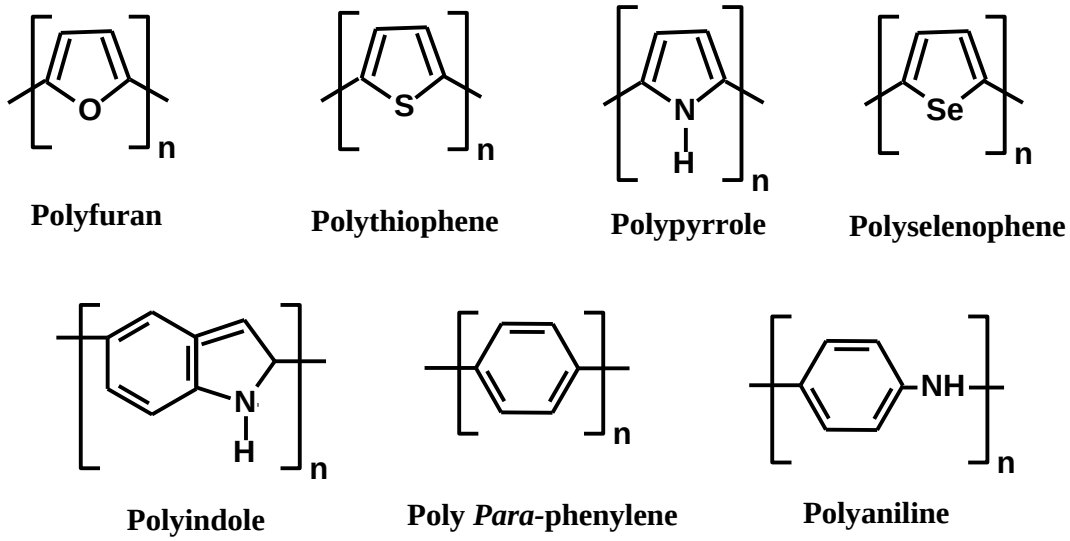

Figure 2.1: Molecular structures of several conjugated polymers.

2.1.1 Electronic conduction in conjugated polymers

The electronic and optical properties of π-conjugated polymers result from a limited number of states around the highest occupied and the lowest unoccupied levels. According to the band theory (Figure 2.2), the highest occupied band, which originates from the highest occupied molecular orbital (HOMO) of each monomer unit, is referred to as the valance band (VB) and the corresponding lowest unoccupied band, originating from the lowest unoccupied molecular orbitals (LOMO) of monomer is known as the conduction band (CB) [18].

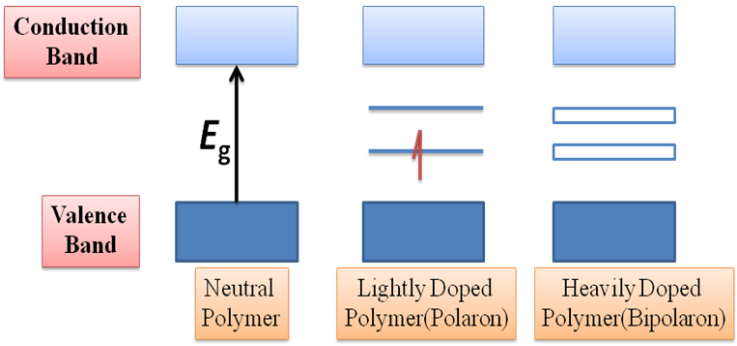

Figure 2.2: Band theory of conjugated polymers.

The energy distance between these two bands is defined as the band gap (E_g), and in neutral conjugated polymers refers to the onset energy of the π-π* transition. The E_g of conjugated polymers can be approximated from the onset of the π-π* transition in the UV-Vis spectrum. Conjugated polymers behave as semiconductors in their neutral state. However, upon oxidation (*p*-doping) or reduction (*n*-doping), the interband transitions between VB and CB can decrease the effective band gap and thereby, resulting in the formation of charge carriers along the polymer backbone. The *p*-doping process involves the removal of an electron from the polymer backbone via the external circuit, while the charge neutrality is maintained via insertion of an anion from the electrolyte solution. The *n*-doping process proceeds withinjection of electrons on the polymer backbone, while cations are inserted into the polymerto maintain charge neutrality (Figure 2.3).

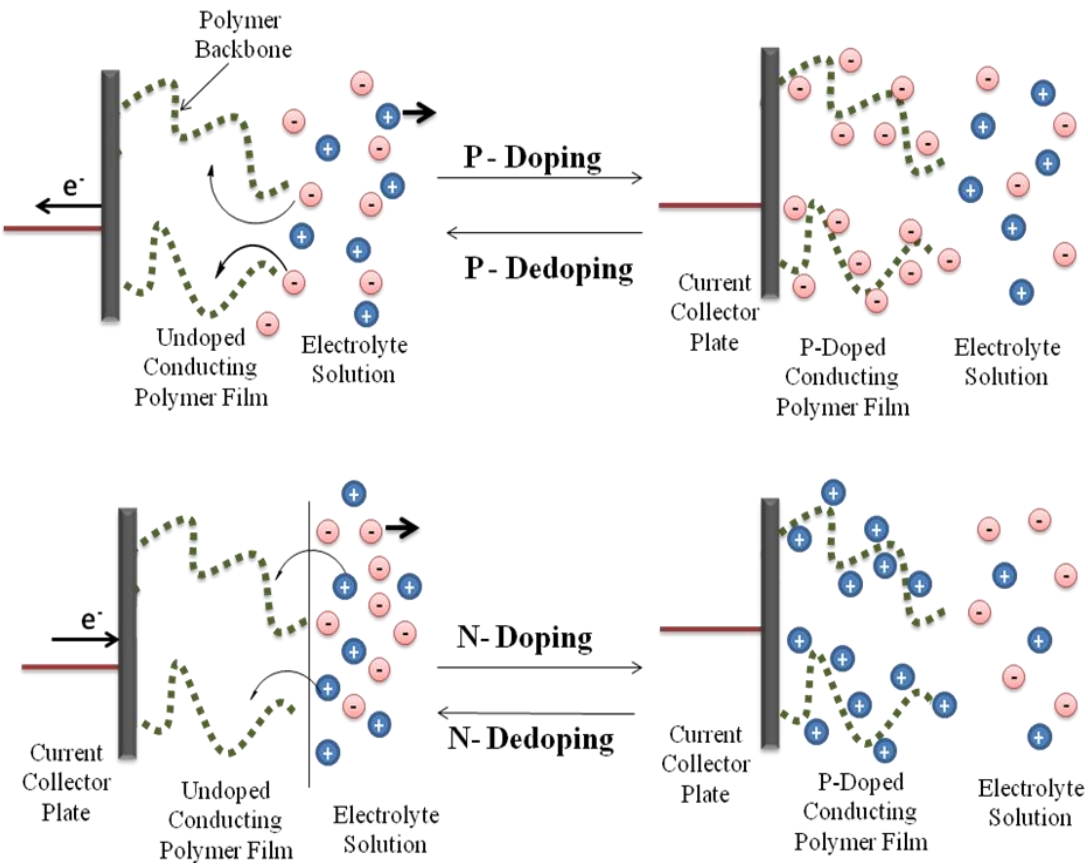

Figure 2.3: *n*-and *p*-doping process in polymers.

Electrochemical doping in which a polymer-coated, working electrode is suspended in an electrolyte solution in which the polymer is insoluble along with separate counter and reference electrodes. An electric potential difference is created between the electrodes which causes a charge (and the appropriate counter ion from the electrolyte) to enter the polymer in the form of electron addition (*n*-doping) or removal (*p*-doping). The reason *n*-type doping is so much less common is that Earth's atmosphere is oxygen-rich, which creates an oxidizing environment. An electron-rich *n*-type polymer will react immediately with elemental oxygen to de-dope (re-oxidize to the neutral state) the polymer. Thus, chemical *n*-type doping has to be done in an environment of inert gas (e.g., argon). Electrochemical *n*-type doping is far less common in research, because it is much more difficult to exclude oxygen from a solvent in a sealed flask.

A brief summary of the theoretical models of the electronic conductivity of conjugated polymers, using polythiophene as example, is given in Figure 2.4. In heterocyclic polymers, where two non-degenerate regions are separated by a topological defect, the formation of single solitons like polyacetylene is energetically unfavorable [19], and paired sites are formed [20]. This is the case for polythiophene, which can be drawn with either aromatic (Fig. 2.4a) or quinoid (Fig. 2.4b) structures, of which the latter possesses a higher energy configuration. Two neutral radicals on a single chain will recombine to eliminate the structural defect [19], although, if one is charged, a polaron is formed, which is delocalized over about four rings (Fig. 2.4c). However, when both defects are charged, they are predicted to pair up to form a ‘bipolaron’ [19], consisting of a doubly charged defect with no spin (Fig. 2.4d) and extending over a number of rings to a similar polaron. At higher doping levels, bipolarons may also combine to form ‘bipolaron bands’ within the gap [21].

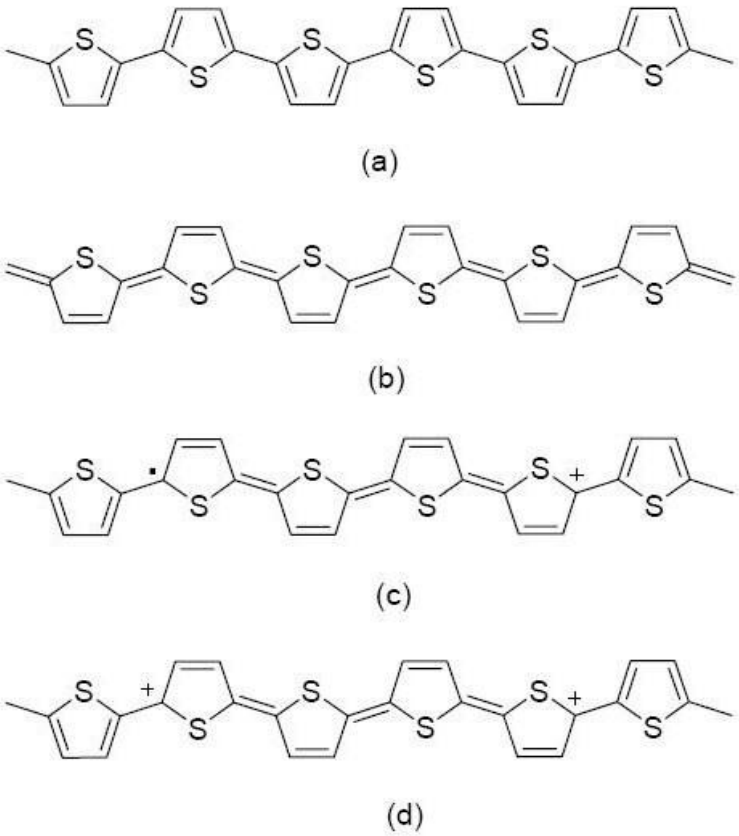

Figure 2.4: Possible structures of polythiophene showing the non-degenerate (a) and quinoid (b) configurations; a polaron defect (c) and a bipolaron defect (d).

Although these charge carriers are responsible for electrical conductivity in conjugated polymers, many structural imperfections are present in all polymers and thus when discussing mechanisms of bulk conductivity, these defects need to be considered. Conductivity is not only a result of charge transfer along the chain, but is also due to electron hopping between chains and between different conjugated segments of the same chain. In addition to these effects, which act at molecular level, bulk conductivity values are also dominated by electron transfer between grain boundaries and variations in morphology [22,23].

2.1.2 Synthesis of conducting polymers

Electrically conductive polymers may be synthesized by any one of the following methods [24].

- Chemical polymerization
- Electrochemical polymerization
- Photochemical polymerization
- Emulsion polymerization

The most widely used technique is based on the oxidative coupling. Oxidative coupling involves oxidation of monomers to form a cation radical followed by coupling to form a dication. Repetition leads to the desired polymer. This can be performed by chemical or electrochemical polymerization.

Chemical polymerization [25, 26] is the versatile technique for preparing large amounts of conducting polymers. Chemical synthesis can be carried out in a solution containing the monomer and an oxidant in an acidic medium. However, control over polymer morphology is extremely limited, purification can be problematic and processing is virtually impossible.

Electropolymerization is a standard oxidative method for preparing electrically conducting conjugated polymers. Smooth, polymeric films can be efficiently electrosynthesized on conducting substrates where their resultant electrical and optical properties can be probed easily by several electrochemical and coupled in situ techniques. Electrosynthesis can be carried out in three ways: (1) potentiostatic (constant potential) method; (2) galvanostatic (constant current) method; (3) potentiodynamic (potential scanning or cyclic voltammetric) method.

Electrochemical synthesis of conducting polymers offers many advantages over chemical synthesis, including the in situ deposition of the polymer at the electrode surface, and, hence, eliminating processibility problems and the control of the thickness, morphology and degree of polymer doping by quantity of passed charge. In addition, the polymers are simultaneously oxidized to their doped conducting forms during polymer growth. Electrochemical polymerization is the method of choice for rapid characterization of conjugated polymers and is achieved by the electrooxidation of the heterocycle in an inert organic solvent containing supporting

electrolyte. Whether using cyclic, potentiostatic, or galvanostatic methods, electrochemical polymerization allows for synthesis of the desired polymer on an electrode's surface that allows for both electrochemical and optical studies. As shown in Figure 2.5, EDOT is converted to its radical cation by removal of an electron under an applied electric field. This intermediate is stabilized by the ethylenedioxy pendant group. Two reactions can then occur by the attack of the radical cation on a neutral monomer or coupling of two radical cations. Both routes yield an intermediate that is rearomatized upon loss of two protons to give a dimer unit. Repeated coupling results in synthesis of the polymer.

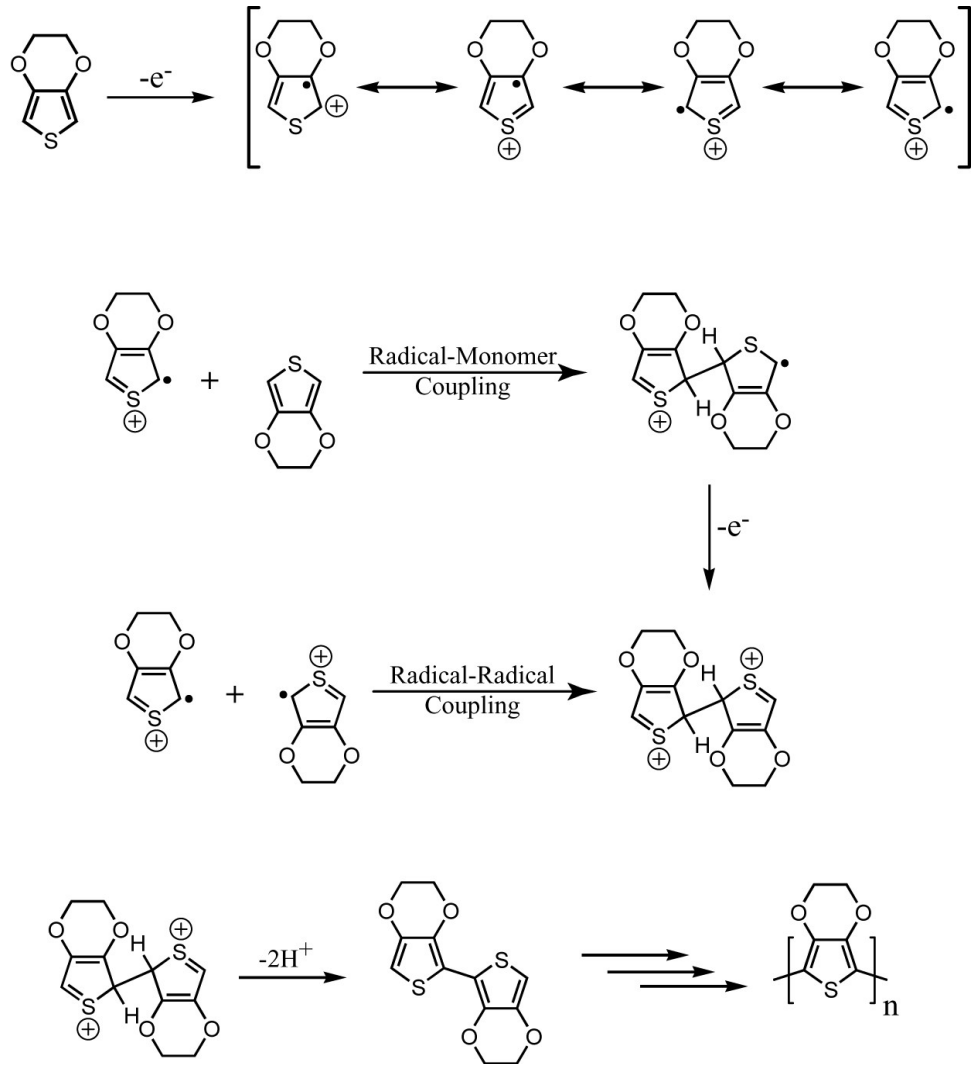

Figure 2.5: Electrochemical polymerization mechanism of EDOT.

2.1.3 Applications of conducting polymers

The susciptiblity of π-electrons of the conjugated polymers to oxidation or reduction alters the electrical, optical and electrooptical properties of the polymers. Since,

mostly the redox processes in the conjugated polymers are reversible, therefore, the electrical and optical properties can be tuned systematically, with appreciable degree of precision by suitably controlling both the chemical or electrochemical oxidation and reduction. It is even possible to swich from a conducting to an insulating state and vice versa.

Conducting polymers are thought to replace metals in future because they have superior properties, such as ease of preparation, light weight and low-cost fabrication, to metals which are also toxic and hazardous to the environment [27]. An assessment of the applica-tion potential of organic conductive polymers in organic electronics [28], in chemical sensors [29], biosensors [30] or as antistatic, corrosion protective [31] or as electrochromic coatings [32] resulted in its extensive investigations during the last decade. So far, numerous publications about various applications of electrically conducting polymers can be divided into two main groups [29]: one is used as materials or elements for construction of various devices based on electronic, optoelectronic and electromechanical principles; the other is as sensitive materials in chemical sensors based on electronic, optical [33], mass [34-35] or transduction mechanisms.

2.2 Poly (3,4-alkylenedioxythiophene)s Derivatives

Due to its high oxidation potential, thiophene itself is difficult to polymerize electrochemically. However, upon alkyl substitution the monomer oxidation potential is lowered to an easily accessible range, which has resulted in the extensive study of poly(3-methylthiophene) and poly(3-alkylthiophene) [36]. While these substituents do lower the oxidation potential and stabilize the oxidized form of the polymers to nucleophilic attack, they also lead to severe steric interactions that distort the π-conjugated system [37] decreasing the degree of conjugation and lowering the conductivity. To overcome this drawback, poly(3,4-cycloalkylthiophenes) were synthesized, and it was demonstrated that carbocycles at the 3- and 4- positions reduced the steric hindrance, especially in the case of poly(3,4-cycloalkylthiophenes). This strategy was taken a step further and the methylene adjacent to the heterocycle was replaced by a heteroatom making the oxidized form even more stable with less steric distortion. As a result, polythiophenes carrying 3,4-dialkoxy and 3,4-alkylenedioxy substituents exhibit the most pronounced stability.

As a class of conducting and electroactive polymers that can exhibit high and quite stable conductivities, a high degree of optical transparency as a conductor, and the ability to be rapidly switched between conducting doped and insulating neutral states, poly(3,4-alkylenedioxythiophene)s (PXDOTs) (Figure 2.6), have attracted attention across academia and industry.

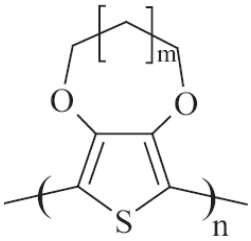

Figure 2.6: Poly(3,4-alkylenedioxythiophene)s (PXDOTs).

The 3,4-ethylenedioxy derivative of PTh (PEDOT) stands out as an excellent candidate for use in a variety of applications such as electrochromic devices, LEDs, capacitors and sensors. Initially developed to give a processable polymer (as an aqueous dispersion) with a high degree of order due to the lack of α−β and β−β couplings, PEDOT showed other very interesting properties worth pursuing by both industry and academia. In addition to its high conductivity (300-400 S/cm), PEDOT exhibits high electrochromic contrast with the major advantage of being almost transparent in thin, doped films [38-39]. Other advantages include low monomer oxidation potential, high stability in the doped form and an ease of derivatization at the ethylenedioxy ring, thus allowing for state-of-the-art tuning of the materials' electronic and optical properties. The industrial use of the polymer as an antistatic layer in photographic films makes it the most widely used conducting polymer to date [40].

In this context, the past ten years have witnessed the emergence of an impressive variety of EDOT derivatives [40]. Functionalization of the monomer with long alkyl or alkoxy pendant groups affords materials that can be processed by common methods including spraying, printing, spin coating or solution casting [41,42]. Moreover, the introduction of water-soluble sodium salt units as pendant groups allows water-processability along with self-doping. This type of polymer has been deposited on several substrates via the electrostatic adsorption technique [43-45]. To expand the range of substituted 3,4-alkylenedioxy thiophenes, monomers were

synthesized having several ring sizes, such as 7-membered (ProDOT) [46] and 8-membered (BuDOT) rings [41] ProDOT has received special attention, as the monomer can be symmetrically derivatized at the central carbon of the propylene bridge, resulting in a regiosymmetric polymer.

The bandgap of EDOT-containing polymers can be modified by varying the degree of π-overlap along the polymer backbone via steric interactions and by controlling the electronic character of the π-system with electron donating or accepting units. The latter is accomplished by using substituents and co-repeat units that adjust the energy of the highest occupied molecular orbital (HOMO) or valence band and the lowest unoccupied molecular orbital (LUMO) or conduction band, thus obtaining polymers with a broad range of colors. In this manner, materials with higher gaps than the PEDOT parent have been prepared, some of which are used as anodically coloring polymers in electrochromic devices [47-49]. Further work using a donor-acceptor methodology has led to low band gap polymers able to p- and n- dope along with exhibiting multi-color electrochromism [50].

2.2.1 Poly (3,4-Propylenedioxythiophene) [Poly(ProDOT)]

P(ProDOT) was synthesized by the traditional double-Williamson etherification route, having Δλ%T of 66% at λmax compared to the 54% transmittance change for PEDOT[51]. ProDOT exhibited higher contrast in comparison to conjugated polymers from EDOT [52].

Side-chain derivatization is possible due to ProDOT flexibility of the conjugated backbone structure. The dimethyl and diethyl derivatives especially exhibit enhanced electrochromic contrasts throughout the visible region [53] and high capacitive behaviors [54 ,55].

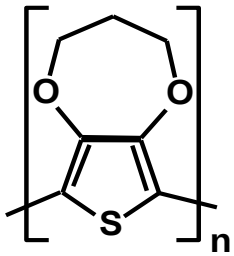

Figure 2.7: Poly(3,4-Propylenedioxythiophene).

A series of Poly(ProDOTs) are disubstituted with long chain esters. This functionality enhances solubility in polar solvent [56]. Electropolymerization of hydroxymethyl-substituted 3, 4- Propylene dioxythiophene monomer (ProDOT-OH) was easily performed [57]. Multiwalled carbon nanotubes (MWNTs) were functionalized with Poly(ProDOT) by oxidative polymerization and MWNT-g-PProDOT hybrid was prepared and showed that improved thermal stability [58]. High capacitances and good reversibility for the poly(2,2-dimethyl-3,4-propylenedioxythiophene) on CFMEs were observed recently [59]. A dibenzyl substituted poly(3,4-propylene dioxythiophene) deposited on ITO coated glass is found to exhibit 89% electrochromic contrast in the visible region with fast switching time [60].

2.3 N-Phenylsulfonyl Pyrrole (PSP)

The chemical synthesis of N-Phenylsulfonyl pyrrole (PSP) was reported in [61] for the purposes of implementing a gas sensor. Additionally, N-phenyl sulfonyl-1H-pyrrole-3-sulfonyl chloride was synthesized in acetonitrile by using chronosulphonic acid [62].

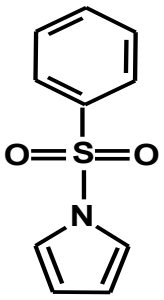

Figure 2.8: N-phenylsulfonyl pyrrole (PSP).

2.4 Dopamine ($C_8H_{11}NO_2$) and Ascorbic Acid ($C_6H_8O_6$)

Dopamine (DA), Figure 2.9, is a catecholamine neurotransmitter that is widely present in both the brain and the peripheral nervous system.

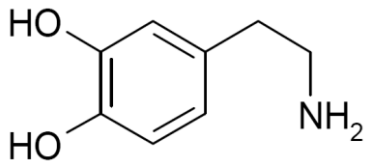

Figure 2.9: Structure of Dopamine.

Schizophrenia occurs because the number of DA receptors in the schizophrenic brain are believed to be higher than in the normal brain. Therefore, the normal amount of DA in the schizophrenic brain has too powerful an action. Again, there is no instant cure, however, the sensitivity of the system can be reduced by blocking the DA receptors with antipsychotic drugs [63].

DA has been linked with the debilitating ailment, Parkinson's disease and the severe mental disorder, schizophrenia. The symptoms of Parkinson's disease arise when the DA containing neurons in the brain start to deteriorate. They eventually disappear as the disease progresses. Currently, there is no immediate cure for patients with Parkinson's disease. The administration of L-Dopa has been found to be helpful but it becomes less effective over time [64].

DA is also believed to play a central role in Huntington's disease, a fatal, genetic neurodegenerative movement disorder for which there is no cure. However, decreasing the release of DA with tetrabenazine has emerged as an effective treatment in suppressing Huntington's disease [65]. Furthermore, it has been shown that DA plays a very important role in drug addiction [66] and attention disorders [67] and it has even been associated with HIV infection [68]. Accordingly, the development of simple analytical methods for the determination of DA concentrations is important.

Moreover, according to other recent clinical studies [69], it seems that the content of Ascorbic Acid (AA) and DA can be used to assess the amount of oxidation stress in human metabolism, linked to cancer [70], diabetes mellitus [71], and hepatic diseases [72]. However, it is almost impossible to detect this component electrochemically by direct oxidation on a conventional electrode (i.e., glassy carbon, graphite, Au, Pt) because of its high overpotential and because of electrode fouling, poor reproducibility, low selectivity and poor sensitivity. AA, Figure 2.11, is a sugar acid with antioxidant properties and it is the most problematic interfering compound in electrochemical DA detection. The typical concentration in the brain of DA is 10^{-8} to 10^{-6} mol dm^{-3} while AA concentrations as high as 10^{-4} mol dm^{-3} have been reported [73].

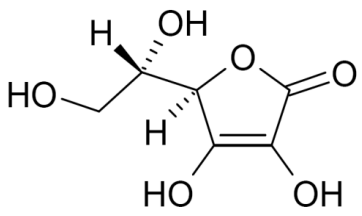

Figure 2.10: Structure of Ascorbic Acid.

Moreover, the oxidation waves of AA and DA, which coexists with AA in biological liquids, are nearly at the same potential and therefore overlapped, which results in the poor selectivity and reproducibility [74]. In addition, the products of AA oxidation foul the electrode surface causing a decrease in the peak currents at most solid electrodes [75]. Furthermore, AA reacts with the oxidised DA product (dopamine-o-quinone, DOQ) which is generated through the electrochemical oxidation of DA. This reaction leads to the oxidation of AA and the regeneration of DA. The catalytic regeneration of DA makes it available for further electrochemical oxidation, and thus complicates the analyses. The mechanism of this reaction has been explained by Bilewicz et al. [75] and by Zhang and Jiang [76]. It involves a redox reaction between the oxidised DA product (DOQ) and AA which results in the oxidation of AA and the regeneration of initial DA. This DA can then be re-oxidised at the electrode surface generating a greater signal than expected for a given concentration of DA. This mechanism is outlined in Figure 2.11.

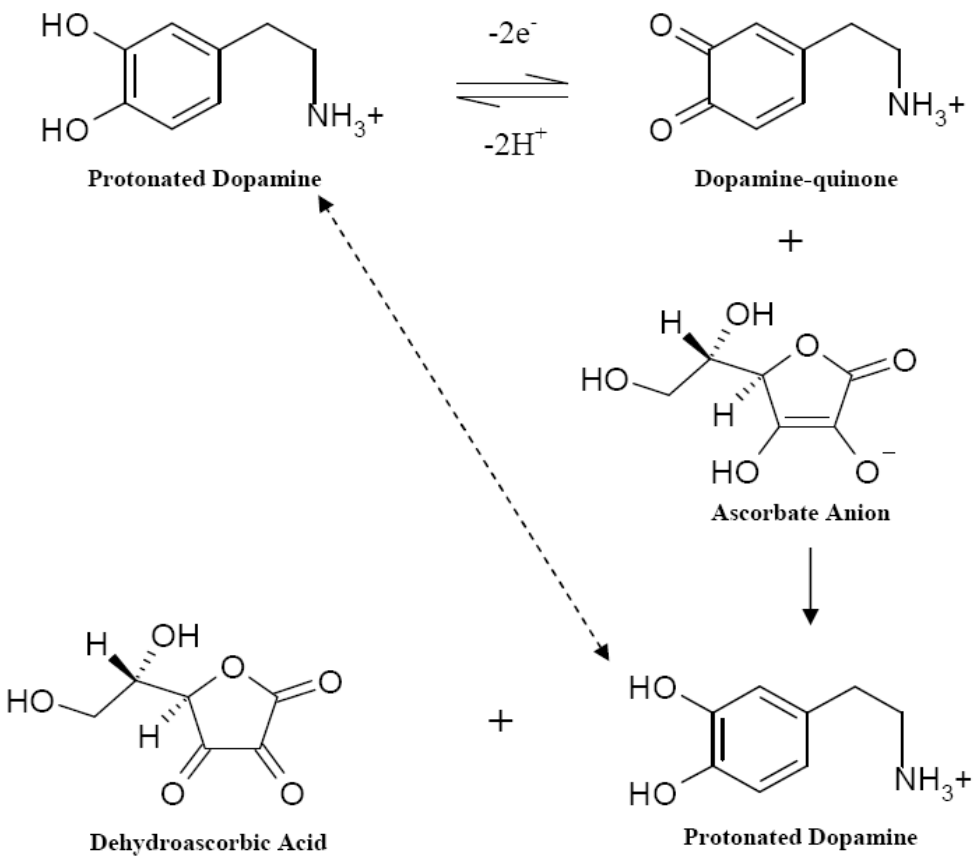

Figure 2.11: Mechanism of the electrocatalytic oxidation of AA by DA.

Thus, the ability to determine AA or DA selectively in the presence of one another has been a major goal for electroanalytical research and the development of chemical sensors for in vivo monitoring. During these last years, many efforts [77] have gone into solving this particular problem but, no satisfactory results have been obtained, especially for clinical, and bio-medical monitoring in real samples.

2.5 Electrochemical Techniques Used in the Synthesis of Conductive Polymers

2.5.1 Chronoamperometry

Chronoamperometric method is used to measure the current as a funtion of time, is a method of choice to study the kinetic of polymerization and especially the first steps. As a potential step is large enough to cause an electrochemical reaction is applied to an electrode, the current changes with time. The study of this current response as a function of time is called chronoamperometry (CA). CA is a useful tool for determining diffusion coefficients and for investigating kinetics and mechanisms. Unlike CV, CA can yield this information in a single experiment.

In CA, the current is monitored as a function of time. It is important to note that the basic potential step experiment is CA; that is, during the experiment, the current is recorded as a function of time. However, after the experiment, the data can also be displayed as charge as a function of time (the charge is calculated by integrating the current). Hence, chronocoulometry data can be obtained.

Chronoamperometry is an electrochemical technique in which the potential of working electrode is stepped and the resulting current from faradaic processes occuring at the electrode is monitore as a function of time.

The current-time curve is described as Cottrel equetion ($I=nFACD^{1/2}\pi^{-1/2}t^{-1/2}$). Where:

n = number of electrons transferred/molecule

F = Faraday's constant (96,500 C mol^{-1})

A = electrode area (cm^2)

D = diffusion coefficient (cm^2s-^{1})

C = concentration (mol cm^{-3}).

2.5.2 Chronopotentiometry

Chronopotentiometric method is used to measure the potential as a function of time. For this technique constant current is applied for elapsed time, than uniformity of coated structure could be decided by checking the linearity of the potential difference with the time. Chronopotentiometry is also named as galvanostatic method and reaction could either be done via galvanostat. Common applications of the galvanostat include constant current stripping potentiometry and constant current electrolysis. One advantage of all constant current techniques is that the ohmic drop due to solution resistance is also constant, as it is equal to the product of the current and the solution resistance.

2.5.3 Cyclic voltammetry

Among electrochemical methods, cyclic voltammetry (CV) has becoming increasingly popular as a mean to study redox states, due to its simplicity and versatility. Cyclic voltammetry refers to the electrochemical technique where the resulting current is measured as dependent variable of the potential varying linearly in time. The reduction or oxidation potential of a conducting polymer can be easily located by CV. The ability to generate a new redox species during the first potential scan and then probe the fate of species on the second and subsequent scans, is regarded as an important aspect of this technique. Therefore, CV can be used both for monitoring the growth of a polymer film on the electrode surface and the subsequent characterization of the polymer within a single set of experiment. Additionally, information about the stability of the polymer films can be obtained from CV during multiple redox cycles. Since the rate of potential scan is variable, both fast and slow reactions can be followed.

During a CV experiment, the potential is increased linearly from an initial potential to a final potential and back to the initial potential again, while the current response is measured. For freely diffusing species, as the potential is increased, oxidizable species near the electrode surface react, and a current response is measured. When the direction of the scan is reversed, the oxidized species near the electrode surface are reduced, and again a current response is measured. The peak current is related to the scan rate according to the Randles - Sevcik equation [78]:

$$i_p = (2.69 \times 10^5)\, n^{3/2}\, C^b\, A\, D^{1/2}\, v^{1/2} \qquad \textbf{(2.1)}$$

where n is the number of electrons, A is the surface area of the electrode (cm^2), D is the diffusion constant (cm^2/s), C^b is the bulk concentration of electroactive species (mol/cm^3), and v is the scan rate (V/s). Therefore, for a diffusion-controlled process, the peak current is proportional to the square root of the scan rate. Since electroactive polymer is adhered to the electrode surface, the process is not diffusion controlled. For surface bound species the peak currents scale linearly with scan rate according to the equation [79]:

$$i_p = n^2 F^2 \Gamma v / 4RT \qquad \textbf{(2.2)}$$

where Γ is the concentration of surface bound electroactive centers (mol/cm^2) and F is Faradays constant (96,485 C/mol).

In CV experiments the current response derives from the application (in an unstirred solution) of a triangular potential waveform (Figure 2.12a), which produces a forward and a reverse scan. Each experiment can consist of one full cycle, a partial cycle or several cycles. The interval of potential scanned in every experiment depends on the voltage at which diffusion-controlled oxidation or reduction of the sample can be observed.

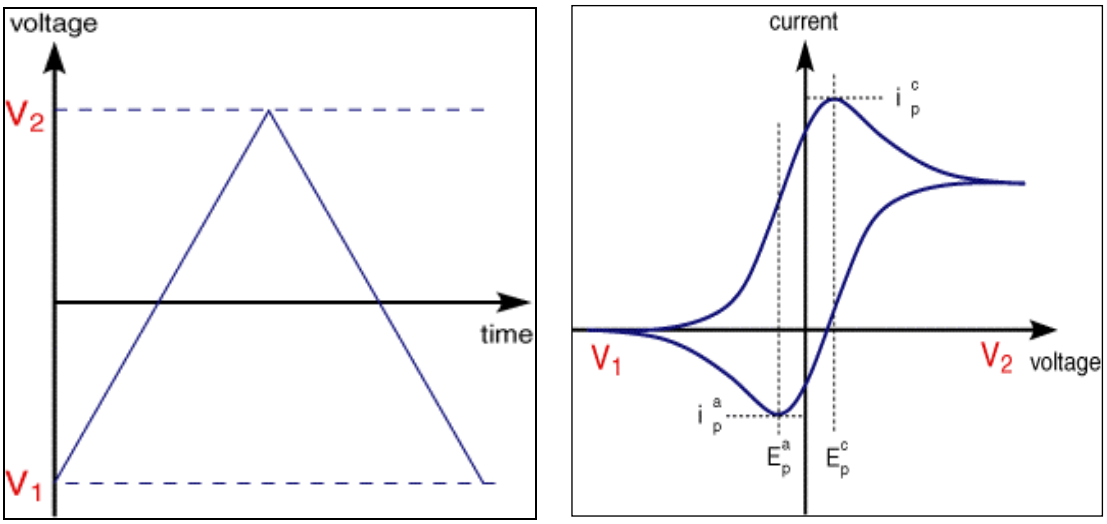

Figure 2.12: Voltage vs time excitation signals used in voltammetry and corresponding current responses: cyclic voltammentry potential **(a)** and corresponding current response **(b)**.

The most useful parameters in a cyclic voltammogram are the cathodic peak potential, Epc, the anodic peak potential, Epa, the cathodic peak current, ipc, and the anodic peak current, ipa (Figure 2.12b). They allow determination of the reversibility of the electron transfer reaction and the consequent similarity of the system to a Nernstian behaviour [80]. For a reversible electrode reaction, the ratio between anodic and cathodic peak currents should be equal to 1, also the peak currents are proportional to the square root of the scan rate. Moreover, at 25°C the difference in peak potentials, ΔEp, is expected to be 0.059/n, where n is the number of electrons involved in the half-reaction. Higher ΔEp indicates irreversibility due to slow electron transfer kinetics (Figure 2.13).

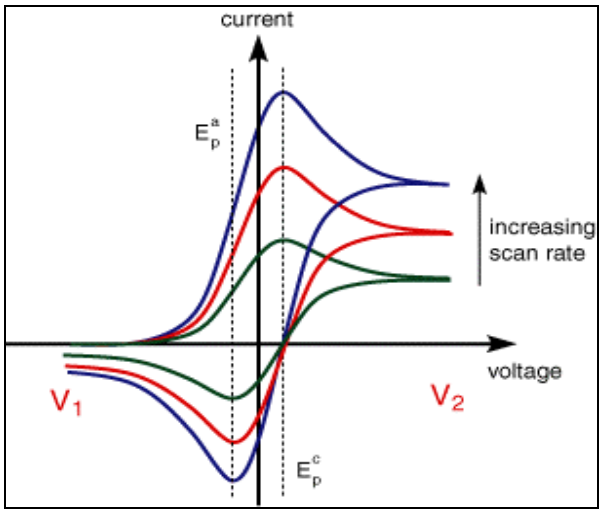

Figure 2.13: A typical cyclic voltammogram for an reversible process.

The CV cases where the electron transfer is not reversible show considerably different behaviour from their reversible counter parts. The Figure 2.14 shows the voltammogram for a quasi-reversible reaction for different values of the reduction and oxidation rate constants.

The first curve shows the case where both the oxidation and reduction rate constants are still fast, however, as the rate constants are lowered the curves shift to more reductive potentials. Again this may be rationalised in terms of the equilibrium at the surface is no longer establishing so rapidly. In these cases the peak separation is no longer fixed but varies as a function of the scan rate. Similarly the peak current no longer varies as a function of the square root of the scan rate.

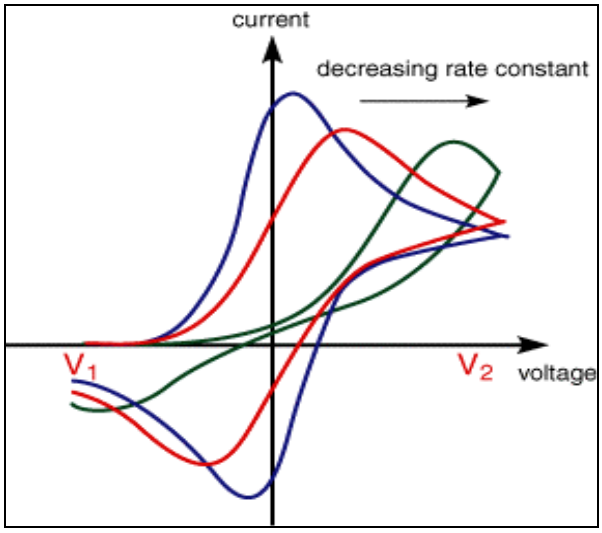

Figure 2.14: A typical cyclic voltammogram for an irreversible process.

2.6 Factors Affecting the Electropolymerization

Presence of alkyl group gives solubility to copolymers obtained both chemically and electrochemically [81]. The substituents on the Nitrogen atom can influence the conductivity: the greater the steric interaction between repeat units is the weaker the conductivity will be. The influence of N-substitution on the electropolymerization characteristics was examined by Waltman [82].

The polymer yield and the rate of oxidation were found the decrease as the size of the alkyl group increases. Bonding large substituents to the Nitrogen atom or to the β-carbon stabilizes to cation radical without stopping the polymerization [83]. If this intermadiate is too stable it can diffuse into the solution and form soluble products. As a result, the yield and the molecular weight of the polymer will be low.

The choice of an electrolyte is made by considering its solubility and nucleophilicity. Moreover the anion oxidation potential should be higher than the monomer. The nature of the anion has an impact on the quality of the film produced which depends on the hydrophobic character of the anion and the interactions between the polymer and the anion. For instance, Kassim et al. [84] have shown that in aqueous solution, the utilization of a large aromatic sulfate anion gives stable conducting polymers with better mechanical properties than when a perchlorate anion is used because of their hydrophobic interaction with water, one of roles played by these organic anions is to orient polymer chain parallel to the electrode surface. This chain orientation increases the order in the polymer structure [85]. On the other hand, anion nucleophilicity interferes with the reaction by increasing the formation of soluble products. The polymer of the highest conductivity is produced when elevated concentrations of electrolyte are used [86].

The copolymer possessing cation recognition properties have been subjected to a sustained interest in recent years. The electrochemical properties were analyzed in the presence of the different alkali cations (Li^+, Na^+, K^+). In each case addition of incremental amounts of cation produces a positive shift of the anodic peak potential and a decrease of electroactivity [87]. The size of the cation can have an influence on the polymer conductivity. It is shown that the larger cation, the lower conductivity of the polymer [88].

The solvent used for electropolymerization is an important factor governing not only the quality of the conducting polymer obtained, but also its conductivity, morphology and subsequently the electrochemical behavior. The solvent must minimize the nucleophilicity reactions. Among these solvents, ACN is the most commonly used. Nucleophilic solvents like DMF or DMSO do not allow polymer formation to occur unless a protic acid, like p-toluenesulfonic acid is added [89]. In ACN, the addition of small quantities of water has a big influence on the kinetics of the reaction and the properties of the polymer formed [90]. This effect is due to the stabilization of the cation radical intermediate by the water molecules which have a larger polarity than ACN.

Film formation is influenced by the strength of the interactions between the solvent and the cation radicals. The basicity of the solvent is the principal factor affecting the selectivity in polymer formation. On the other hand, the solvent polarity will affect the strength of the interactions between the solvent and the electrolyte anions.

Ko et al. have studied the morphology and the film properties in aqueous and nonaqeous solution (in the case of ACN) [91]. They have found that the film prepared in ACN are more homogeneous and better conductors as compared to the polymers prepared in aqueous solution undergo attack by water molecules during reaction which is responsible for their irregular morphology and their weak properties. Unsworth et al. have shown that the adsorption of oxygen gas formed during water oxidation is a source of surface defects in the polymer [92]. In dried ACN, acid catalyzed formation of a pyrrole trimer having a broken conjugation yields a partly conjugated and poorly conductive PPy which passivates the electrode after deposition.

The flavorable effect of water comes from its stronger basicity than pyrrole and therefore it has the ability to capture the protons released during the electropolymerization. This prevents the formation of the trimer and thus avoids the passivation of the electrode.

Solvent retention within the polymer matrix, retention of solvent affinity sites, are important factors. Thus, for instance, several polypyrrole derivatives, when electropolymerized in ACN or PC show a well electrochemically cycle in the solvent of electropolymerization [93]. Solvents may also be too nucleophilic: besides its high solvation capability for even doped CPs, DMF is also poor electropolymerization solvent due to high nucleophilicity; if this is reduced with addition of protic solvents, electropolymerizations are observed [94].

Electropolymerization temperature has a substantial influence on the kinetics of polymerization as well as on the conductivity, redox properties and mechanical characteristics of the films. Films prepared at lower temperatures have a more rugged appearance and poorer adhesion than those prepared at higher temperatures [95].

a) A conjugated polymer's conductivity decreases with decreasing temperature.

b) A semiconductor's DC conductivity decreases with decreasing temperature, remains finite at low temperatures.

c) A metal DC conductivity increases slightly with decreasing temperature [96].

One of the first characteristics of CV of a CP film that one searches for is the dependence of the peak current (I_p) on the scan rate (υ). According to well established electrochemical treatments, for a behavior dominated by diffusion effects, I_p is proportional to $\upsilon^{1/2}$, whilst for a material localized on an electrode surface, such as CP film, I_p is proportional to υ. For most CP films the latter case obtains, thus indicating surface localized electroactive species. As more detailed analysis shows, however, this is so only for CP films that are not inordinately thick, not inordinately compact and not doped with very large dopant, ions which have inordinately small diffusion coefficients. If any of the latter conditions prevail, however i.e., wherever dopant diffusion effects can predominate I_p can be proportional to $\upsilon^{1/2}$, as in the case of copolymer.

2.7 Electrochemical Impedance Spectroscopy (EIS)

Electrochemical Impedance Spectroscopy (EIS) is a powerful tool to investigate chemical and physical processes at liquid/solid interfaces. EIS is becoming increasingly popular for a number of applications such as: characterisation of batteries, fuel cells, organic coatings, ceramics, semiconductors, sensors, and conducting polymers as well as for corrosion studies [97-98].

In dc theory, the applied potential E (Volt) is related to the current I (Ampere) by Ohm's law defining the resistance R (Ohm):

$$E=I.R \qquad \textbf{(2.3)}$$

In ac theory, in the analogous equation of R the impedance Z is defined:

$$E=I.Z \qquad \textbf{(2.4)}$$

Figure 2.15 shows the relationship between current and voltage in impedance measurements.

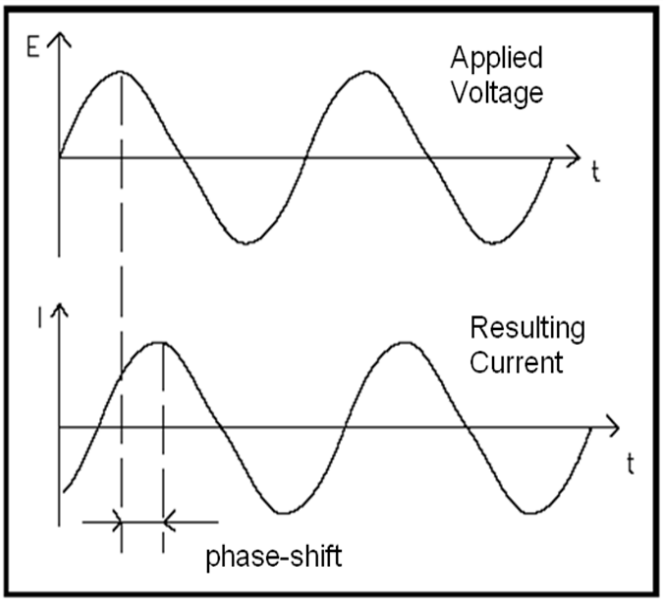

Figure 2.15: Relationship between current and voltage in impedance measurements.

In an EIS measurement, a small excitation signal is applied and electrochemical impedance response is measured. In a linear system, the current response to a sinusoidal potential will be a sinusoid at the same frequency but shifted in phase. The excitation signal that is applied to the cell has the form:

$$E(t) = E_o \sin(\omega t) \quad \textbf{(2.5)}$$

E(t) is the potential at time t_r E_o is the amplitude of the signal, and ω is the radial frequency. The relationship between radial frequency ω (expressed in radians/second) and frequency f (expressed in hertz) is:

$$\omega = 2\pi f \quad \textbf{(2.6)}$$

For the linear system, the resulting current is given by the equation:

$$I_t = I_o \sin(\omega t + \varphi) \quad \textbf{(2.7)}$$

Here φ is the phase difference between the voltage and the current

The perturbation potential and the current respond can be written as complex function:

$$E_t = E_o \exp(j\omega t) \quad \textbf{(2.8)}$$

$$I_t = I_o \exp(j\omega t - \varphi) \quad \textbf{(2.9)}$$

The impedance is defined as the ratio between potential and current:

$$Z = \frac{E}{I} = Zo\exp(j\phi) = Zo(\cos\phi + j\sin\phi) \quad \textbf{(2.10)}$$

In the complex plane the impedance of a single frequency can be represented by a vector of length with argument φ (angle between the real axis of the impedance Z' and the vector). Z'' is the imaginary part of the impedance.

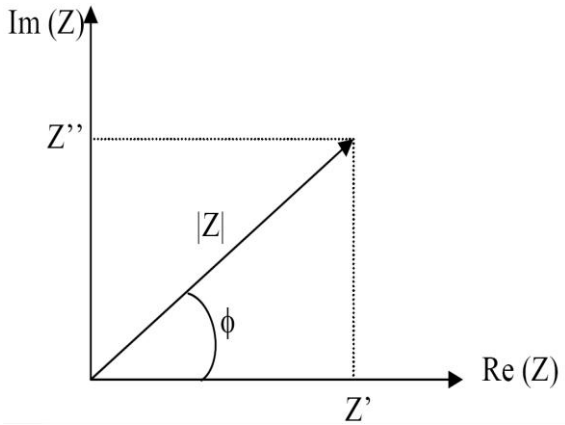

The |Z| and φ are related to Z' and Z'' by the equation:

$$|Z| = \sqrt{Z'^{2} + Z''^{2}} \quad \textbf{(2.11)}$$

And the phase angle is defined:

$$\tan\varphi = \frac{Z''}{Z'} \quad \textbf{(2.12)}$$

Impedance data is typically represented in two types of plots: the Nyquist Plot and the Bode Plots.

The Nyquist Plot, where the X-axis represents the real part and the Y-axis represents the imaginary part of the complex number. In the case of plotting impedance data, the positive Y-axis conventionally represents the negative imaginary portion of the impedance and there is a complex impedance point for every frequency at which the impedance was measured, creating a plot with impedance features.

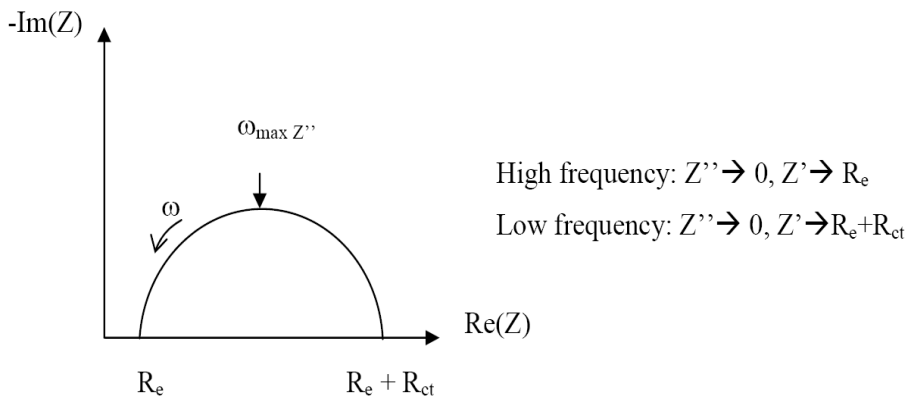

Figure 2.16: Nyquist plot of the impedance of a simple electrode reaction.

The Nyquist plot of the impedance of the simple electrode reaction is a semicircle (Figure 2.16). The intercept of the plot with the axis (high frequency) is R_e. The other intercept at low frequency is the sum of R_e and R_{ct}. The Nyquist plot has some advantages and disadvantages.

Advantages:

- A simple representation of the R_e.
- The shape of plot does not change when the ohmic resistance is changed.
- A simple representation of the charge transfer resistance as diameter of the semi circle.

Disadvantages:

- Indirect representation on frequency.

The Bode Plot consists of two graphs. Impedance Z and phase angle φ are presented as a function of frequency (in logarithmic form). The R_e and $R_e + R_{ct}$ value can be taken from the value of |Z| for ω→∞ and ω→0. At intermediate frequencies, the plot of logZ should be a straight line with slope –1. Extrapolating this line to ω →1 gives the value of $1/C_{dl}$.

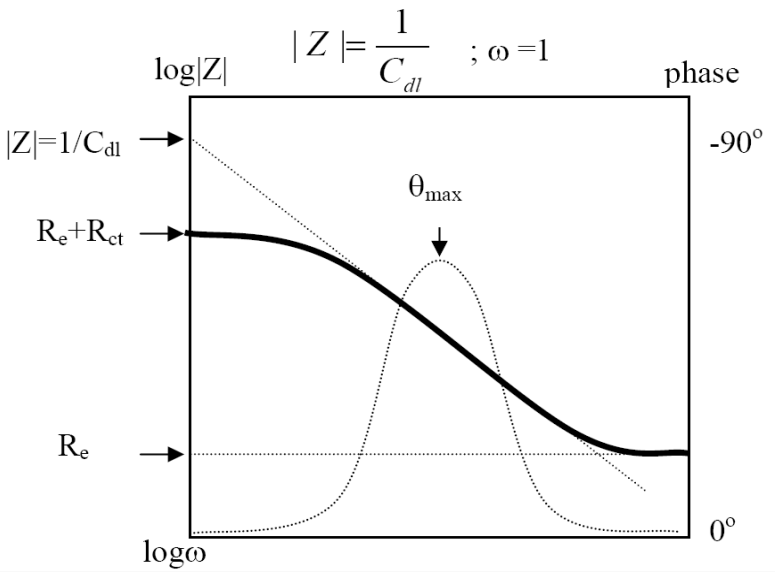

Figure 2.17: Bode plot for a simple electrochemical system (impedance - solid line, phase angle - dotted line).

The phase angle is nearly zero for ω→∞ and ω→1. It has the maximum for medium frequencies. The Bode plot provides a clear description of the frequency-dependence of the electrochemical parameters.

2.8 Equivalent Circuit Modelling (ECM)

In EIS, impedance is measured for a number of frequencies that span a range from few milli hertz to 100 kilohertz, and the result is a complex number. To make use of the complex numbers that are obtained from EIS measurement, can be represented by electrical equivalent circuits, the system under test is modeled as a collection of electronic components such as resistors and capacitors. As shown in Figure 2.18.

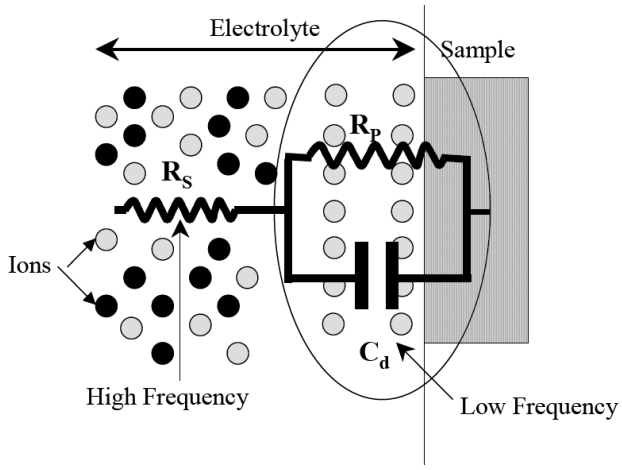

Figure 2.18: Electrical Circuit (Randles Circuit).

The nature of these models involves a number of these components and the ways in which they are connected. The commonly used circuit elements are resistor, capacitors, and inductors. The circuit elements and their impedance response are tabulated in Table 2.1. The impedance of the resistor is independent of the frequency and has only real component. Since there is no imaginary impedance, the current through the resistor is always in phase with the voltage.

Table 2.1: Electrical elements and their impedance response.

Component	Current Vs.Voltage	Impedance
resistor	E = IR	Z = R
inductor	E = L di/dt	Z = jwL
capacitor	I = C dE/dt	Z = 1/jwC

From the table C and L are defined as capacitance and inductance. The impedance of the capacitor does not have a real component and its imaginary component is a function of frequency, where $\omega = 2\pi f$ (ω = angular frequency and f, is the frequency). In a capacitor impedance decreases with the increase in the frequency. The current through a capacitor is phase shifted –90 degrees with respect to the voltage, with current leading the voltage. Since the impedance of the capacitor varies inversely with the frequency, $Z=(j\omega C)^{-1}$, at high frequencies a capacitor acts as a short circuit: its impedance approaches zero. At low frequencies, a capacitor acts as an open circuit, and the impedance approaches infinity.

The impedance versus frequency behavior for an inductor is opposite to that of a capacitor. Inductors have only imaginary impedance component and the current through the inductor is always 90 degrees out of phase with respect to the voltage. As the frequency increases, the impedance of an inductor increases. It acts as a short circuit (i.e., zero impedance) at infinitely low frequencies and has infinite impedance at very high frequencies.

The complex electrical circuits that are used to model the given system will usually comprise of serial and parallel combinations of simple elements like the resistors, capacitors and inductors; the impedance values of the individual components can be combined according to some simple rules governing the system impedance for circuit elements both in parallel and series combinations. For linear impedance elements in series, we can calculate the equivalent impedance from:

$$Z_{eq} = Z_1+Z_2+Z_3 \qquad \textbf{(2.13)}$$

where Z_1, Z_2, Z_3 are the impedance of the elements (resistor or capacitor or inductor). For linear impedance elements in parallel, we can calculate the equivalent impedance from:

$$\frac{1}{Z_{eq}} = \frac{1}{Z_1} + \frac{1}{Z_2} + \frac{1}{Z_3} \qquad \textbf{(2.14)}$$

2.8.1 Equivalent circuit elements

Equivalent circuit models employ mathematical or computer models of fundamental electric circuit components, such as resistors and capacitors, to model complex electrochemical processes. Simple equivalent circuits have long been used to predict the performance characteristics of porous electrodes.

These equivalent circuits primarily have been applied to attempt to capture the behavior of the double-layer at the interface between the electrode pores and electrolyte solution.

Note that, circuits could be used to model a pseudocapacitor model proposes that, because of unique electrosorption bahaior found in micropores, the capacitance per micropore surface area and capacitance per external surface area must be calculated separately. The second model, which is now widely accepted, suggests that electrolyte ions cannot diffuse into pores beneath a size treshold and therefore the surface area of those pores cannot contribute to the capacitance. In considering the second model, there have been efforts to determine the optimal pore size and size distribution needed to maximize ion accessability. As a corollary result, an inverse relationship between pore size and ESR has also been demostrated.

Table 2.2: Circuit elements used in the models.

Equivalent element	Admittance	Impedance
R	1/R	JωC
C	jωC	1/jωC
L	1/jωL	jwL
W(Infinite)	$Yo\sqrt{(j\omega)}$	$1/Yo\sqrt{(j\omega)}$
O (Finite)	$\left[Yo\sqrt{(j\omega)}\right]\coth(B\sqrt{(j\omega)})$	$Tanh(B\sqrt{(j\omega)}/\left[Yo\sqrt{(j\omega)}\right]$
Q(CPE)	$Yo(j\omega)\alpha$	$1/Yo(j\omega)\alpha$

Looking at the electrode/polymer/electrolyte system from the viewpoint of the impedance characteristics, at variance with an electrified membrane inside an electrolytic solution, it constitutes a so-called ‘asymmetrical’ configuration [82], the current flow requiring the transport of electrons across the metal/polymer interface and of ions through the polymer/electrolyte interface; the charge percola tion inside the polymer bulk should be additionally considered.

The generalised transmission line circuit model predicts the relevant impedance features of such a system in terms of a Nyquist plot, based on a mathematical approach. The two semi-circles at the highest frequencies, induced by the processes at the metal/polymer and polymer/solution interfaces, are, in practice, not always detectable. Sometimes, only one or even one-half semi-circle is observed; at other times, these two semi-circles are partially overlapped to each other, the actual situation observed depending on the characteristics of the interfacial processes in terms of energy (resistance) to overcome at the relevant interface.

Moreover these semi-circles are very often depressed, most probably due to non-homogeneous separation surfaces [99]. Furthermore, they can also overlap to the mid-frequency Warburg impedance quasi-45°-slope segment that reflects the diffusion-migration of ions at the boundary surface between solution and polymer, inside the latter medium. Finally, 90°-trend at the lowest frequencies, due to a capacitive impedance, accounts for the charge transport process inside the bulk of the film.

An ionic conductivity often constitutes the slow step in the overall charge percolation process through the CP-modified electrode system [100]. When the ionic conductivity is definetely very low, so that a very thin diffusion layer accounts for the transport of ions inside the polymer, the generalised transmission line-circuit can be considered infinitely extended, simulating a semi-infinite diffusion-migration, the boundary surface being the polymer/solution one.

Therefore, the trend attributable to a Warburg impedance extends so much down to low frequencies that the capacitive impedance 90°-slope trend may not be observed. In this case the generalised transmission line circuit can be simplified into the classical Randless circuit.

On the opposite side, when the ionic conductivity is relatively high, the impedance value of the polymer bulk is correspondingly low, both ions being present in the bulk of the permselective polymer. The study of this situation for the case of polypyrrole, carried out by Duffit and Pickup [101-102], has led the authors to define a condition they call ‘enhanced ionic conductivity’: for polypyrrole, electrolyte concentrations as high as 3 M are proposed.

For intermediate situations the whole generalised transmission line circuit has to be considered. In the impedance plot of such a circuit the presence of an additional semi-circle at the highest frequencies is also predictable, which is described to the impedance of the polymer bulk but cannot, however, be generally observed using instrumentation with non-extraordinary performances. If one is mainly interested in the study of ionic conductivity, the generalised transmission line circuit can then be simplified into the circuit proposed by Albery and Mount [103].

Electrolyte Resistance: Solution resistance is often a significant factor in the impedance of an electrochemical cell. A modern three electrode potentiostat compensates for the solution resistance between the counter and reference electrodes.

The resistance of an ionic solution depends on the ionic concentrations, type of ions, temperature and the geometry of the area in which current is carried. In a bounded are with area A and length l carriying a uniform current the resistance is defined as:

$$R=\rho.\ 1/A \qquad \textbf{(2.15)}$$

In this equation R is the solution resistivity. The conductivity of the solution, k, is more commonly used in solution resistance calculations. Its relationship with solution resistance is:

$$R=1/k.A \text{ as a result } k=1/R.A \qquad \textbf{(2.16)}$$

For other solutions, k was calculated from specific ion conductance. The units for k are Siemens per meter (S/m). The siemens is the reciprocal of the ohm, so S=1/Ohm. The value of the double layer capacitance depends on many variables including electrode potential, temperature, ionic concentrations, types of anions, oxide layers, electrode roughness, impurity adsorption, etc.

Double Layer Capacitance (C_{dl}): An electric double layer exists at the interface between an electrode and its surrounding electrolyte. This double layer is formed as ions from the solution stick on the electrode surface. Charges in the electrode are separated from the charges of these ions. The separation is very small, on the order of angstroms.

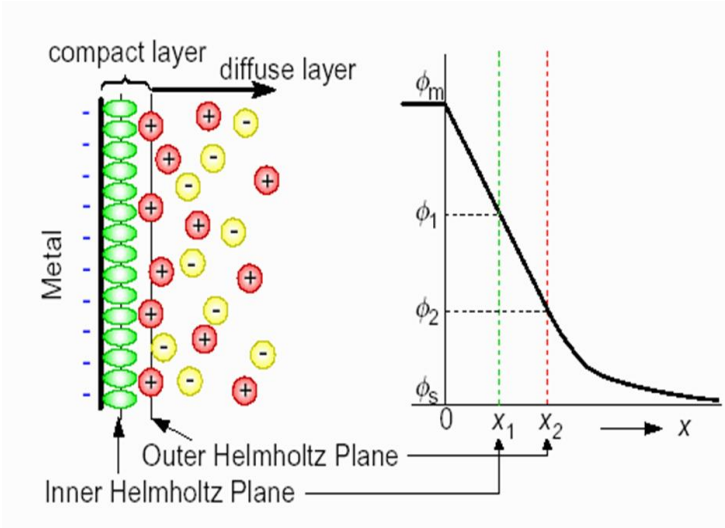

Figure 2.19: Scheme of the electrical double layer, IHP: Inner Helmholtz Plane, OHP: Outer Helmholtz Plane.

The main feature of the double layer region concerns the molecular and ionic populations three-dimensionally distributed near the metal surface. In a first approximation this region has been described by Helmholtz as being equivalent to a parallel plate capacitor, where one plate is the metal surface and the other plate is composed by solvated ions present in the electrolyte. In this case, the first layer in contact with the electrode surface is composed by orientated water dipole molecules and by ions specifically adsorbed (independent of the electrode potential). The imaginary plane crossing the radius of the specific adsorbed ions is termed inner Helmholtz plane (IHP). Next to the IHP, the ions become solvated and the imaginary plane cross the centre of these solvated ions. The position of these ions defines the outer Helmholtz plane (OHP). The two regions confined by the IHP and the OHP are two-dimensional (internal layer) whereas the region comprised between the OHP and the end of the double layer is a three-dimensional one dominated by thermal interactions of the species called diffuse layer as schematically given in Figure 2.19.

Charge Transfer (Polarization) Resistance: Whenever the potential of electrode is forced away from its value at open circuit, is referred to as polarizing the electrode. When an electrode is polarized, it can cause current to flow via electrochemical reactions that occur at the electrode surface. The amount of current is controlled by the kinetics of the reactions and the diffusion of reactants both towards and away from the electrode.

In cells where an electrode undergoes uniform corrosion at open circuit, the open circuit potential is controlled by the equilibrium between two different electrochemical reactions. One of the reactions generates cathodic current and the other anodic current. The open circuit potential ends up at the poteantial where the cathodic and anodic currents are equal each others. It is referred to as a mixed potential. The value of the current for either of the rections is known as the corrosion current, a new parameter, R_p, the polarization resistance.

Diffusion: Diffusion can create impedance known as the Warburg impedance. This impedance depends on the frequency of the potential perturbation. At high frequencies the Warburg impedances small since diffusing reactants don't have to move very far. At low frequencies the reactants have to diffuse further, thereby increasing the Warburg impedance. The equation for the infinite Warburg impedance is:

$$Z=\sigma\ (w)^{-1/2}(1-j) \qquad \textbf{(2.17)}$$

On a Nyquist plot the infinite Warburg impedance appears as a diagonal line with a slope of 0.5. On a Bode plot, the Warburg impedance exhibits a phase shift of 45°.

Constant Phase Element: Capacitors in EIS experiments often do not behave ideally. Instead, they act like a constant phase element (CPE) as defined below. The impedance of a capacitor has the form:

$$Z=A(j.w)^{-a} \qquad \textbf{(2.18)}$$

When this equation describes a capacitor, the constant A=1/C (the inverse of the capacitance) and the exponent a=1. For a constant phase element, the exponent a is less than one. The double layer capacitor on real cells often behaves like a CPE instead of resembling a capacitor. Several theories have ben proposed to account for the non-ideal behavior of the double layer but none has been universally accepted.

2.9 Carbon Fiber Micro Electrodes

Carbon due to different allotropes (graphite, diamond, ly.fullerens / nanotubes), various microtextures (more or less ordered) owing to the degree of graphitization, a rich variety of dimensionality from 0 to 3D and ability for existence under different forms (from powders to fibers, foams, fabrics and composites) represents a very attractive material for electrochemical applications , especially for storage of energy. Carbon electrode is well polarizable; however, its electrical conductivity strongly depends on the thermal teatment, microtexture, hybridization and content of heteroatoms. Additionally, the amphoteric character of carbon allows use of the rich electrochemical properties of this element from donor to acceptor state. Apart from it, carbon materials are environmentally friendly. During the last years a great interest has been focused on the application of carbons as electrode materials because of their accessability and easy processability and relatively low cost. They are chemically stable in different solutions (from strongly acidic to basic) and able for performance in a wide range of temperatures. Already well-established chemical and physical methods of activation allow producing materials with a developed surface area and controlled distribution of pores that determine the electrode / electrolyte interface for electrochemical applications. The possibility of using the activated carbon without binding substance, e.g., fibrous fabrics or felts, gives an additional profit from construction point of view.

As the technology of textile reinforced composites expanded, a growing demand from the aerospace industry for composite materials with superior properties emerged. In particular, materials with higher specific strength, higher specific modulus and low density were required. Other desirable properties were good fatigue resistance and dimensional stability.

Electropolymerization on carbon fiber microelectrode (CFME) can improve the interfacial properties between the carbon fiber and polymeric matrix. Generally electrocoating of conjugated polymers or copolymers on carbon fiber easily allows the characterization of the deposited films by spectroscopic, morphological and electrochemical techniques. Conducting polymers which were coated electrochemically on CFMEs were studied in detail [104-106].

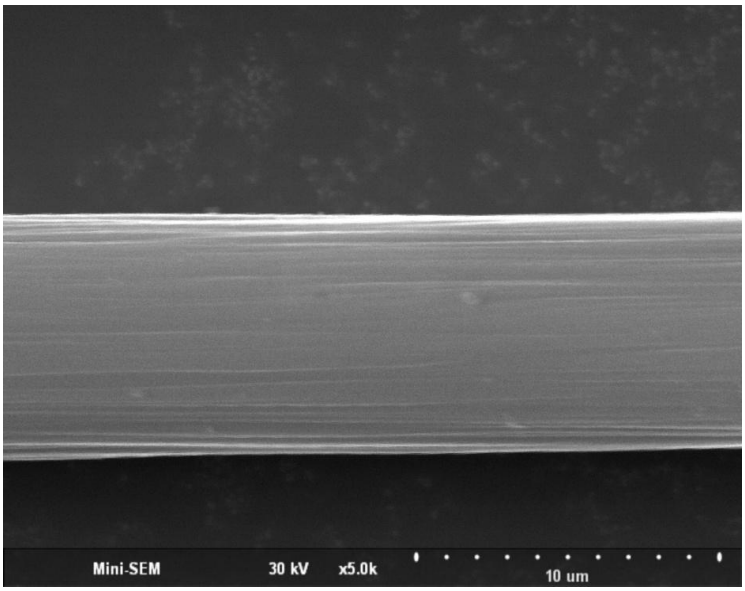

Figure 2.20: SEM image of single carbon fiber microelectrode (SCFME).

Polymer coated carbon fiber microelectrodes (CFMEs) have been used in the detection of biologically important analysts such as dopamine [107-108], and micron-sized reversible conductive polymer electrodes and actuators [109]. The fibers are stable and readily available from a number of commercial sources. The disposable character of these electrodes has opened up a wide range of possible applications, for example in the determination of enzyme substrates [110], neurotransmitters [111], proteins [112] and other redox species [113-114].

2.10 Biosensors

Rapid, reliable, low cost, and in some cases, continuous measurement of analytes has been a major goal in analytical sciences. Since biosensors offer many advantages over conventional analytical techniques in terms of simplicity, detection limit, specificity and sensitivity, the development of biosensors for analytical purposes has attracted a great deal of interest in recent years. Biosensors have widespread applications in medical analysis; environmental monitoring and industrial process control [115-116].

Biosensors are devices, ideally small and portable, that allow the selective quantitation of chemical and biochemical analytes. They consist of two components: the transducer and the chemical recognition element. Chemical recognition is accomplished by exploiting the natural selectivity of biochemical species such as enzymes, antibodies, chemoreceptors, and nucleic acids. In the presence of the analyte, these agents, immobilized at the surface of the transducer, cause a change in a measurable property in the local environment near the transducer surface. The transducer monitors this property, and converts the chemical recognition event into a measurable electronic signal [117-118].

2.10.1 Electrochemical biosensors

Biosensors are classified and evaluated on the basis of design and functional characteristics such as sensitivity, cost, selectivity, versatility, range, availability, future adaptability and simplicity. On these bases, electrochemical biosensors are favoured over optical sensors mainly because of cost and availability, while piezoelectric and thermal sensors are fairly poorly rated on all characteristics [119].

The biochemical transducer or biocomponent imparts to the biosensor, selectivity or specificity. A transducer converts the biochemical signal to an electronic signal. The transducer of an electrical device responds in a way that a signal can be electronically amplified, stored and displayed. Suitable transducing system can be adapted in a sensor assembly depending on the nature of the biochemical interaction with the species of interest.

Amperometric enzyme biosensors operate at a fixed potential with respect to a reference electrode, while the measured signal is the working electrode current generated by the oxidation or reduction of electroactive species at its surface.

Immobilized antibodies can also be used as highly selective reagents in biosensors. Unlike the enzyme-based biosensors where either the co-substrate or the product of an enzyme reaction is monitored, antibody-based biosensors detect antigen or antibody concentration either by direct changes in the transducer output resulting from the binding event, or by means of indirect competitive and displacement reactions using optical, piezoelectric, or electrochemical techniques. Nevertheless, the majority of the reported antibody-based biosensors (immunosensors) makes use of irreversible binding chemistry; these biosensors are therefore not reusable and thus

expensive. Depending upon the electrochemical property to be measured, electrochemical biosensors can be further divided into conductimetric, potentiometric and amperometric biosensors. Conductimetric biosensors measure the changes in conductance/impedance of a solution as consequence of the biological component using noble metal electrodes [120]. If the biocatalyst produces ionic products, or consumes ions, and the support solution has low electrical conductivity, this is often a convenient and simple technique. A deoxyribonucleic acid (DNA) biosensor using Faradic impedance spectroscopy based on use of biotinylated oligonucleotide and avidin-HRP (horseradish peroxidase) conjugate has been described [121].

Potentiometric biosensors measure the potential difference between the working electrode and a reference electrode under conditions of zero current flow [122]. The potential generated is directly proportional to the logarithm of the concentration of an ion in an ideal solution. The basis of this type of biosensor is the Nernst equation, which relates the electrode potential (E) to the concentration of the oxidized and reduced species. For the reaction:, the Nernst equation can be described as the following,

$$E= E^0 +RT/nF\ [ln\ ([C_A]^a / [C_B]^b\ )] \qquad \textbf{(2.19)}$$

where is the standard redox potential, R is the gas constant, T is the absolute temperature, F is the Faraday constant, n is the number of exchanged electrons in the reaction, and, C_A and C_B are the concentration of oxidized and reduced species, respectively. A potentiometric urease-based biosensor for detection of heavy metal ions has been reported [123].

Amperometric biosensors measure the currents resulting from the electrochemical oxidation or reduction of an electroactive species under a constant potential applied to working electrodes. The most important of these is the glucose biosensor, which has been successfully commercialized for blood glucose monitoring in diabetics [124]. Other examples of enzyme-based amperometric biosensors include the phenol sensors, which utilize cellobiose dehydrogenase (CDH) or glucose dehydrogenase (GDH) [125]; the lactate biosensor, which is based on lactate oxidase immobilized to a conducting copolymer through glutaraldehyde [126]; and the alcohol biosensor, which is based on peroxidase and alcohol oxidase [127]. Most of the electrochemical immunosensors are based on enzyme-linked immunosorbent assay principles, with sensor-immobilized antibodies or antigens where the enzyme label such as

peroxidase, alkaline phosphatase or GOx, is indicated amperometrically by measuring the produced iodine, p-aminophenol or hydrogen peroxide, respectively [128-130].

2.10.2 Dopamine sensors

In particular, there has been much interest in the development of electrochemical sensors. This is because DA is electroactive and thus the oxidation of DA can be followed using electrochemical techniques. Electrochemical sensors are usually inexpensive to manufacture, highly sensitive and easy to employ. Furthermore, the electrodes used in the sensing can be miniaturised and conveniently placed in the living organism for real time analysis. This is not possible with non-electrochemical techniques. The electrochemical oxidation of DA occurs via an ECE mechanism [131, 132], Figure 2.21.

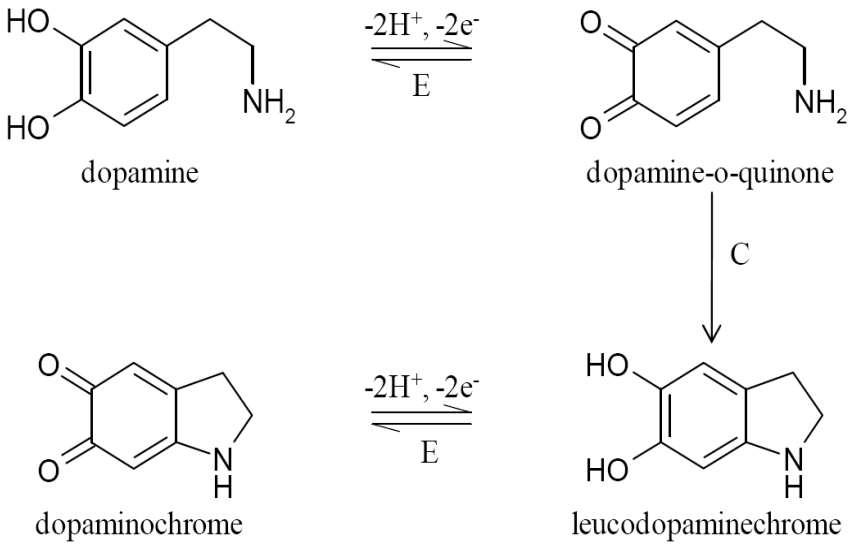

Figure 2.21: The ECE mechanism for DA oxidation.

A two electron exchange results in the formation of dopamine-o-quinone. This molecule can then undergo an intermolecular addition, which results in a cyclisation reaction generating leucodopaminechrome which, in turn, is oxidised further via another two electron transfer to dopaminochrome. In this scheme, ‘E’ denotes the electrochemical reactions and ‘C’ denotes the chemical reactions.

Monitoring the concentration of DA is particularly challenging using electrochemical methods because DA co-exists with many interfering compounds in biological samples. These interfering compounds are usually present at concentrations much

higher than DA and, moreover, they are oxidised at similar potentials to DA at most solid electrodes. This is particularly true of ascorbic acid (AA), the main interfering compound in the determination of DA. Consequently, modified electrodes have been employed for the determination of DA. The most popular strategies include polymer modified electrodes [133], self-assembled monolayer modified electrodes [134] and surfactant modified electrodes [135].

2.11 Characterizations

2.11.1 Attenuated total reflection Fourier transform infrared spectroscopy (FTIR-ATR)

FTIR is a fundamental tool that is used to probe substances to determine the nature of their molecular bonds. FTIR has commonly been used for the identification of functional groups among organic molecules. It can often easily distinguish between a variety of molecular bonds involving carbon, hydrogen, nitrogen, oxygen, phosphorus, sulfur, and halogens. There are many methods available for infrared spectroscopy. Traditionally, FTIR is used with a transmission cell or a KBr pellet. However, in the surface science community, infrared spectroscopy is used in a different manner.

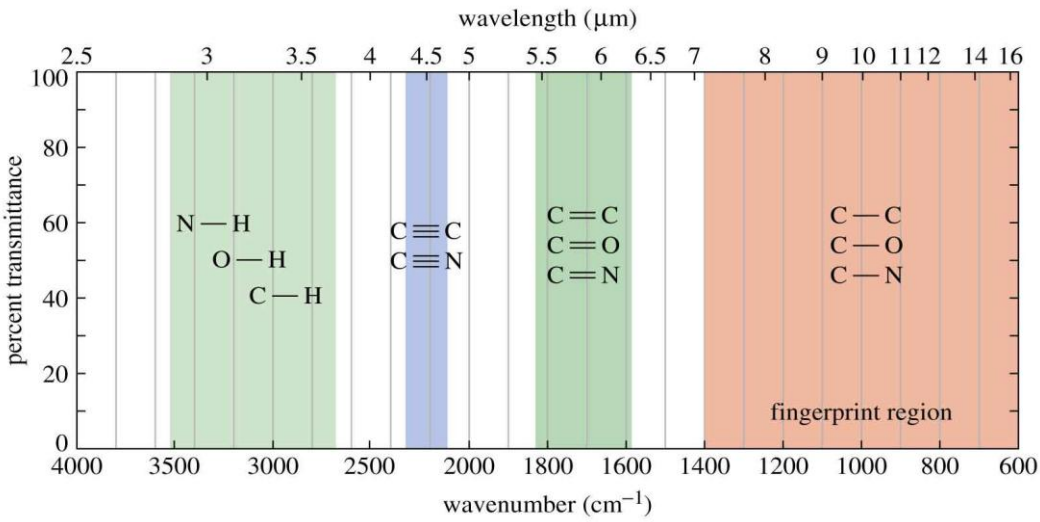

Figure 2.22: Infrared spectrum bands for general subtitutions.

Attenuated Total Reflection (ATR) is an accessory of transmission IR spectrometers that significantly enhances surface sensitivity. As the name implies, ATR refers to a

particular type of reflection geometry. In contrast to transmission FTIR, in which the infrared beam travels in a straight path through a sample, in ATR, the infrared beam is reflected internally through a crystal. The beam is oriented to bounce within the crystal at an angle that ensures total internal reflection. Just above each point of reflection exists an evanescent wave that can probe substances within about a micrometer of the crystal surface (Figure 2.23).

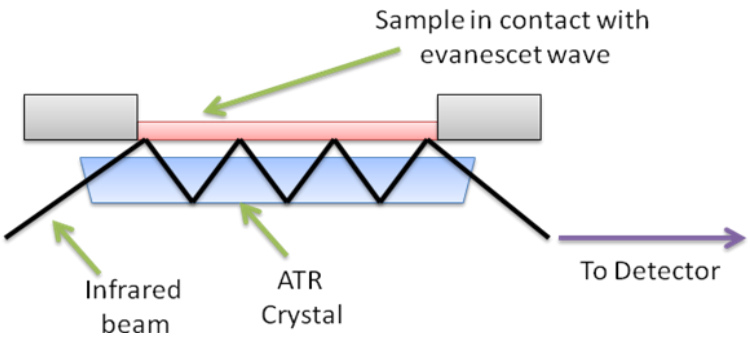

Figure 2.23: A multiple reflection ATR system.

2.11.2 Scanning electron microscopy (SEM)

SEM is a method for high-resolution imaging of surfaces. The SEM uses electrons for imaging, like a light microscope which uses visible light. A finely focused electron beam scanned across the surface of the sample generates secondary electrons, backscattered electrons, and characteristic X-rays. These signals are collected by detectors to form images of the sample displayed on a cathode array tube screen. SEM typically is used for conductive samples. Scanning electron microscopy is one of the most widely used techniques in nanomaterials characterization. This method usually is applied to get information about the grain size, surface roughness, porosity, particle size distributions, material homogeneity, and intermetallic distribution and diffusion. The electron beam, which typically has an energy ranging from a few hundred eV to 50 keV, is focused by one or two condenser lenses into a beam with a very fine focal spot sized 1 nm to 5 nm. The beam passes through pairs of scanning coils in the objective lens, which deflect the beam in a raster fashion over a rectangular area of the sample surface. Through these scattering events, the primary electron beam effectively spreads and fills to teardrop-shaped volume, known as the interaction volume, extending from less than 100 nm to around 5μm into the surface.

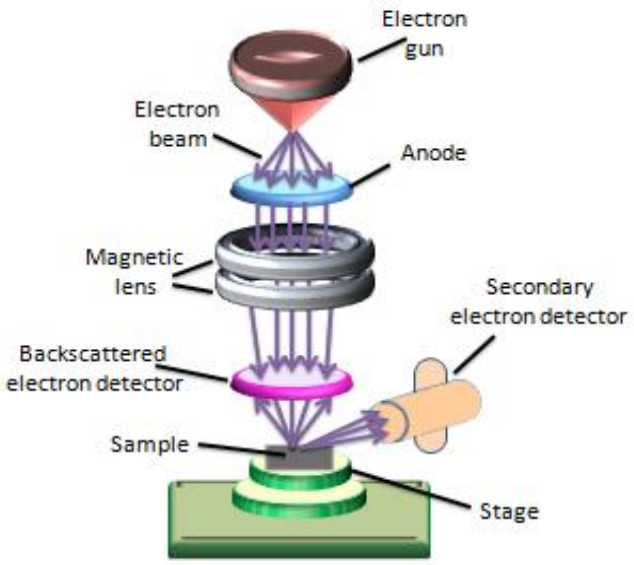

Figure 2.24: Schematic diagram of scanning electron microscopy.

Interactions in this region lead to the subsequent emission of electrons which are then detected to produce an image. X-rays, which are also produced by the interaction of electrons with the sample, may also be detected in an SEM equipped for energy-dispersive X-ray spectroscopy or wavelength dispersive X-ray spectroscopy.

2.11.3 Atomic force microscopy (AFM)

AFM is one of the most powerful tools for determining the surface topography of native biomolecules at subnanometer resolution. The technique involves imaging a sample through the use of a probe, or tip, with a radius of 20 nm. The tip is held several nanometers above the surface using a feedback mechanism that measures surface–tip interactions on the scale of nanoNewtons. Variations in tip height are recorded while the tip is scanned repeatedly across the sample, producing a topographic image of the surface. Atomic force microscope is capable to produce images in different modes including tapping, magnetic force, electrical force, and pulsed force.

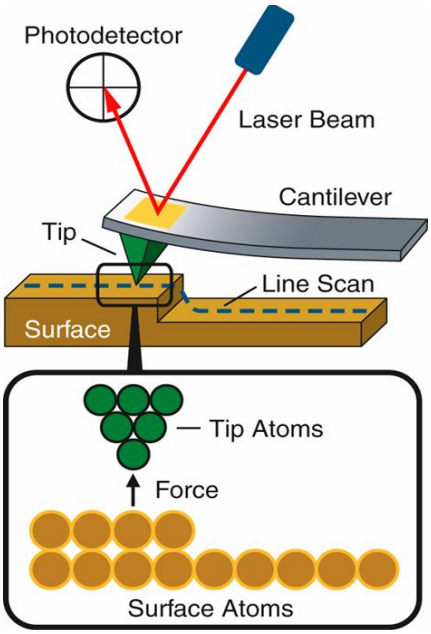

Figure 2.25: Schematic diagram of atomic force microscope.

AFM works by bringing a cantilever tip in contact with the surface to be imaged. An ionic repulsive force from the surface applied to the tip bends the cantilever upwards. The amount of bending, measured by a laser spot reflected on to a split photo detector, can be used to calculate the force. By keeping the force constant while scanning the tip across the surface, the vertical movement of the tip follows the surface profile and is recorded as the surface topography by the AFM.

3. EXPRIMENTAL

3.1 Chemicals

3,4-Propylenedioxythiophene (ProDOT) monomer and N-phenylsulfonyl pyrrole (PSP) monomer were purchased from Sigma-Aldrich and used as received. Electrochemical polymerizations (electrocoatings) were performed in acetonitrile (ACN, Merck) containing $NaClO_4$ (Sigma-Aldrich) at the same scan rate (30mV/s) and deposition cycle numbers (10 cycles) (applied charges). Buffer solution (Potassium dihydrogen phosphate-di-Sodium hydrogen phosphate / Carlo Erba), Dopamine (Sigma-Aldrich) and Ascorbic acid (Lancaster) were purchased and used without any further purification.

3.2 Electrocopolymerizations

Electrocopolymerizations by cyclic voltammetry were performed using a Princeton Research Potentiostat (model 2263) potentiostat/galvanostat, interfaced to a PC computer with Power Suite Software package. The potentiostat was also connected to a Faraday cage (BAS Cell Stand C3). A three electrode system, employing carbon fiber as working electrode, Pt button as counter electrode and Ag button as a reference electrode, was used.

3.3 Electrode Preperations

SGL SIGRAFIL C 320B (A carbon fiber with high strength, high modulus of elasticity, and high electric conductivity, manufactured by SGL Carbon Group) containing single filaments in a roving was used as the working electrode. Fabrication of all single carbon fiber micro electrodes (SCFMEs) was carried out as follows. A single carbon fiber SGL SIGRAFIL HM485 (~ 7µm in diameter, approx. 4 cm in length) was inserted on a 5 cm long teflon tape, while 2.5 cm of the fiber was kept out. A filament of carbon fibers with a length of 8 cm (approximately 25 fibers) were sticked on the single carbon fiber for providing connections and electrical

conductivity. A second teflon tape with the same length was mounted and wrapped around the composition. Silver paste was used on carbon fiber filament to improve conductivity.

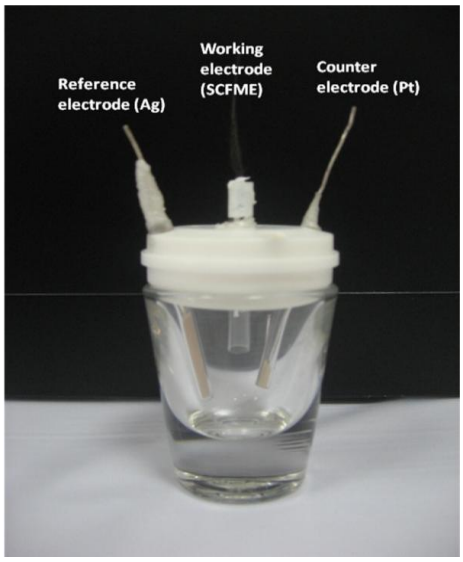

Figure 3.1: A geometry of one compartment-3 electrode cell.

The electrode area was kept constant ~ $2x10^{-3}$ cm^2 by adjusting the dipping length (~ 1cm). The button electrodes were prepared by using Ag and Pt wires in glass capillary (~4.45 mm diameter) filled with methylmetacrylate (MMA), electrodes were then polymerized by UV light, which was inert against the electrolyte solution. The surface area of the reference and the counter electrodes were kept constant (~ 0.47 mm^2) during the experiments.

3.4 Electrochemical Impedance Spectroscopy (EIS) and Equivalent Circuit Modelling (ECM)

EIS measurements were taken at room temperature (~ 25 ^oC) using a conventional three electrode cell configuration. The electrochemical cell was connected to a Potentiostat (PAR 2263) connected to a PC. An electrochemical impedance software, PowerSine, was used to carry out impedance measurements between 10 mHz and 100 kHz, with an applied AC signal amplitude of 10mV. The impedance spectra was analyzed using ZSimpWin V3.10, an AC-impedance data analysis software.

3.5 Fourier Transform Infrared-Attenuated Total Reflectance (FTIR-ATR)

For spectroscopic measurements, Poly(ProDOT-co-PSP) copolymers were synthesized on ITO-PET (NV Innovative Sputtering Technology, PET 175μm,Coating ITO-60) in the potential range from −0.8 to 1.5V at a scan rate of 30 mV/s in 0.1M $NaClO_4$/ACN. Polymer films on ITO-PET were analysed using an ATR-FTIR reflectance spectrometer (Perkin Elmer, Spectrum One, having a universal ATR attachment with a diamond and ZnSe crystal C70951).Perkin Elmer Spectrum software was used to carry out FTIR-ATR measurements between 650-4000cm^{-1}.

3.6 Scanning Electron Microscopy (SEM)

Thin films of copolymers, electrocoated on carbon fibers were analyzed by scanning electron microscopy on a Nanoaye Desktop Mini-SEM Instrument. The excitation energy used 5 keV. Avarage values of the increase in fiber thickness were obtained from SEM images, taking into account the diameter of the ungrafted fiber. The diameters for the fibers were calculated from an average of 5-6 measurements on individual fibers.

3.7 Atomic Force Microscopy (AFM)

Thin film of copolymer, electrocoated on ITO-PET, were analyzed by atomic force microscopy using a Nanosurf Easyscan AFM Instrument with a 10 μm AFM head. The Nanosurf Easyscan 2 software was used to carry out the AFM measurement.

4. RESULTS AND DISCUSSION

4.1 The Experimental Details of Electrochemical Copolymerization of 3,4-Propylene dioxythiophene (ProDOT) and N-Phenylsulfonyl Pyrrole (PSP) on SCFME in Different Mole Fractions of PSP

Synthesis of polymer films on SCFMEs were performed cyclic voltammetrically at normal ambient conditions on 1 cm long dipped into ~5 ml electrolytic solution, using a standart three electrode cell (surface area of working electrode is $2x10^{-3}$ cm^2). Pt and Ag button electrodes were used as counter and pseudo reference electrodes, respectively (each was placed ~ 1 cm distance from each other).

For electrocopolymerization of ProDOT and PSP, 10 mM ProDOT and 5, 10, 20 mM PSP was used. Electrocopolymerizations were performed for the monomers with 0.1 M $NaClO_4$ in ACN at a scan rate of 30 $mV.s^{-1}$ and 10 cycles.

After ProDOT and PSP were electrochemically polymerized on SCFME, the working electrode (modified SCFME) was removed from the cell and then washed throughly with ACN to remove monomer molecules and electrochemical impedance measurements were carried out in the same electrolyte solution.

Finally, modified carbon fibers were characterized in monomer free solutions to find out their redox behavior at different scan rates between 25 $mV.s^{-1}$ and 200 $mV.s^{-1}$ by cyclic voltammetry.

4.2 Electrocopolymerization of ProDOT and PSP

ProDOT and PSP were electrochemically copolymerized on SCFMEs in the potential range from −0.8 to 1.5V at a scan rate of 30 mV/s in 0.1M $NaClO_4$/ACN. The amount of PSP concentration was increased from 5mM to 20mM when ProDOT concentration was held constant (10 mM). Three copolymers with different compositions were synthesized with by using X_{PSP} = [(PSP/ (ProDOT+PSP)] mole fraction [CP1 (0.33), CP2 (0.50), and CP3 (0.66)].

The potential shift to the positive direction with an increase of PSP concentration in the feed indicates that the monomer ratio affects the copolymer composition and its electrochemical properties. The obvious peak potential shift provided information about the increase in the electrical resistance in the copolymer film. As shown at multisweep cyclic voltammograms of ProDOT (10 mM) in the presence of PSP (5; 10; 20 mM); the intensity of the current peaks increased with increase in the number of potential cycle indicating a continuous growth of electroactive copolymer on the electrode (Figure 4.1, Figure 4.2, Figure 4.3).

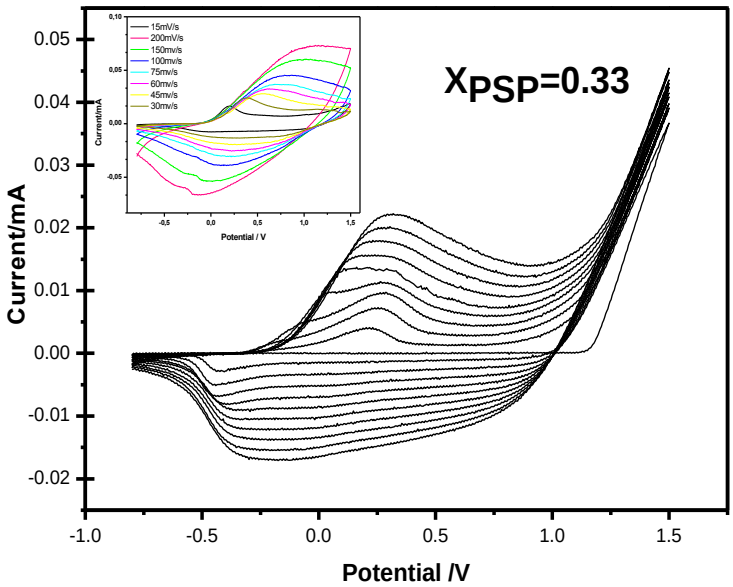

Figure 4.1: Cyclic voltammogram of electrogrowth of 10 mM ProDOT and 5 mM PSP in 0.1 M $NaClO_4$/ACN at 30mV.s^{-1}, 10 cycle on SCFME. Inset: CV of monomer free of Poly(ProDOT-co-PSP) film in 0.1 M $NaClO_4$/ACN at different scan rates between 15 and 200 mV.s^{-1}.

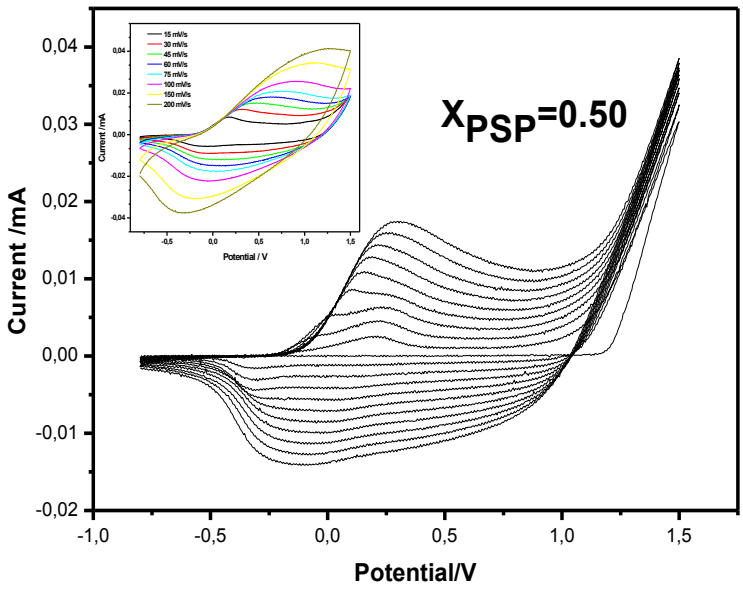

Figure 4.2: Cyclic voltammogram of electrogrowth of 10 mM ProDOT and 10 mM PSP in 0.1 M $NaClO_4$/ACN at 30mV.s^{-1}, 10 cycle on SCFME. Inset: CV of monomer free of Poly(ProDOT-co-PSP) film in 0.1 M $NaClO_4$/ACN at different scan rates between 15 and 200 mV.s^{-1}.

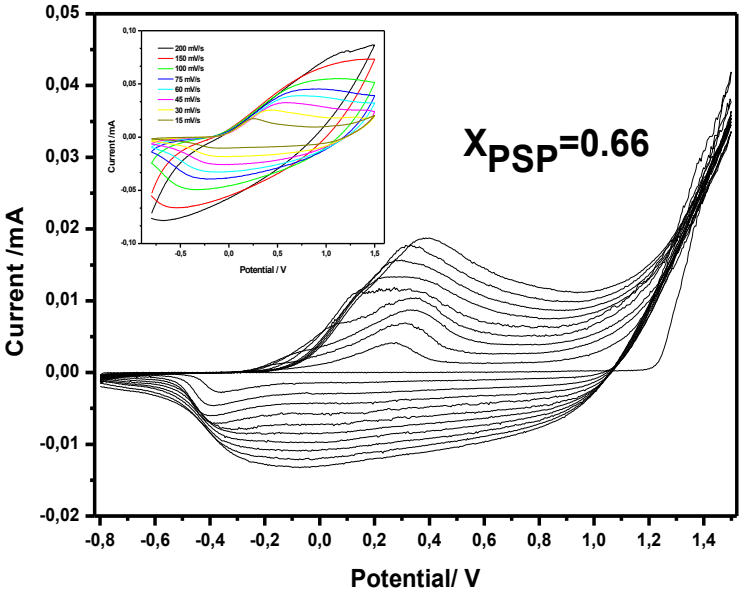

Figure 4.3: Cyclic voltammogram of electrogrowth of 10 mM ProDOT and 20 mM PSP in 0.1 M $NaClO_4$/ACN at 30mV.s^{-1}, 10 cycle on SCFME. Inset: CV of monomer free of Poly(ProDOT-co-PSP) film in 0.1 M $NaClO_4$/ACN at different scan rates between 15 and 200 mV.s^{-1}.

For repeated cycling the cathodic peak current decreases and the anodic one increases until a steady-state pattern. Also the current during the first cycle was quite different from that in the second cycle. After 5 cycles the system has settled down. Results obtained from multiple cycling showed that the first five cycles of the voltammogram were usually in unstable stage. After five cycles, achieve steady state condition (6th cycle) in cyclic voltammetry.

As well known, a copolymerization could be induced by one of the comonomers' radical cation or its oligomer generated on the surface of the working electrode. Therefore, the copolymerization of PSP and ProDOT could be initiated by the radical cations of ProDOT or its oligomer and formed a copolymer under a potential lower than the oxidation onset potential of PSP (Figure 4.4).

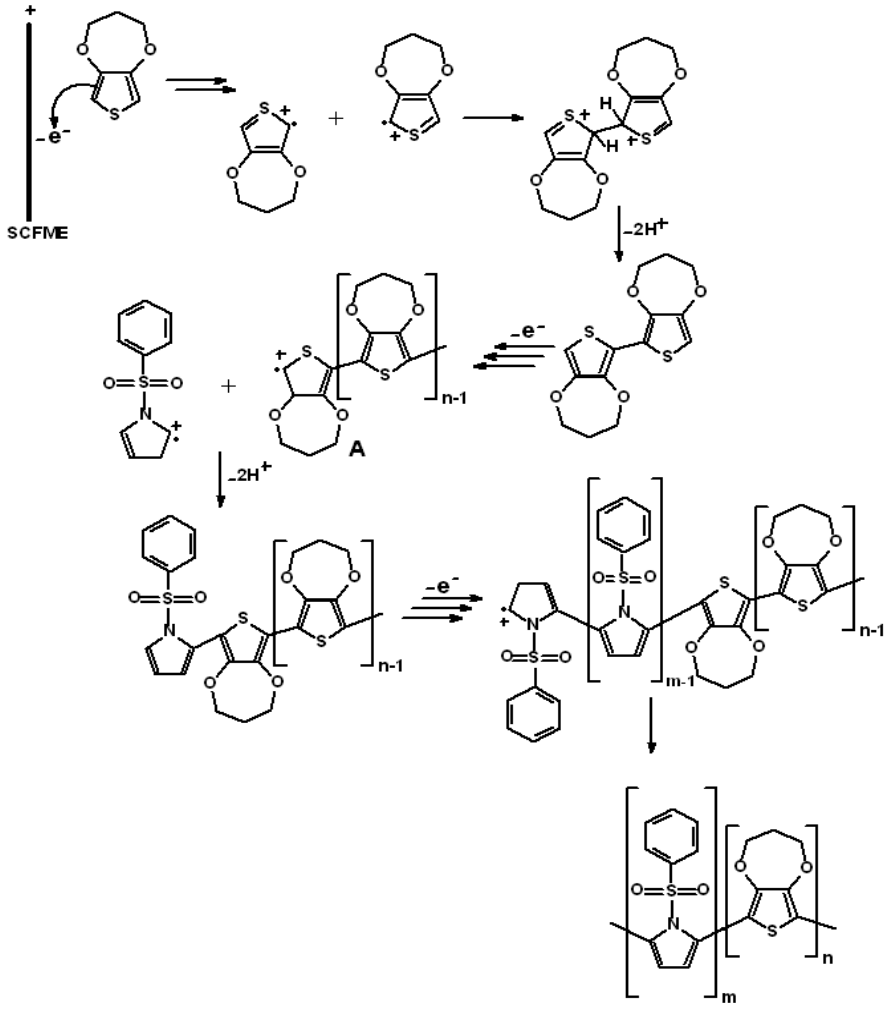

Figure 4.4: Mechanism of electrochemical copolymer formation of ProDOT and PSP on SCFME.

Oxidation potentials (E_{ONSET}) of X_{PSP} = 0.33 and X_{PSP} = 0.50 were obtained as 1.139 V and 1.127 V higher than oxidation potential of X_{PSP} = 0.66 (1.19 V) during the electrogrowth process. This is due to increased PSP concentration in feed ratio. The strong electron–withdrawing sulphonyl group in PSP can be stabilized by using the radical cation intermediates to diffuse away from the electrode and thus inhibiting electropolymerization (Table 4.1). The peak current decreased in direct proportion with decrease of oxidation potential (Figure 4.5).

Table 4.1: Comparison of thickness of copolymer coated SCFME, ΔQ, C_{LF} and phase angle of copolymer films.

X_{PSP} =	**0.33**	**0.50**	**0.66**
ΔQ (mC)	7.184	5.498	3.305
Thickness of copolymer coated SCFME (μm)	19.86	15.75	11.15
C_{LF} ($mF.cm^{-2}$)	173.5	172.3	65.5
~i_{pa} (mA)	0.044	0.038	0.018
E_{onset} (V)	1.139	1.127	1.119
Phase of Z (degree)	66.99°	51.18°	43.28°

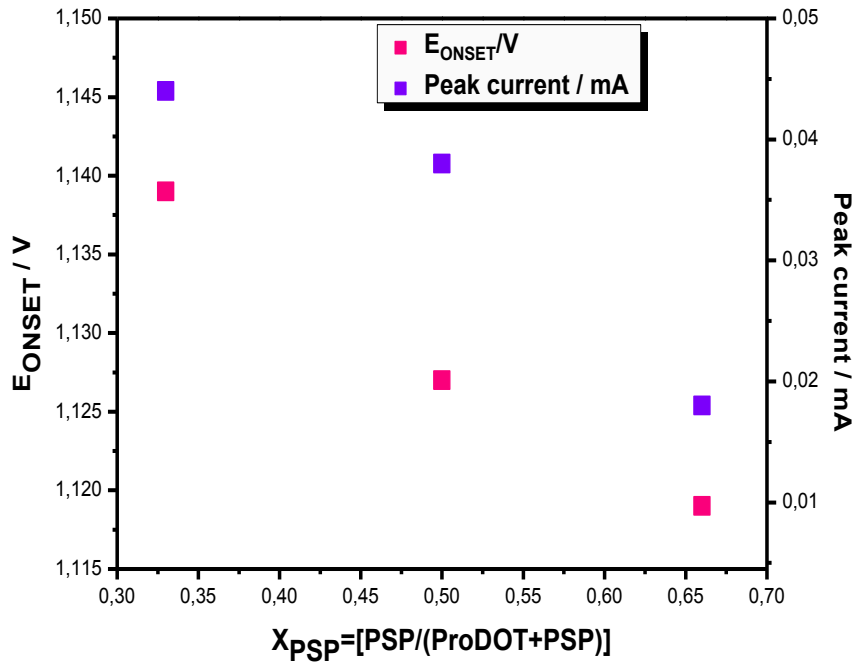

Figure 4.5: Plot of oxidation potential and peak current obtained from CV for different mole fraction of Poly(ProDOT-co-PSP).

The anodic and cathodic peak current increased with increase in square root of scan rate and scan rate. Figure 4.6 and 4.7 show that the anodic and cathodic redox

reaction for the copolymers formed in 0.1 M $NaClO_4$/ACN. The scan rate dependence of the anodic and cathodic peak currents presents a linear dependence on scan rate and square root of scan rate, as evidenced by linearity of the plot, R value varies in the range of 0.9782 to 0.9970. It demonstrates that the electrochemical processes are diffusionally-controlled and entirely reversible even at high scan rates.

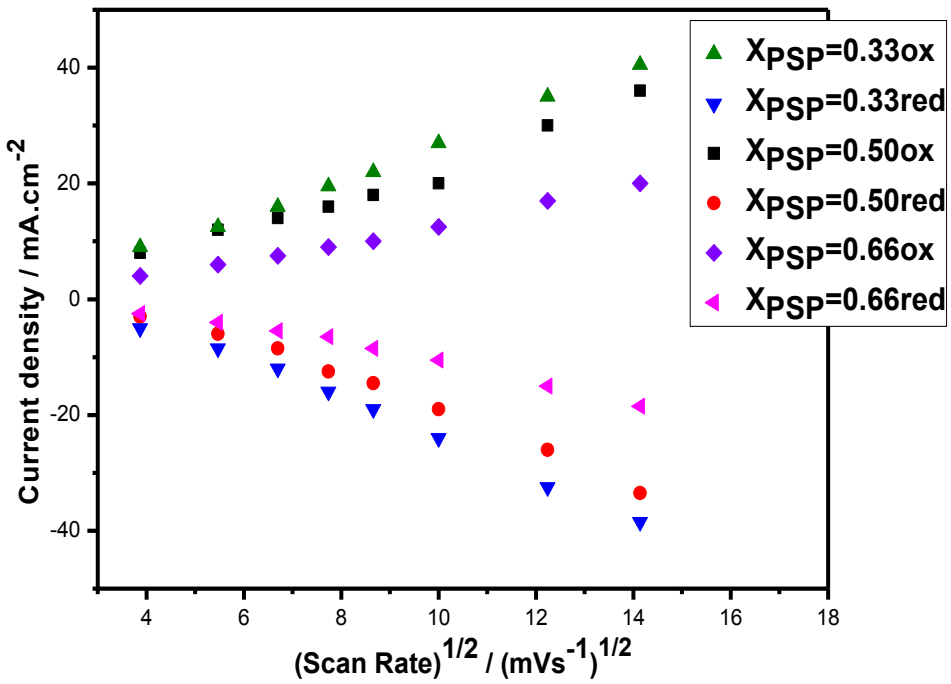

Figure 4.6: Plots of anodic and cathodic peak current density vs. square root of scan rates for the copolymer films in monomer free solution (in 0.1M $NaClO_4$ / ACN).

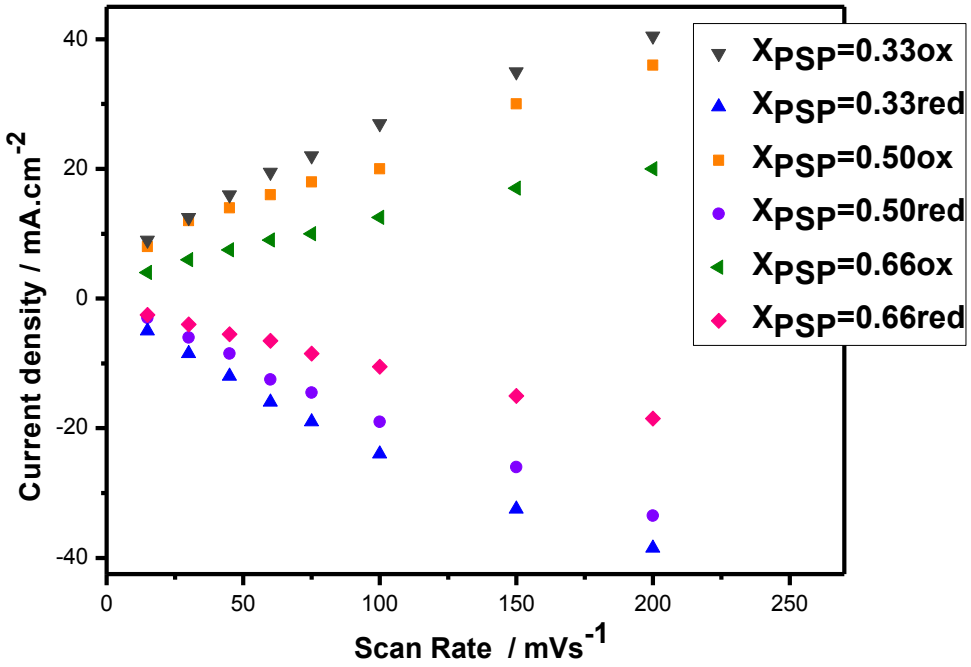

Figure 4.7: Plots of anodic and cathodic peak current density vs. scan rates for the copolymer films in monomer free solution(in 0.1M $NaClO_4$ / ACN.)

4.3 Ex-situ FTIR-ATR Measurements of Poly(ProDOT-co-PSP) and Poly(ProDOT)

For spectroscopic characterization of Poly(ProDOT-co-PSP) films, the same mole fractions of the copolymers were also prepared by cyclic voltammetry on ITO-PET with the same conditions of random Poly(ProDOT-co-PSP) films formation on SCFME (Figure 4.8).

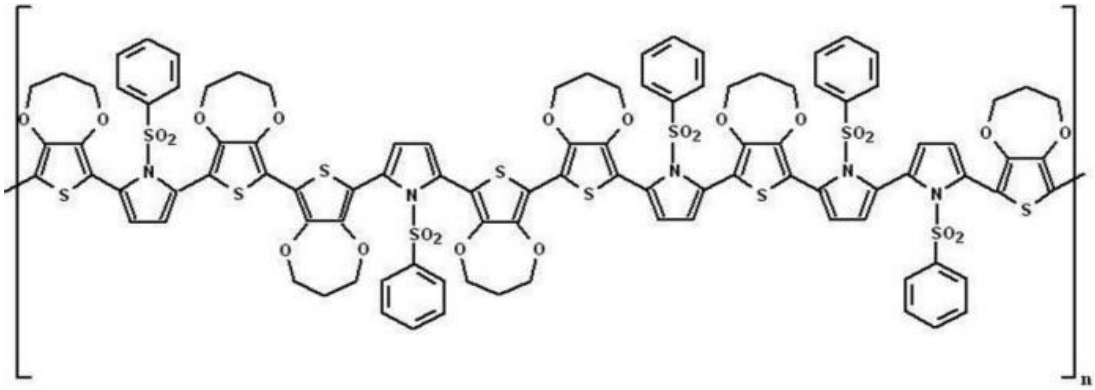

Figure 4.8: Chemical structure of random Poly(ProDOT-co-PSP).

Inclusion of PSP into the electrocopolymerized thin film, and doping with the respective anion of the supporting electrolyte were followed by FTIR-ATR (Figure 4.9). This technique allows us to assign corresponding functional groups in the resulting copolymer.

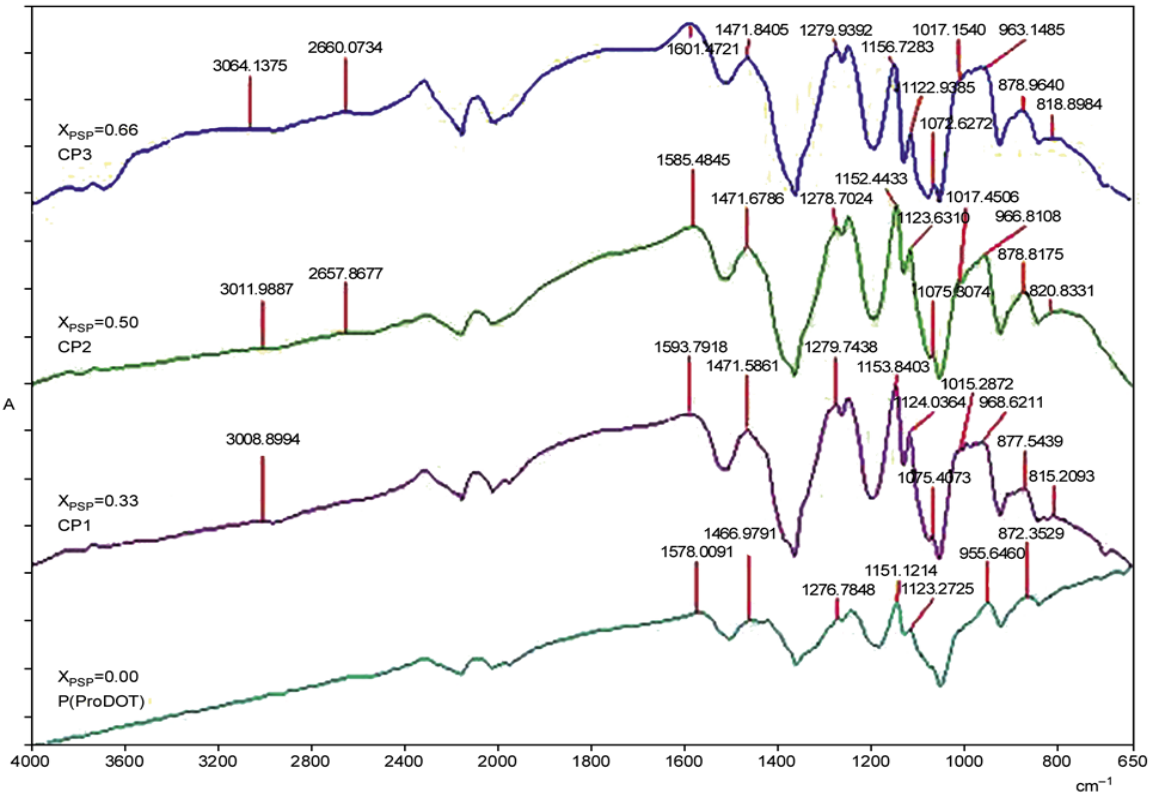

Figure 4.9: Ex-Situ FTIR-ATR spectrum of Poly(ProDOT-co-PSP) and Poly(ProDOT) films on ITO-PET.

The band at 1466-1471 cm^{-1} (stretching of C=C bond) and the peak at 1276-1279 cm^{-1} (the stretching quonidal structure of thiophene) are known to be characteristic vibrational peaks of polythiophene. Vibrations at 1151-1156 cm^{-1} are assigned to stretching in the alkylenedioxy group(C-O-C bond). The band at 1015-1018 cm^{-1} (C-N stretching) originated from the N-substitued pyrrole of PSP. Sulfonyl stretching at 1072-1075 cm^{-1}, aromatic C-H bending (815-820 cm^{-1}) and aromatic C-H stretching (3008-3064 cm^{-1}) become distinct when PSP ratio is increased in the copolymer. Further vibrations from the C-S bond, in the thiophene ring, can be seen at 872-879 cm^{-1}, attributed to C-S stretching. All assignments were denoted in Table 4.2.

Table 4.2: FTIR-ATR assignments of Poly(ProDOT-co-PSP)s and Poly(ProDOT).

(cm^{-1})	**X_{PSP}=**	**0.00**	**0.33**	**0.50**	**0.66**
C-H stretching (aromatic)		-	3008	3011	3064
C-H deformation (aromatic)		-	-	2657	2660
CH_2 wagging		1123	1122	1124	1123
C=C stretching (thiophene ring)		1466	1471	1471	1471
Sulfonyl stretching		-	1075	1075	1072
The stretching quonidal structure of thiophene		1276	1279	1278	1279
C-O-C group stretching		1151	1153	1152	1156
C-N stretching (N-substitued pyrrole)		-	1015	1018	1017
C-O bending		955	963	968	966
C-H bending (aromatic)		-	815	820	818
C-S stretching		872	877	878	879

4.4 Morphological Analyses of Poly(ProDOT-co-PSP) Films via SEM and AFM

Morphological analysis were made via SEM and AFM. SEM images of Poly(ProDOT-co-PSP) copolymers, SEM images were obtained at 5 kV, and illustrated in Fig. 4.10, Fig 4.11, and Fig 4.12. By using small size electrolyte anions as ClO_4^-, a high density of pores was obtained. SEM images of copolymers of this study have similar porous structure with ProDOT-Et_2 [136]. The observed differences at film thicknesses were obtained due to an increase of PSP in the feed (Table 4.1).

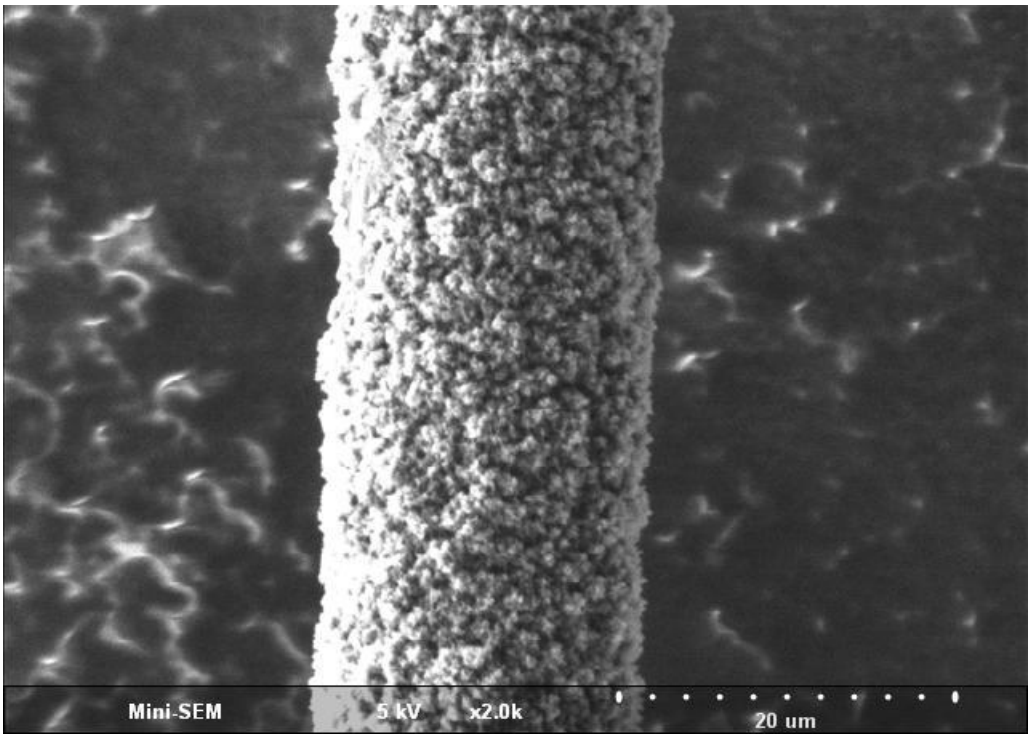

Figure 4.10: SEM image of the copolymer coated SCFME of X_{PSP} = 0.33.

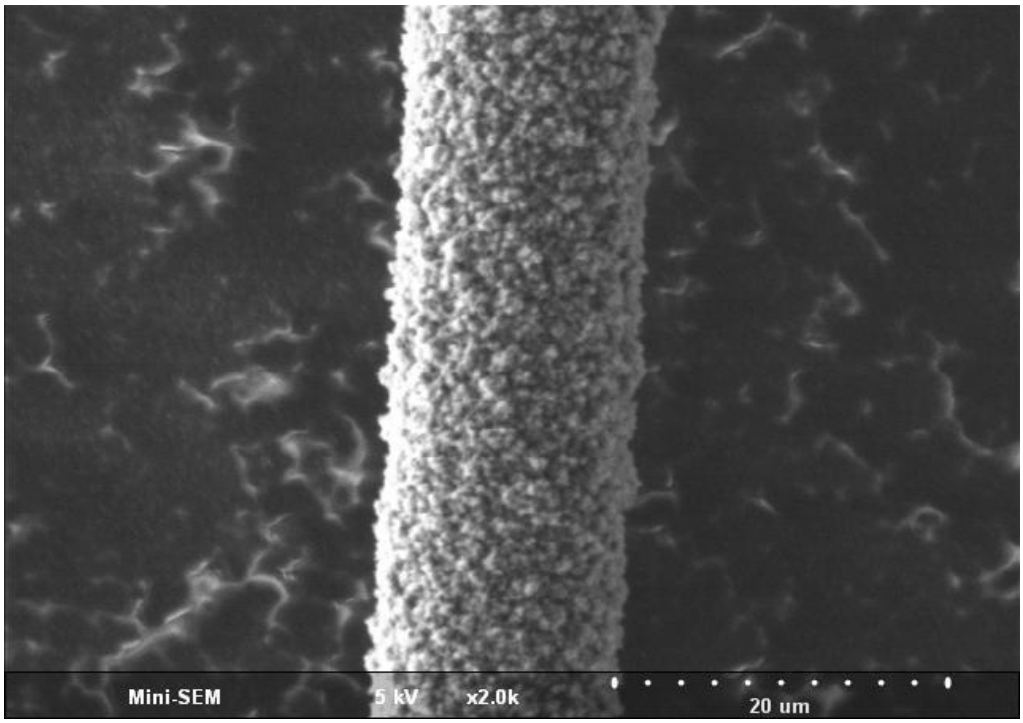

Figure 4.11: SEM image of the copolymer coated SCFME of X_{PSP} = 0.50.

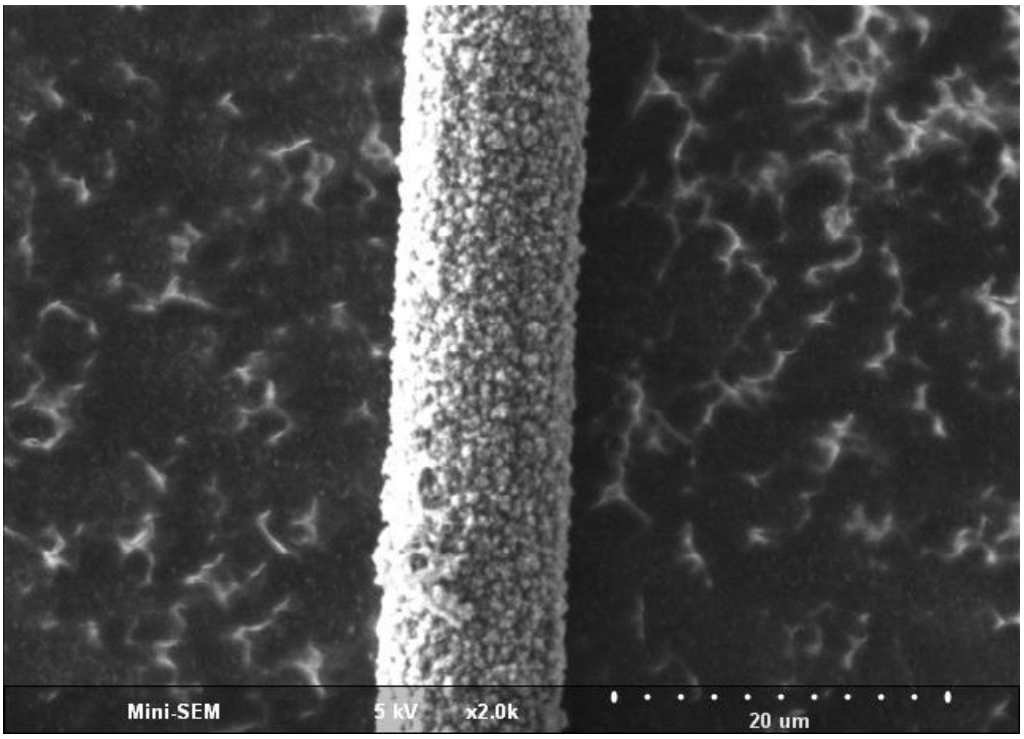

Figure 4.12: SEM image of the copolymer coated SCFME of X_{PSP} = 0.66.

This thickness difference helps us to follow the incorporation of PSP on the copolymer structure. The difference in the capacitance is also due to change of film thickness and fiber morphology in the course of their modification. A continuous increase in current with successive scans is observed, indicating an increase in the thickness, and also in the conductivity of the polymeric film formed on the electrode surface, which is followed by CV measurements.

The monomer mixture of ProDOT (10mM) and PSP (5mM) was copolymerized by CV on ITO-PET for AFM analysis. The images were obtained at none-contact mode AFM (Fig. 4.13 and Fig. 4.14). Root mean square (RMS), roughness value was calculated via Nanosurf Easyscan 2 software programme by selecting raw data (RMS: 65.8 nm).

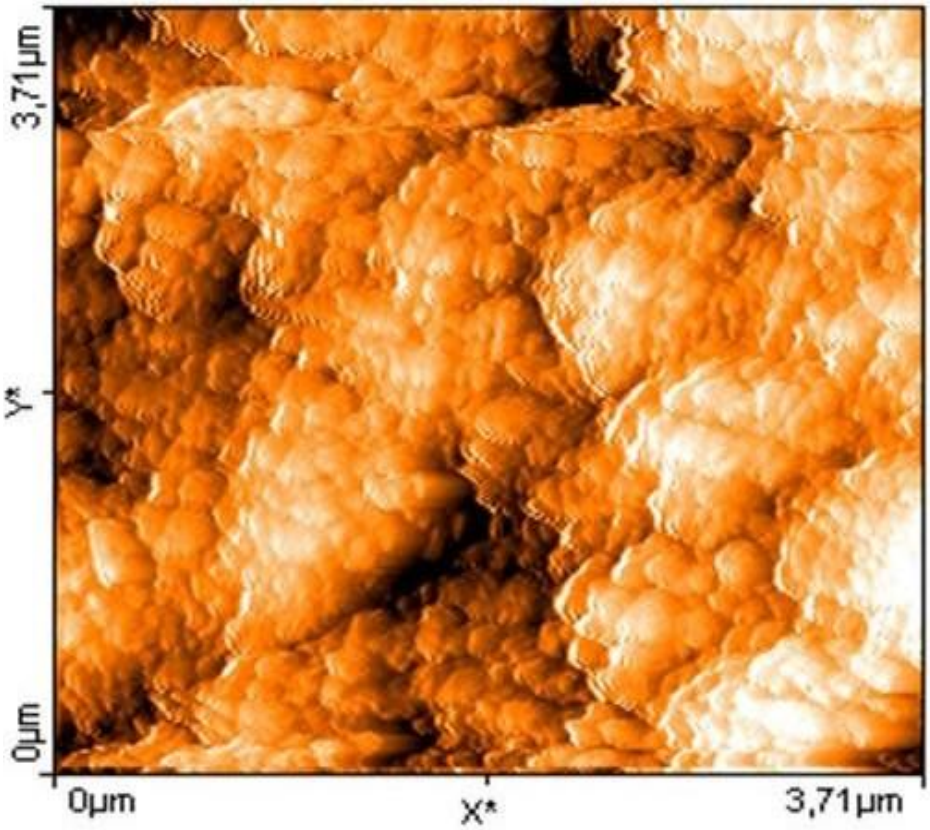

Figure 4.13: AFM image of Poly(ProDOT-co-PSP) coated ITO-PET.

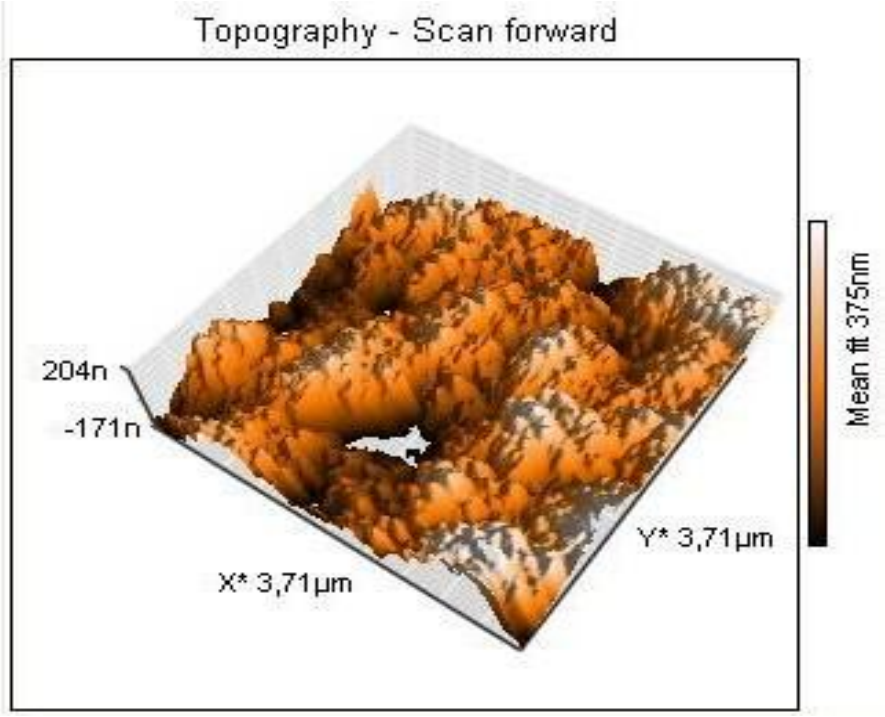

Figure 4.14: AFM topography image of Poly(ProDOT-co-PSP) coated ITO-PET.

The SEM image was also obtained for modified ITO-PET (Fig. 4.15). These spherical-shape aggregates were obtained by the growth of much smaller nanoscale aggregates dependent on the polymerization charge.

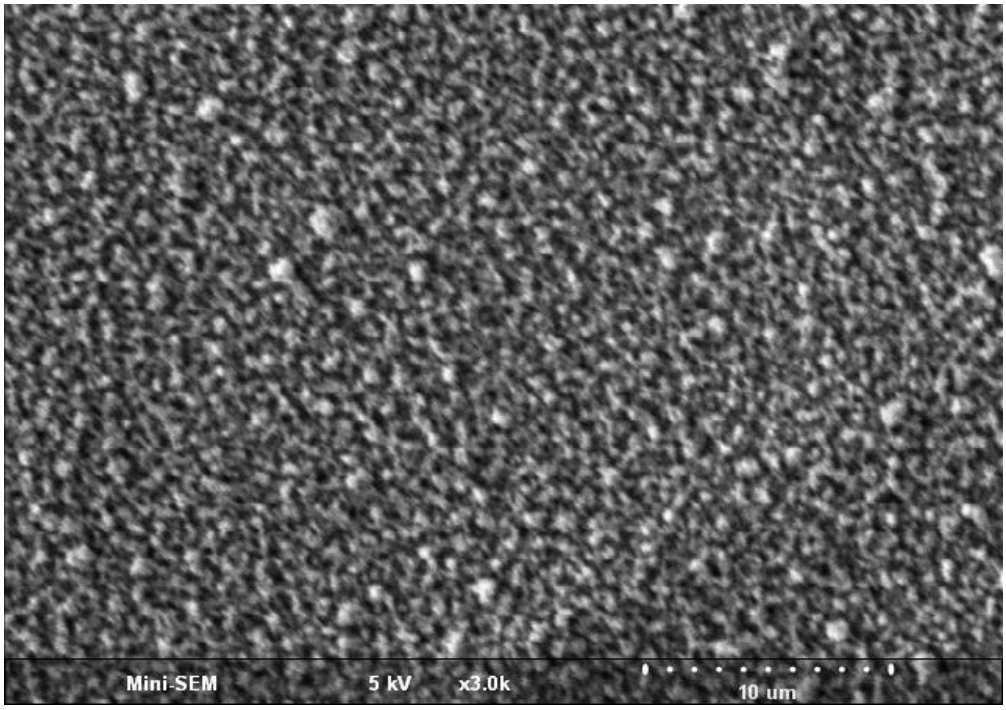

Figure 4.15: SEM image of Poly(ProDOT-co-PSP) coated ITO-PET.

4.5 EIS Investigation of Poly(ProDOT) and Poly(ProDOT-co-PSP) on SCFME

The electrical properties of Poly(ProDOT) and copolymers on SCFMEs were determined by electrochemical impedance measurements in monomer free solution. The Nyquist, Bode Magnitude and Bode Phase plots of thin films were given in the frequency range 0.01 Hz - 100 kHz (Fig. 4.16, Fig. 4.17 and Fig. 4.18).

The copolymers are also exhibiting different impedance data from that of Poly(ProDOT) which shown an ideal capacitive line (Bode phase angles close to 90^0) by the application of which was obtained from–electrochemical impedance spectroscopic measurements, indicating fast charge transfer at the carbon fiber/polymer and polymer/solution interfaces, as well as fast charge transport in the polymer bulk. Bode-phase angles which approached the maximum at 0.01 Hz were ~ 66.99° for X_{PSP} = 0.33, ~ 51.18° for X_{PSP} = 0.50 and ~ 43.28° for X_{PSP} = 0.66, respectively. That indicates the presence of PSP in copolymer structure.

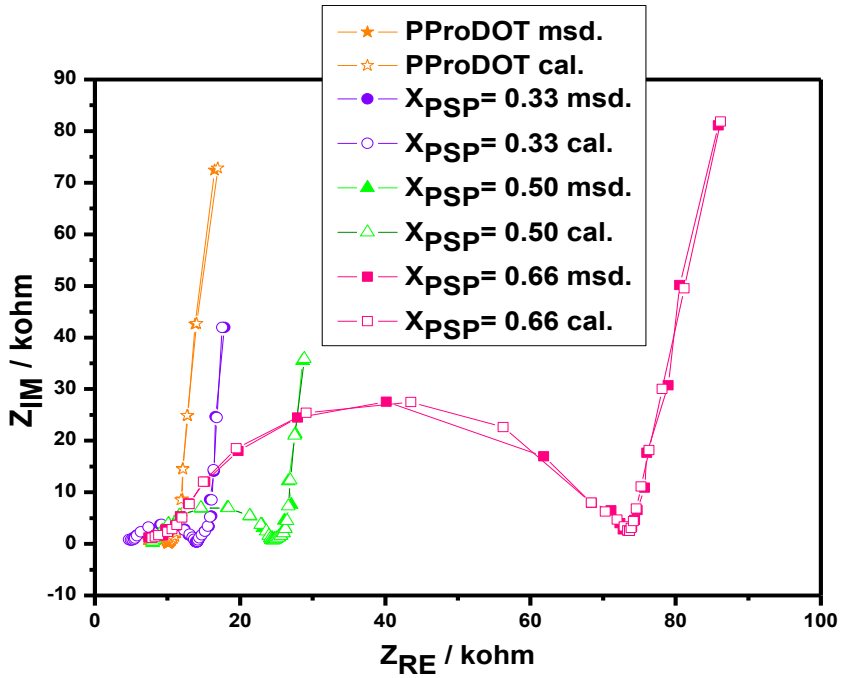

Figure 4.16: Nyquist plots of Poly(ProDOT) and different mole fractions of Poly(ProDOT-co-PSP) electrografted on SCFMEs; correlated with the calculated data from the equivalent circuit model; (R(W(CR)(QR))(CR)).

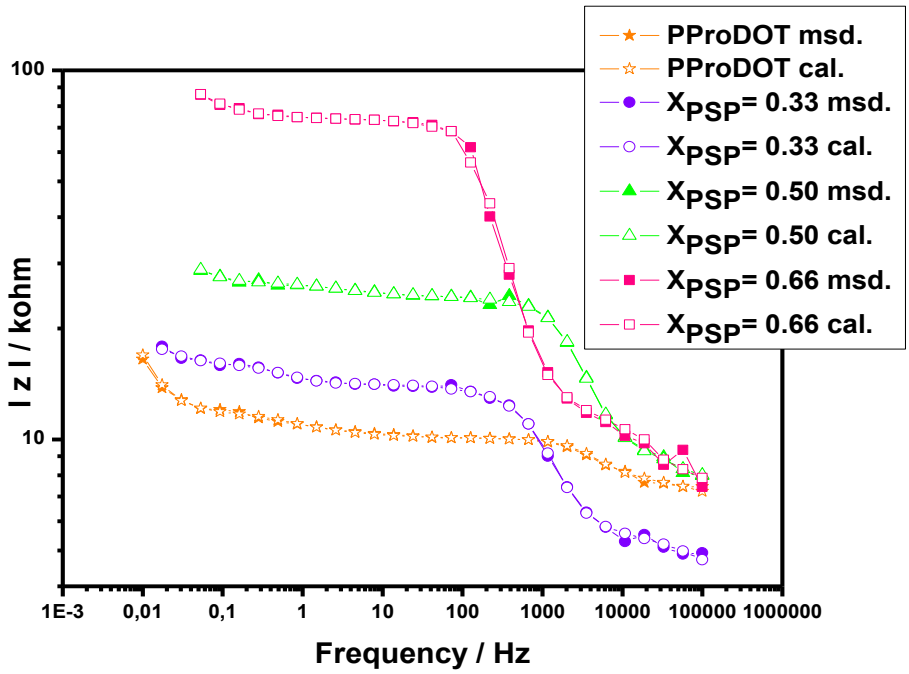

Figure 4.17: Bode Magnitude plots of Poly(ProDOT) and different mole fractions of Poly(ProDOT-co-PSP) electrografted on SCFMEs; correlated with the calculated data from the equivalent circuit model; (R(W(CR)(QR))(CR)).

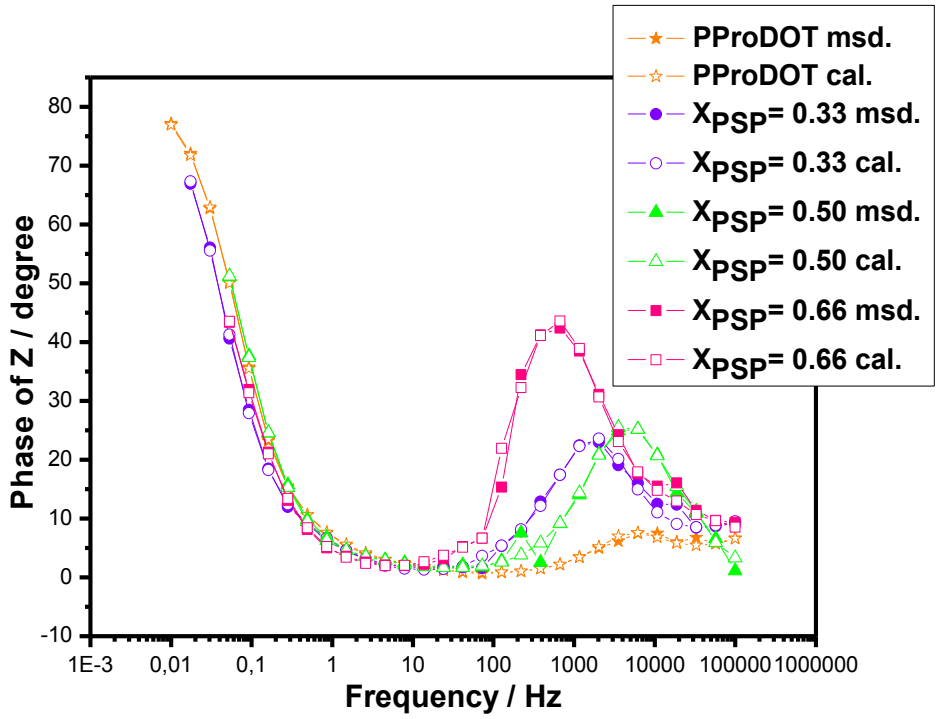

Figure 4.18: Bode Phase plots of Poly(ProDOT) and different mole fractions of Poly(ProDOT-co-PSP) electrografted on SCFMEs; correlated with the calculated data from the equivalent circuit model; (R(W(CR)(QR))(CR)).

The Bode- phase peaks of the copolymers in the frequency range of 10Hz -10000 Hz appeared which should be caused by the transition from resistor to capacitor with the increase of PSP ratio. The Bode magnitude plots for copolymers were presented in Fig. 4.17, X_{PSP} = 0.33 had higher conductivity compared to X_{PSP} = 0.50 and X_{PSP} = 0.66. Nyquist plots were also used to estimate the low-frequency redox capacitance (C_{LF}) of the copolymer-modified SCFMEs. The low frequency capacitance ($C_{LF} = -1/2\pi f Z_{IM}$) values from the impedance spectroscopy were obtained by using imaginary component (Z_{IM}) corresponding to f = 0.01 Hz.

The C_{LF} and film thickness of copolymers decreased which indicates the increase of PSP concentration in the feed. Total charges were obtained during electrogrowth process as 7.184 mC, 5.489 mC and 3.305mC (Table 4.1). The increase of PSP concentration in the feed resulted in the decrease of film thickness and growth rate of copolymer. This is confirmed from the cyclic voltammetry of mixture of monomers, the decrease found in the total charge, film thickness and C_{LF} in the plot of it against the increase of PSP mole fraction in copolymer (Fig. 4.19).

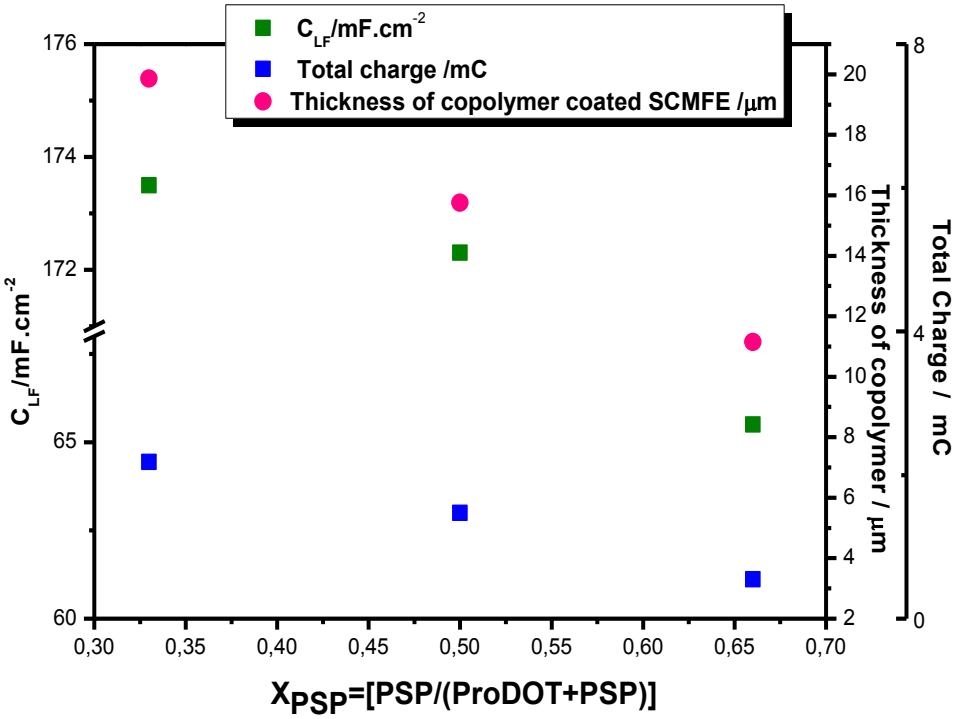

Figure 4.19: Graph of thicknesses of copolymer coated SCFMEs obtained from SEM, low frequency capacitances and total charges (ΔQ) which were applied during the electropolymerization vs. mole fractions of Poly(ProDOT-co-PSP).

The electrodes which were showing the The Nyquist plots (complex plane plots) with semi-circle behaviour seems to be ideal electrode systems for biosensing [137]. The diameter of the semi-circle increased with an increase of PSP in the feed that destroys the integrated heterocyclic and conjugated system of polythiophene. It corresponds to the increase of the charge transfer resistance which included in the equivalent circuit (Fig.4.20) as the resistance of the modified electrode.

4.6 Equivalent Circuit Modelling of Poly(ProDOT) and Poly(ProDOT-co-PSP) on SCFME

The EIS data were fitted with an equivalent electrical circuit in order to characterize the electrochemical properties of copolymer. The experimental results obtained from equivalent circuit shown that both the double-layer and the film capacitances decreased with the increase of incorporated PSP ratio into copolymer structure, while the charge-transfer and the pore resistance increased.

The impedance spectra for copolymers may be described by the equivalent circuit of (R(W(CR)(QR))(CR)) Fig. 20,. The model is composed of the electrolyte and pore resistance (Rs), the adsorption capacitance and resistance (C_a and R_a), double-layer capacitance and charge-transfer resistance (C_{dl} and R_{ct}), Warburg impedance (W), resitance and capacitance of the copolymer film on SCMFE (R_f and C_f). R_a and C_a connected with the charging / discharging process in the surface of the film. Both of these parameters improve the quality-of-fit of the frequency dispersion transition between the charge transfer semi-circle and the Warburg impedance or capacitance line. C_{dl} and R_{ct} formed by the inward penetration of ClO_4^- anion along pores at the electrolyte|copolymer interface. W is related to diffusion of species along the micropores and depends on the electrode geometry (spherical diffusion at microelectrode).

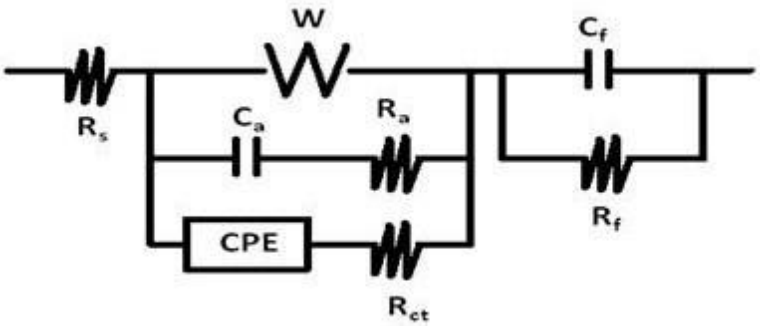

Figure 4.20: The equivalent circuit model of Poly(ProDOT), X_{PSP} = 0.33, X_{PSP} = 0.50 and X_{PSP} = 0.66 coating on a single carbon fiber electrode. (R_s=solution and pore resistance and W=Warburg impedance, Z_W; R_a and C_a are the resistance and the adsorption capacitance; R_{ct}= charge transfer resistance; CPE is used for modelling the double layer capacitance, C_{dl}; R_f and C_f are film resistance and film capacitance of coated copolymer film on carbon fiber microelectrode).

The most widely used is the constant phase element (CPE), which has a non-integer power dependence on the frequency. CPE is used in a model in place of a capacitor C_{dl} (double layer capacity) to compensate for roughness of the electrode, porosity and nonhomogeneity in the system. A rough or porous surface can cause a double-layer capacitance to appear as a CPE with a n value between 0.9 and 1 [138]. In this study, CPE was used as double layer capacitance due to a porous structure (n~1) (Table 4.3).

Table 4.3: Mole fraction dependence of parameters calculated from the equivalent circuit model for Poly(ProDOT) and Poly(ProDOT-co-PSP).

X_{PSP} →	**0.00 Poly(ProDOT)**	**0.33**	**0.50**	**0.66**
$R_S/\Omega.cm^2$	2.528	4.738	12.574	14.656
$W/Y_0/\mu Ss^{-n}.cm^{-2}$	0.0253	0.218	0.278	0.528
$C_a/mF.cm^{-2}$	92.35	41.35	27.98	5.08
$R_a/\Omega.cm^2$	8.25	11.37	15.57	34.06
$C_{dl}/ mF.cm^{-2}$	466.95	176.05	118.80	55.30
n	0.946	0.974	0.902	0.906
$R_{ct}/ \Omega.cm^2$	19.75	41.66	78.34	167.84
$C_f/ mF.cm^{-2}$	117.22	0.02	0.013	0.0053
$R_f/ \Omega.cm^2$	3.85	19.19	25.26	107.60
Chi Squred/$\chi 2$	$1.95x10^{-4}$	$7.56x10^{-4}$	$7.87x10^{-4}$	$2.97x10^{-3}$

At Nyquist plots of copolymers, appeared semi-circle in high frequency range was associated with anion transfer at the film|solution interface and can be described by the charge transfer resistance R_{ct}, in series combination with a CPE. The increase in diameter of the circle, i.e., higher the charge transfer resistance (R_{ct}), is most useful for biosensing [137]. After the charge transfer semi-circle, straight line at the x- axis can be related to Warburg impedance, Z_W, due to the diffusion of charged species in the film at low frequency.

The copolymers have high electrolyte and pore resistivity (Rs), resulted from the decrease in pore size and film thickness, making it more difficult to maintain connectivity between the pores and cause the lowest interfacial area for charge transport. Film capacitance (C_f), double-layer capacitance (C_{dl}) and adsorption capacitance (C_a) were found to be inversely proportional to the concentration of PSP (Fig. 4.21).

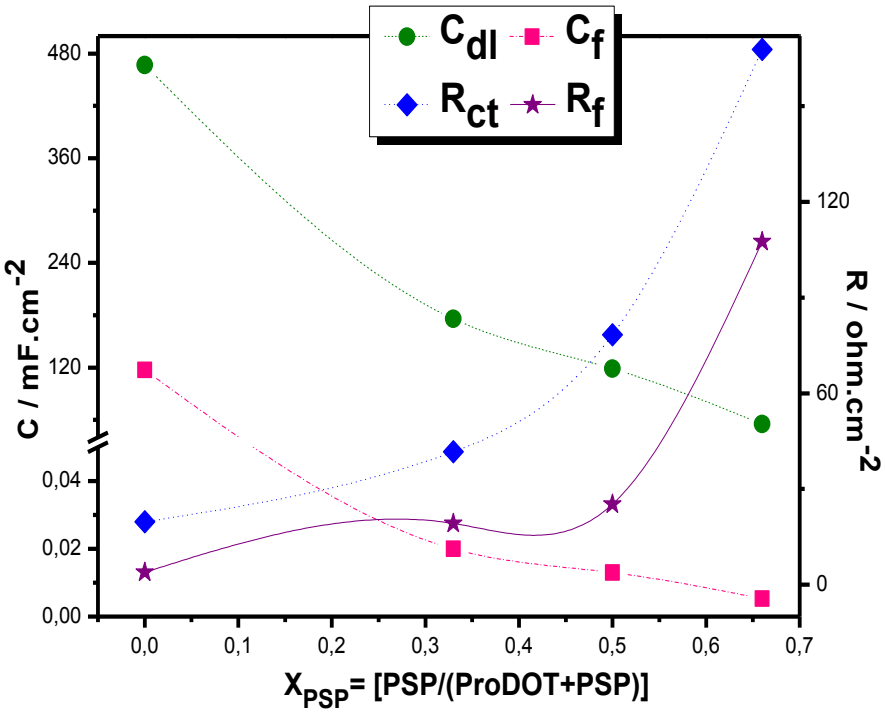

Figure 4.21: Charge transfer (R_{ct}) and film (R_f) resistances; double layer (C_{dl}) and film (C_f) capacitances obtained rom ECM for Poly(ProDOT), X_{PSP} = 0.33, X_{PSP} = 0.50 and X_{PSP} = 0.66.

4.7 Sensor Behaviours of Poly(ProDOT) and Poly(ProDOT-co-PSP) Microelectrodes

Cyclic voltammetry was used for the determination of DA and AA. Potential scanning was performed over the range -1.0 to 1.0 V at a scan rate of 50 mV/s in buffer solution (BS) on Poly(ProDOT) and Poly(ProDOT-co-PSP) microelectrodes at room temperature.

4.7.1 Electrochemical behaviour of Dopamine and Ascorbic Acid at the Poly(ProDOT) and Poly(ProDOT-co-PSP) microelectrodes

Figure 4.22 shows the cyclic voltammograms of 1 mM DA at the Poly(ProDOT) and Poly(ProDOT-co-PSP), X_{PSP}=0.66 microelectrodes in buffer solution (Potassium dihydrogen phosphate-di-Sodium hydrogen phosphate). Poly(ProDOT) exhibited a poor electrochemical response. At the Poly(ProDOT-co-PSP), DA exhibited a good electrochemical response, and the voltammograms showed a pair of clear redox peaks with a potential value of 0.6 V for the oxidation peak and -0.2 V for the reduction peak. The above result revealed that the Poly(ProDOT-co-PSP) film exerted stronger electro-catalytic effect on DA than Poly(ProDOT).

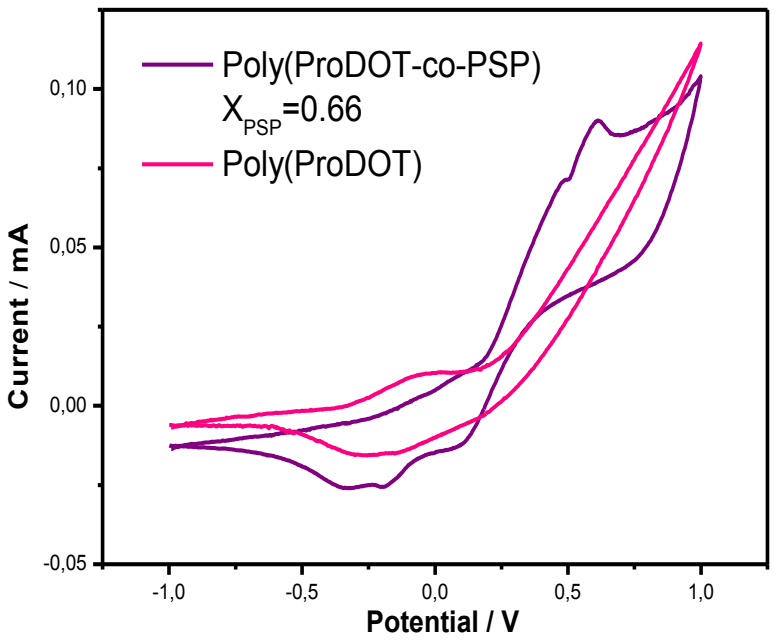

Figure 4.22: Cyclic voltammograms of DA at the Poly(ProDOT) and Poly(ProDOT-co-PSP) microelectrodes in a buffer solution at scan rate 50mV/s.

Since AA and DA coexist in the extra-cellular fluid of the central nervous system, both have a similar oxidation potential at most solid electrodes, and determination of these species is very difficult due to the overlapping signals. To evaluate the sensitivity and selectivity of the present system for the quantification of AA and DA, the electrochemical behaviour of a mixture of AA (100 μM) and DA (1mM) was investigated. Fig. 4.23 shows the cyclic voltammograms of a mixture of AA and DA at the Poly(ProDOT) and Poly(ProDOT-co-PSP) microelectrodes in buffer solution.

Two well-defined oxidation peaks at a potential of 0.02 and 0.6 V in buffer solution were observed for the oxidation of AA and DA at the Poly(ProDOT-co-PSP) film, respectively.

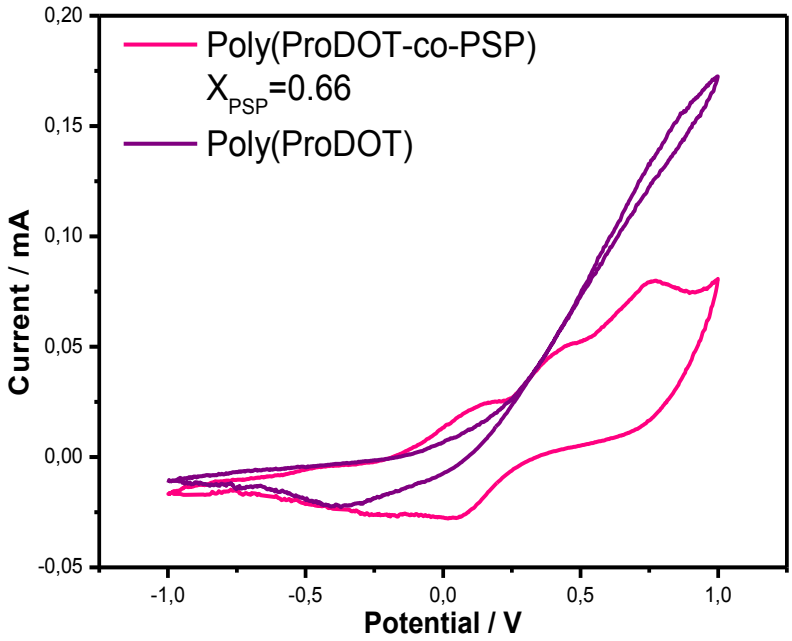

Figure 4.23: Cyclic voltammograms of DA and AA at the Poly(ProDOT) and Poly(ProDOT-co-PSP) microelectrodes in a buffer solution at scan rate 50mV/s.

These results indicate that the Poly(ProDOT-co-PSP) film exhibits excellent catalytic activity and well-separated peak potentials for the determination of AA and DA. The improvement of the sensivity of the modified sensor to DA is due to PSP in copolymer structure.

4.7.2 Determination of concentration of Dopamine by CV (Calibration Curve)

The determination of DA concentration in presence of AA for Poly(ProDOT-co-PSP) modified SCFME was performed by CV (Fig. 4.24). The oxidation peak current density of dopamine was chosen as the analytical signal. Oxidation peak current of AA almost doesn't change due to concentration of AA held constant at 100µM. The results showed that anodic peak current density was proportional to concentration intervals of DA, from 10^{-4} M to 10^{-11} M as shown in Fig. 4.25. The oxidation peak currents of DA are proportional to its concentrations.

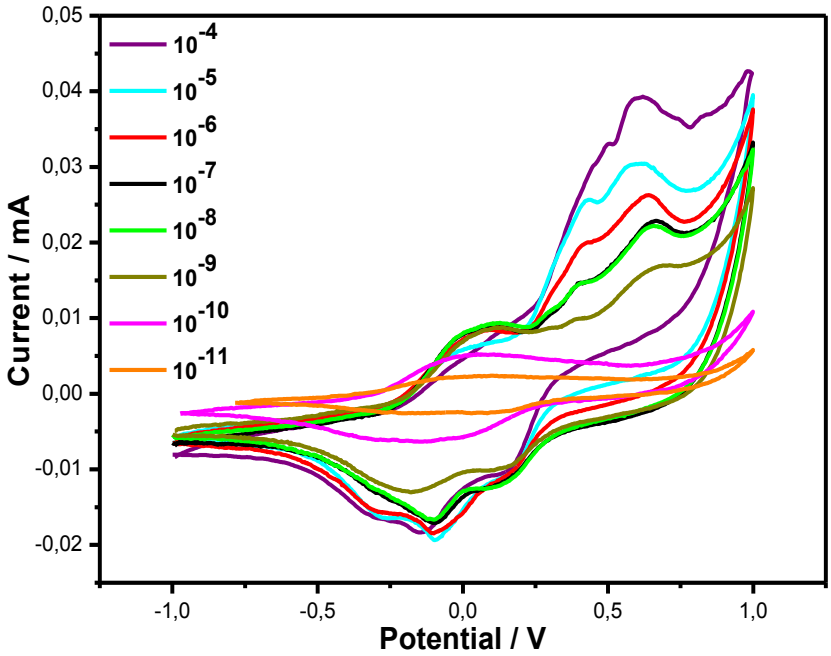

Figure 4.24: CV of Poly(ProDOT-co-PSP) modified SCFME in buffer solution containing 100µM AA different concentration of DA.

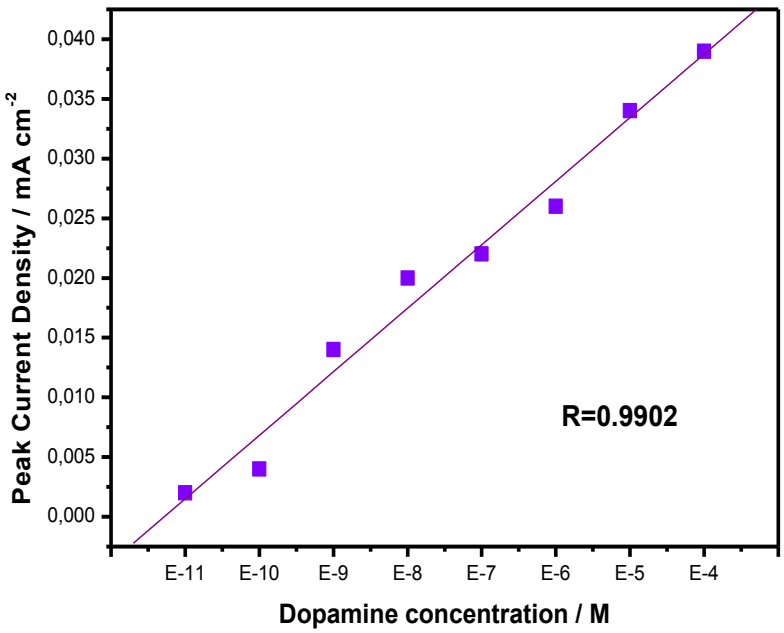

Figure 4.25: Changes in anodic peak current density by dopamine concentration for Poly(ProDOT-co-PSP) modified SCFME in 10^{-4} M to 10^{-11} M dopamine-containing buffer solution.

A detection limit of 1nM was obtained in the presence of AA using cyclic voltammetry, which is sufficient to detect DA in a pharmaceutical product. The linear range of DA concentration is 10^{-4} M-10^{-11} M with a correlation coefficient of 0.9902. The relative standard deviation (%R.S.D.) was less than 2.0% for eight determinations of 1nM dopamine.

The Poly(ProDOT-co-PSP) modified electrode showed good reproducibility (± 2.0% relative standard deviation), a low detection limit (1 nM), high sensitivity, a wide dynamic range of detection (1 mM), and great selectivity (presence of AA).

5. CONCLUSIONS

A new copolymer, obtained from 3,4- Propylenedioxythiophene (ProDOT) and (N-phenylsulfonyl pyrrole) PSP by the cyclic voltammetry, was successfully synthesized. The experimental results from CV and EIS and the theoretical results obtained from equivalent circuit correlated with morphological characterization.

FTIR-ATR characteristic peaks of PSP indicate the inclusion into copolymer. The decrease in peak currents and total charges of copolymer was observed as compared to homopolymer of Poly(ProDOT). The changing of the capacitance properties, film thickness and fiber morphology was found to be inversely proportional with the increasing PSP concentration in the feed. These information hints that sulphonyl group in PSP has very strong electron-withdrawing effect thus making it difficult to polymerize electrochemically. The capacitance properties of copolymers at lower frequency become weak as compared to Poly(ProDOT), hence suggesting an increase in the sulphonyl content in the copolymer due to the addition of PSP, which in turn suggests more sulphonyl structure in the copolymer. The changing of the capacitance of the copolymer is reflected on to the equivalent circuit model by the dependency of the mole fractions. The decreasing of the film thickness obtained from SEM and the decrease of capacitance values clearly indicates the inclusion of PSP into copolymer.

The Poly(ProDOT-co-PSP) modified SCFME exhibits highly electro-catalytic activity for the oxidation of dopamine (DA) and ascorbic acid (AA). Moreover, peak separations between DA and AA allow this modified electrode to analyze DA and AA by using cyclic voltammetry with good stability, sensitivity and selectivity. The detection limit of 1nM is lower, thus affords an alternative pathway for the determination of DA. The well-defined electrochemistry of Poly(ProDOT-co-PSP) films on SCMFEs opens up the possibility for bioelectrochemical sensor electrodes.

REFERENCES

[1] **Kimura, G. and Yamada, K.,** 2009: Electrochromism of poly(3,4-ethylenedioxythiophene) films on Au nano-brush electrode, *Syntetic Metals*, **159**, 914-918.

[2] **Bokria, J.G., Invernale, M.A., Lee, K.R., Mamangun, D.M.D., Ombaba, M., Sotzing, G.A.,** 2010: Variable-color poly(3,4-propylenedioxythiophene) electrochromics from precursor polymers. *Polymer*, **51**, 378-382.

[3] **Cheng, Y., Hobson, T., Hou, Y., Jie, L.J.,** 2010: Design and Synthesis of Hierarchical MnO_2 Nanospheres/Carbon Nanotubes/Conducting Polymer Ternary Composite for High Performance Electrochemical Electrodes, *Nano Letters*, **10** , 2727–2733.

[4] **Chen, H.W., Hu, C.W., Ho, K.C., Hsu, C.Y., Lee, K.M.,** 2010: A dye-sensitized photo-supercapacitor based on PProDOT-Et_2 thick films, *Journal of Power Sources*, **195**, 6232-6238.

[5] **Wan, M., Wei, Z., Xia, L.,** 2010: Conducting polymer nanostructures and their application in biosensors, *Journal of Colloid and Interface Science*, **341**, 1-11.

[6] **Garnier, F., Tourillon, G.,** 1984: Structural effect on the electrochemical properties of polythiophene and derivatives, *Journal of Electroanalytical Chemistry*,**161**, 51-58.

[7] **Oberlin, A.,** 1984: Carbonization and graphitization, *Carbon*, **22**, 521–541.

[8] **Sarac, A.S., Sezgin, S., Ates, M., Turhan, C.M.,** 2008: Electrochemical impedance spectroscopy and morphological analyses of pyrrole, phenyl pyrrole, and methoxy phenyl pyrrole on carbon fiber microelectrodes, *Surface Coatings Technology*, **202**, 3997-4005.

[9] **Abidian, M.R., Martin, D.C.,** 2008: Experimental and theoretical characterization of implantable neural microelectrodes modified with conducting polymer nanotubes, *Biomaterials*, **29**, 1273-1283.

[10] **Bobacka, J., Ivaska, A., Lewenstam, A.,** 2000: Electrochemical impedance spectroscopy of oxidized poly(3,4-ethylenedioxythiophene) film electrodes in aqueous solutions, *Journal of Electroanalytical Chemistry*, **489**,17-27.

[11] **Aziz, I., Xiang, M., Zhang, Q.,** 2010: Using EIS to evaluate anti-corrosion properties of the SiC_p/5A06 aluminium MMC treated by cerium conversion coatings, *Journal of Rare Earths*, **28**, 109-116.

[12] **Huang, M.R., Li, X.G., Lu, Q.F.,** 2007: Synthesis and Heavy-Metal-Ion Sorption of Pure Sulfophenylenediamine Copolymer Nanoparticles

with Intrinsic Conductivity and Stability, *Chemistry – A European Journal*, **13**, 6009–6018.

[13] **Aleman, C., Ocampo, C., Oliver, R.,** 2007: Copolymers of *N*-methylpyrrole and 3,4-ethylenedioxythiophene: structural, physical and electronic properties, *Polymer International*, **56**, 803–809.

[14] **Chiang, C.K., Fincher, C.R., Gau, S.C., Heeger, A.J., Louis, E.J., MacDiarmid, A.G., Park, Y.W., Shirakawa, H.,** 1977: Electrical Conductivity in Doped Polyacetylene, *Physical Review Letters*, **39,** 1098-1101.

[15] **Chiang, C.K., Heeger, A.J., Louis, E.J., MacDiarmid, A.G., Shirakawa, H.,** 1977: Synthesis of electrically conducting organic polymers: halogen derivatives of polyacetylene, $(CH)_x$, *Journal of the Chemical Society, Chemical Communications*, 578-580.

[16] **Skotheim, T.A., Elsenbaumer, R.L. and Reynolds, J.R.,** 1998: Handbook of Conducting Polymers, 2nd ed., Marcel Dekker, New York.

[17] **Chien, J.C.W.,** 1984: Polyacetylene: Chemistry, Physics and Materials Science Academic, Orlando.

[18] **A. Ajayaghosh, A.,** 2003: Donor–acceptor type low band gap polymers: polysquaraines and related systems, *Chemical Society Reviews*, **32**, 181-191.

[19] **Bredas, J.L., Chance, R.R. and Sileby, R.,** 1982: Comparative theoretical study of the doping of conjugated polymers: Polarons in polyacetylene and polyparaphenylene, *Physical Review B*, **26**, 5843–5854.

[20] **Bredas, J.L., Themans, B., Andre,J.M., Chance, R.R., Boudreaux, D.S. Silbey, R.,** 1983: Theoretical studies of the physics of charged defect formation in doped organic polymers : towards a coherent theoretical picture, *Journal de Physique Archives*, **44,** 373-379.

[21] **Bredas, J.L. and Street, G.B.,** 1985: Polarons, bipolarons, and solitons in conducting polymers, *Accounts of Chemical Research*, **18,** 309-315.

[22] **Qian, R. and Qiu, J.,** 1987: Electrochemically Prepared Polypyrroles from Aqueous Solutions, *Polymer Journal*, **19,** 157-172.

[23] **Roncali,J., Garnier, F., Lemaire, M. and Garreau, R.,** 1986: Poly mono-, bi- and trithiophene: Effect of oligomer chain length on the polymer properties, *Synthetic Metals*, **15,** 323-331.

[24] **Kumar, D. and Sharma, R.C.,** 1998: Advances in conductive polymers, *European Polymer Journal*, **34,** 1053-1060.

[25] **Chen, S.A. and Tsai, C.C.,** 1993: Structure/properties of conjugated conductive polymers. 2. 3-Ether-substituted polythiophenes and poly(4-methylthiophenes), *Macromolecules*, **26(9),** 2234-2239.

[26] **Okada, T., Ogata, T., and Ueda, M.,** 1996: Synthesis and Characterization of Regiocontrolled Poly(2,5-di-*n*-butoxy-1,4-phenylene) by

Oxovanadium-Catalyzed Oxidative Coupling Polymerization, *Macromolecules,* **29(24),** 7645–7650.

[27] **Stenger-Smith, J.D.,** 1998: Intrinsically electrically conducting polymers: synthesis, characterization and their applications, *Progress in Polymer Science,* **23,** 57-79.

[28] **Janata, J.,** 2002: Electrochemical Sensors and Their Impedances: a Tutorial, *Critical Review in Analytical Chemistry,* **32,** 109-120**.**

[29] **Janata, J. and Josowicz, M.,** 2003: Conducting polymers in electronic chemical sensors, *Nature Materials,* **2(1),** 19-24.

[30] **Gerard,M., Chaubey, A. and Malhotra, B.D.,** 2002: Application of conducting polymers to biosensor, *Biosensors & Bioelectronics,* **17,** 345-559.

[31] **Conroy, K.G. and Breslin, C.B.,** 2003: The electrochemical deposition of polyaniline at pure aluminium: Electrochemical activity and corrosion protection properties, *Electrochimica Acta,* **48,** 721-732.

[32] **Pron, A. and Rannou, P.,** 2002: Processible conjugated polymers: from organic semiconductors to organic metals and superconductors, *Progress in Polymer Science,* **27**, 135-160.

[33] **Leclerc, M.,** 1999: Optical and Electrochemical Transducers Based on Functionalized Conjugated Polymers, *Advanced Materials,* **11,** 1491-1498.

[34] **Milella, E. and Penza, M.,** 1998: SAW gas detection using Langmuir Blodgett polypyrrole films, *Thin Solid Films,* **694**, 327-329.

[35] **Hwang, B.J., Yang, J.Y. and Lin, C.W.,** 2001: Recognition of alcohol vapor molecules by simultaneous measurements of resistance changes on polypyrrole-based composite thin films and mass changes on a piezoelectric crystal, *Sensors and Actuators B: Chemical,* **75**, 67-75.

[36] **Roncali, J.**, 1992,Conjugated poly(thiophenes)-synthesis, functionalization and applications, *Chemical Reviews,* **92(4),** 711-738.

[37] **Tourillon, G., Garnier, F**., 1984: Structural effect on the electrochemical properties of polythiophene and derivatives, *Journal of Electroanalytical Chemistry and Interfacial Electrochemistry,* **161,** 51- 58.

[38] **Dietrich, M., Heinze, J., Heywang, G., Jonas, F.,** 1994: A variety of monomers can be electropolymerized in polar organic solvents, and these films have been used to make both OLEDs and organic FETs, *Journal of Electroanalytical Chemistry,* **369,** 87-92.

[39] **Heywang, G., Jonas, F.,** 1992: Poly(Alkylenedioxythiophene)S - New, Very Stable Conducting Polymers, *Advanced Materials,* **4,** 116-118.

[40] **Groenendaal, B. L., Jonas, F., Freitag, D., Pielartzik, H., Reynolds, J. R.,** 2000: Poly(3,4-ethylenedioxythiophene) and Its Derivatives: Past, Present, and Future. Advanced Materials, **12,** 481-494.

[41] **Welsh, D. M., Kumar, A., Meijer, E. W., Reynolds, J. R.,** 1999: Enhanced Contrast Ratios and Rapid Switching in Electrochromics Based on Poly(3,4-propylenedioxythiophene) Derivatives, *Advanced Materials*, **11,** 1379-1382.

[42] **Smith, L.A. and Ma P.X.,** 2004: Nano-fibrous scaffolds for tissue engineering, *Colloids and Surfaces B: Biointerfaces*, **39,** 125-131.

[43] **Rouse, J.H. and Lillehei, P.T.,** 2003: Electrostatic Assembly of Polymer/Single Walled Carbon Nanotube Multilayer Films, *Nano Letters*, **3(1),** 59–62.

[44] **Ai, H., Jones S.A. and Lvov, Y.M.,** 2003: Biomedical applications of electrostatic layer-by-layer nano-assembly of polymers, enzymes, and nanoparticles, *Cell Biochemistry and Biophysics*, **39**, 23-43.

[45] **Cutler, C. A., Bouguettaya, M., Reynolds, J. R.,** 2002: PEDOT Polyelectrolyte Based Electrochromic Films via Electrostatic Adsorption, *Advanced Materials*, **14,** 684-688.

[46] **Jonas, F., Lerch, K.,** 1997: Conductive plastics, *Kunststoffe-Plast Europe*, **87,** 1401-1402.

[47] **Schwendeman, I., Hickman, R., Zong, K., Welsh, D. M., Schottland, P., Sonmez, G., Reynolds, J. R.,** 2002: Enhanced Contrast Dual Polymer Electrochromic Devices, *Chemistry of Materials*, **14**, 3118-3122.

[48] **Carpi, F., and Rossi, D.D.,** 2006: Colours from electroactive polymers: Electrochromic, electroluminescent and laser devices based on organic materials, *Optics & Laser Technology*, **38,** 292-305.

[49] **Camurlu, P., Cirpan, A. and Toppare, L.,** 2004: Dual type complementary colored polymer electrochromic devices utilized by 3-ester substituted thiophenes, *Journal of Electroanalytical Chemistry*, **572,** 61-65.

[50] **Irvin, D. J., DuBois, C. J., Reynolds, J. R.,** 1999: Dual p- and n-Type Doping in an Alternating Bi(ethylenedioxythiophene)/Pyridine Polymer, *Chemical Communications*, 2121-2122.

[51] **Kumar, A., Welsh, D.M., Morvant, M.C., Piroux, F., Abboud, K.A., Reynolds, J.R.,** 1998: Conducting Poly(3,4-alkylenedioxythiophene) Derivatives as Fast Electrochromics with High-Contrast Ratios. *Chemistry of Materials*, **10,** 896–902.

[52] **Padilla J., Seshadri V., Filloramo J., Minob K., Mishra P., Radmardd B., Kumar A., Sotzing A., Otero F.,** 2007: High contrast solid-state electrochromic devices from substituted 3,4-propylenedioxythiophenes using the dual conjugated polymer approach, *Synthetic Metals*, **157**, 261-268.

[53] **Gaupp C.L., Welsh D.M., Rauh R.D., Reynolds J.R.,** 2002: Poly(ProDOT-Et2): A high-contrast, high coloration efficiency electrochromic polymer, *Macromolecules Rapid Communications*, **23**, 885-889.

[54] **Hsu, C.Y., Chen, H.W., Lee K.M., Hu, C.W., Ho, K.C.,** 2010: A dye-sensitized photo-supercapacitor based on PProDOT-Et_2 thick films, *Journal of Power Sources,* **195**, 6232-6238.

[55] **Sarac, A.S., Gilsing, H.D., Gencturk, A., Schulz, B.,** 2007: Electrochemically polymerized 2,2-dimethyl-3,4-propylenedioxythiophene on carbon fiber for microsupercapacitor, *Progress in Organic Coatings,* **60**, 281-286.

[56] **Sinha, J., Sahoo, R., Kumar, A.,** 2009: Processable, Regioregular, and "Click"able Monomer and Polymers Based on 3,4-Propylenedioxythiophene with Tunable Solubility, *Macromolecules,* **42,** 2015–2022.

[57] **Mishra, S.P., Sahoo, R., Ambade, A.V., Contractor, A.Q., Kumar, A.,** 2004: Synthesis and Characterization of Functionalized 3,4-propylenedioxythiophene and Its Derivatives, *Journal of Materials Chemistry,* **14**, 1896-1900.

[58] **Kumar, N.A., Kim, S.H., Cho, B.G., Lim, K.T., Jeong, Y.T.,** 2009: Surface functionalization of multiwalled carbon nanotubes with poly(3,4-propylenedioxythiophene) and preparation of its random copolymers: new hybrid materials, *Colloid & Polymer Science,* **287**, 97-102.

[59] **Sarac, A.S., Gilsing, H.D., Gencturk, A., Schulz, B., Serantoni, M.,** 2007: Nanoscale surface morphology and monomer concentration dependence on impedance of electrocoated 2,2-dimethyl-3,4-propylene-dioxythiophene on carbon fiber microelectrode, *Journal of Nanoscience and Nanotechnology,* **7(10),** 3543-3452.

[60] **Mishra, S.P., Krishnamoorthy, K., Sahoo, R., Kumar, A.,** 2005: Synthesis and characterization of monosubstituted and disubstituted poly(3,4-propylenedioxythiophene) derivatives with high electrochromic contrast in the visible region, *Journal of Polymer Science Part A: Polymer Chemistry,* **43(2),** 419-428.

[61] **Castello B.P.J.L., Evans, P., Guernion, N., Ratcliffe, N.M., Sivanand, P.S., Teare, G.G.,** 2000: The synthesis of a number of 3-alkyl and 3-carboxy subtituted pyrroles: their chemical polymerisation on poly(vinylidene fluoride) membranes and their use as gas senstive resistor, *Syntetic Met*als, **114(2),** 181-188.

[62] **Janosik, T., Shirani, H., Whalstorm, N., Malky, I., Stensland, J., Bergman,J**., 2006: Efficient sulfonation of 1-phenylsulfonyl-1-H-pyrroles and 1-phenylsulfonyl-1-H-indoles using chronosulfonic acide in acetonitrile, *Tetrahedron,* **62(8)**, 1699-1707.

[63] **Thompson,R.F.,** 1993: The Brain: A Neuroscience Primer, 2nd ed. W. H. Freeman and Company, New York.

[64] **Revest, P. and A. Longstaff, A.,** 2008: Molecular neuroscience, 3nd ed., Bios, Taylor & Francis, New York.

[65] **Wilson, G.S. and Johnson, M.A.,** 2008: In-vivo electrochemistry: What can we learn about living systems, *Chemical Reviews,* **108,** 2462-2481.

[66] **Phillips, P.E.M., Stuber, G.D., Heien, M., Wightman, R.M. and Carelli, R.M.,** 2003: Subsecond dopamine release promotes cocaine seeking, *Nature,* **422,** 614-618.

[67] **O'Neill, R.D.,** 2005: Long-Term Monitoring of Brain Dopamine Metabolism In Vivo with Carbon Paste Electrodes, *Sensors,* **5,** 317-342.

[68] **Koutsilieri, E., Meulen, V.ter and P. Riederer, P.,** 2001: Neurotransmission in HIV associated dementia: a short review, *Journal of Neural Transmission,* **108,** 767-775.

[69] **Genro, K., Seiji, K., Yukiko, N., Keiji, S., Kazuaki, F., Makoto, G.,** 2003: Relief of oxidative stress by ascorbic acid delays cellular senescence of normal human and Werner syndrome fibroblast cells, *Free Radial Biology and Medicine,* **35,** 438-443.

[70] **Kuo, S.M., Morehouse, F., Jr., Lin, C.P.,** 1997: Effect of antiproliferative flavonoid on ascorbic acid accumulation in human colon adenocarcinoma cells, *Cancer Lett*ers, **16,** 131-137.

[71] **Heitzer, T., Finckh, B., Albers, S., Karoline, K., Kohlscutter, A.,** 2001: Benefical effects of lipoic acid and ascorbic acid on endothelium-dependent, nitric oxide vasodilation in diabetic patients: realtion to parameters of oxidative stres, *Free Radial Biology and Medicine,* **31,** 53-61.

[72] **Wu, Y., Whitman, I., Molmenti, E., Moore, K., Hippenmeyer, P., Pelmutter, D.H.,** 1994: A lag in intracellular degradation of mutant alpha1-antitrypsin correlates with liver disease phenotype in homozygous PiZZ alpha1-antitrypsin deficiency. *Proceedings of the National Academicy of Science USA,* **91,** 9014- 9018.

[73] **Zheng, J. and X. Zhou, X.,** 2007: Preparation and characterization of carbon paste micro-electrode based on carbon nano-particles, *Bioelectrochemistry,* **74,** 405-411.

[74] **Ciszewski, A., Milczarek, G.,** 1999: Polyeugenol-Modified platinum electrode for selective detection of dopamine in the presence of ascorbic acid, *Analytical Chemistry,* **71,** 1055-1061.

[75] **Majewska, U.E., Chmurski, K., Biesiada, K., Olszyna, A.R. and Bilewicz, R.,** 2006: Dopamine Oxidation at Per(6-deoxy-6-thio)-α-Cyclodextrin Monolayer Modified Gold Electrodes, *Electroanalysis,* 18, 1463-1470.

[76] **Zhang, L. and Jiang, X.,** 2005: Attachment of gold nanoparticles to glassy carbon electrode and its application for the voltammetric resolution of ascorbic acid and dopamine, *Journal of Electroanalytical Chemistry,* **583,** 292-299.

[77] **Wang, Z., Liu, J., Liang, Q., Wang, Y., Luo, G.,** 2002: Carbon nanotube-modified electrodes for the simultaneous determination of dopamine and ascorbic acid, *Analyst,* **127,** 653-658.

[78] **Abruna, H.D.,** 1988: Coordination Chemistry in Two Dimensions: Chemically Modified Electrodes, *Coordination Chemistry Reviews,* **86,** 135-189.

[79] **Lane, R.F. and Hubbard, A.T.,** 1973: Electrochemistry of Chemisorbed Molecules. I. Reactants Connected to Electrodes through Olefinic Substituents, *Journal of Physical Chemistry*, **77,** 1401-1410.

[80] **Bard, A. J., Faulkner, L. R.,** 2001: *Electrochemical Methods*, 2nd ed., John Wiley & Sons, Inc., USA.

[81] **Jenden, C.M., Davidson, R.G. and Turner, T.G.**, 1993: A fourier transform-raman spectroscopic study of electrically conducting polypyrrole films, *Polymer*, **34(8),** 1649-1652.

[82] **Waltman, R.J. and Bargon, J.,** 1985: The electropolymerization of polycyclic hydrocarbons-substituent effects and reactivity structure correlations, *Journal of Electroanalytical Chemistry*, **194(1),** 49-62.

[83] **Bauerle, P., Segelbacher, U., Maier, A. and Mehring, M.,** 1993: Electronic structure of monomeric and dimeric cation radicals end-capped oligothiophenes, *Journal of the American Chemical Society*, **115(22),** 10217-10223.

[84] **Kassim, A., Davis, F.J. and Mitchell, G.R.,** 1994: The role of the counter-ion during electropolymerization of polypyrrole camphor sulfonate films, *Synthetic Metals*, **62(1),** 41-47.

[85] **Warren, L.F. and Anderson, D.P.**, 1987: Polypyrrole films from aqueous electrolytes-the effect of anions upon order, *Journal of Electrochemical Society*, **134(1),** 101-105.

[86] **Li, Y.F. and Yang, J.**, 1997: Effect of the electrolyte concentration on the properties of the electropolymerized polypyrrole films, *Journal of Applied Polymer Science*, **65(13),** 2739-2744.

[87] **Bauerle, P. And Scheib, S.,** 1993: Molecular recognition of alkali ions by crown-ether functionalized poly(alkylthiophenes), *Advanced Materials*, **5(11),** 848-853.

[88] **Imanishi, K., Satoh, M., Yasuda, Y., Tsushima, R. And Aoki, S.,** 1988: Solvent effect on electrocehical polymerization of aromatic compounds, *Journal of Electroanalytical Chemistry*, **242(1-2),** 203-208.

[89] **Diaz, A.F. and Bargon, I.,** 1986: Handbook of Conducting Polymers, 1st ed., Ed.T.J. Skotheim, Marcel Dekker, New York, 1337.

[90] **Funt, R.L. and Diaz, A.F.,** 1991: Organic Electrochemistry: an Introduction and Guide, Marcel Dekker, New York, 1337.

[91] **Ko, J.M., Rhee, H.W., Park, S.M. and Kim, C.Y.,** 1990: Morphology and electrochemical properties of polypyrrole films prepared in aqueous solvents, *Journal of Electrochemical Society*, **137(3),** 905-909.

[92] **Unsworth, J., Innis, P.C., Lunn, B.A., Jin, Z. And Norton, G.P.,** 1992: The influence of electrolyte pH on the surface-morphology of polypyrrole, *Synthetic Metals*, **53(1),** 59-69.

[93] **Jones, D., Guerra, M., Favaretto, L., Modelli, A. and Fabrizio, M.,** 1990: Determination of the electronic structure of thiophene oligomers and extrapolation of polythiophene, *Journal of Physical Chemisty*, **94(15),** 5761-5766.

[94] **Suarez, M.F. and Campton, R.G.**, 1999: In-situ atomic force microscopy study of polypyrrole synthesis and the volume changes induced by oxidation and reduction of the polymer, *Journal of Electroanalytical Chemistry*, **462(2),** 211-221.

[95] **Rodrigez, J., Grande, H.J. and Otero, T.F.,** 1997: Handbook of Organic Conducting Molecules and Polymers, John Wiley & Sons, 415.

[96] **Chandrasekhar, P., Zay, B.J., Ross, D., McQueeney, T., Birur, G.C., Swanson, T., Kauder, L. And Dougles, D.,** 2002: Conducting polymer based dynamic IR-electrochromics for supercraft thermal control, Abst. Papers Am. Chem.Soc., **223** D25 287-Poly Part-2.

[97] **Macdolnald, J.R.,**1997: Impedance spectroscopy, John Wiley and Sons, New York.

[98] **Lang, G. And Inzelt, G.,** 1991: Some problems connected with impedance analysis of polymer film electrodes: effect of the film thickness and the thickness distribution, *Electrochimica acta*, **36**, 847-854.

[99] **Macdonald, J.R.**, 1990: Impedance spectroscopy: Old problems and new developments, *Electrochimica Acta*, **35,** 1483.

[100] **Ding, H., Pan, Z., Pigani, L., Seeber, R.**, 2001: Impedance characteristics of poly (4,4 '- bis(butylsulfanyl)-2,2 '-bithiophene) film electrode as a function of different oxidation levels, *Journal of New Materials for Electrochemical Systems*, **4,** 63.

[101] **Duffitt, G.L., Pickup, P.G.**, 1991: Permselectivity of polypyrrole in acetonitrile, *Journal of Physical Chemistry*,, **95**, 9634-9635.

[102] **Duffitt, G.L., Pickup, P.G.**, 1992: Enhanced ionic conductivity of polypyrrole due to incorporation of excess electrolyte during potential cycling, *Journal of the Chemical Society, Faraday Transactions*, **88**, 1417-1423.

[103] **Albery, W.J., Mount, A.R.,** 1994: in: M.E.G. Lyons (Ed.), Electrocative Polymer Electrochemistry, vol I, Plenum Press, New York.

[104] **Sarac, A.S., Sezgin, S., Ates, M., Turhan, C.M., Parlak, E.A., Irfanoglu, B.,** 2008: Electrochemical Impedance Spectroscopy of Poly(N-Methyl pyrrole) on Carbon Fiber Micro Electrodes and Morphology, *Progress in Organic Coatings*, **62**, 331-335.

[105] **Ates, M., Sarac, A.S.,** 2009: Electrochemical Impedance Spectroscopy of Poly(Carbazole-co-p-tolylsulfonyl pyrrole) on carbon fiber microelectrodes, Equivalent Circuits for Modelling, *Progress in Organic Coatings*, **65**, 281-287.

[106] **Sarac, A.S., Ates, M., Parlak, E.A.,** 2006: Electrolyte and solvent effects of electrocoated polycarbazole thin films on carbon fiber microelectrodes, *Journal of Applied Electrochemistry*, **36**, 889-898.

[107] **Dressman, S.F., Peters, J.L. and Michael, A.C.,** 2002: Carbon fiber microelectrodes with multiple sensing elements for in vivo voltammetry, *Journal of Neuroscience Methods,* **119(1),** 75-81.

[108] **Ates, M., Sarac A.S.,** 2009: Conducting polymer coated carbon surfaces, and Biosensor applications, *Progress in Organic Coatings,* **66**, 337-358.

[109] **Sonmez, G. and Sarac, A.S.,** 2003: Structural study of pyrrole-EDOT copolymers on carbon fiber micro-electrodes, *Synthetic Metals,* **135(1-3),** 459-460.

[110] **Pariente, F., Hernandez, L., Abruna, H.D. and Lorenzo, E.,** 1993: Alkaline phosphatase-modified carbon fiber disc microelectrode for the determination of 4-aminophenyl phosphate, *Analytica Chimica Acta,* **273(1-2),** 187-193.

[111] **Brazell, M.P., Kasser, R.J., Renner, K.J., Feng, J., Moghaddam, B. and Adams, R.N**., 1987, Electrocoating carbon fiber microelectrodes with nafion improves selectivity for electroactive neurotransmitters, *Journal of Neuroscience Methods,* **22(2),** 167-172.

[112] **Agui, L., Gonzales-Cortés, A., Yanez.Sedeńo, P. and Pingarrŏn, J.M.,** 1999: Continuous monitoring of amino acids and related compounds with poly(3-methylthiophene) coated cyclindical carbon fiber microelectrodes, *Analytica Chimica Acta,* **401(1-2),** 145-154.

[113] **Csoregi, E., Gorton, L. and Markovarga, G.,** 1993: Carbon fibers as electrode materials for the construction of peroxidase-modified amperometric biosensors, *Analytica Chimica Acta,* **273(1-2),** 59-70.

[114] **Pantano, P. and Kuhr, W.G.,** 1991: Characterization of the chemical arthitecture of carbon fiber microelectrodes 1.carboxylates, *Analytical Chemistry,* **63(14),** 1413-1418.

[115] **Crouch, E., Cowell, D. C., Hoskins, S., Pittson, R. W., Hart, J. P.,** 2005: Amperometric, screen-printed, glucose biosensor for analysis of human plasma samples using a biocomposite water-based carbon ink incorporating glucose oxidase, *Anaytical Biochemistry,* **347,** 17-23.

[116] **Montereali, M. R., Vastarella, W., Della Seta, L., Pilloton, R.,** 2005: Tyrosinase biosensor based on modified screen printed electrodes: measurements of total phenol content, *International Journal of Environmental Analytical Chemistry,* **85,** 795-806.

[117] **De Luca, S., Florescu, M., Ghica, M. E., Lupu, A., Palleschi, G., Brett, C. M. A., Compagnone, D.,** 2005: Carbon film electrodes for oxidase-based enzyme sensors in food analysis, *Talanta,* **68,** 171-178.

[118] **Mikkelsen, S. R., Corton, E.,** 2004: Bioanalytical Chemistry; John Wiley & Sons, Inc., Hoboken, New Jersey.

[119] **Cunningham, A. J.,** 1998: Introduction to Bioanalytical Sensors; John Wiley & Sons, Inc., New York, 207-316.

[120] **Sukeerthi, S., Contractor, A. Q.,** 1994: Applications of conducting polymers as sensors, *Indian Journal of Chemistry - Section A: Inorganic, Physical, Theoretical and Analytical Chemistry,* **33,** 565-571.

[121] **Patolsky, F., Katz, E., Bardea, A., Willner, I.,** 1999: Enzyme-Linked Amplified Electrochemical Sensing of Oligonucleotide - DNA Interactions by Means of Impedance Spectroscopy, *Langmuir*, **15,** 3703-3706.

[122] **Koncki, R., Radomska, A., Glab, S.,** 2000: Potentiometric determination of dialysate urea nitrogen, *Talanta,* **52,** 13-17.

[123] **Ogonczyk, D., Tymecki, L., Wyzkiewicz, I., Koncki, R., Glab, S.,** 2005: Screen-printed disposable urease-based biosensors for inhibitive detection of heavy metal ions, *Sensors and Actuators B-Chemical,* **106,** 450-454.

[124] **Matthews, D. R., Bown, E., Watson, A., Holman, R. R., Steemson, J., Hughes, S., Scott, D.,** 1987: Pen- sized digital 30-second blood glucose meter, *Lancet,* **1,** 778-779.

[125] **Nistor, C., Rose, A., Farre, M., Stoica, L., Wollenberger, U., Ruzgas, T., Pfeiffer, D., Barcelo, D., Gorton, L., Emneus, J.,** 2002: In-field monitoring of cleaning efficiency in waste water treatment plants using two phenol-sensitive biosensors, *Analytica Chimica Acta,* **456**, 3-17.

[126] **Suman, S., Singhal, R., Sharma, A. L., Malthotra, B. D., Pundir, C. S.,** 2005: Development of a lactate biosensor based on conducting co-polymer bound lactate oxidase, *Sensors and Actuators B-Chemical,* **107,** 768-772.

[127] **Alpeeva, I. S., Vilkanauskyte, A., Ngounou, B., Csoregi, E., Sakharov, I. Y., Gonchar, M., Schuhmann, W.,** 2005: Bi-Enzime Alkohol Biosensors on Genetically Engineering Alcohol. Oxidase and Different Peroxidases, *Microchimica Acta,* **152,** 21-27.

[128] **Rishpon, J., Ivnitski, D.,** 1997: An amperometric enzyme- channeling immunosensor, *Biosensors & Bioelectronics,* **12,** 195-204.

[129] **Ducey, M. W., Smith, A. M., Guo, X. A., Meyerhoff, M. E.,** 1997: Competitive nonseparation electrochemical enzyme binding/immunoassay (NEEIA) for small molecule detection, *Analytica Chimica Acta,* **357,** 5-12.

[130] **Benkert, A., Scheller, F., Schossler, W., Hentschel, C., Micheel, B., Behrsing, O., Scharte, G., Stocklein, W., Warsinke, A.,** 2000: Development of a creatinine ELISA and an amperometric antibody-based creatine sensor with a detection limit in the nanomolar range. *Analytical Chemistry,* **72,** 916-921.

[131] **Afkhami, A., Nematollahi, D., Khalafi, L. and Rafiee, M.,** 2005: Kinetic study of the oxidation of some catecholamines by digital simulation of cyclic voltammograms, *International Journal of Chemical Kinetics,* **37**, 17-24.

[132] **Luczak, T.,** 2008: Electrochemical Oxidation of Dopamine in the Presence of Secondary Amine. An Alternative Way for Quantitative Dopamine Determination at a Gold Electrode, *Electroanalysis,* **20**, 1639-1646.

[133] **Hou, S., Zheng, N., Feng, H., Li, X. and Yuan, Z.**, 2008: Determination of dopamine in the presence of ascorbic acid using poly(3,5-dihydroxy benzoic acid) film modified electrode, *Analytical Biochemistry*, **381,** 179-184.

[134] **Weng, J., Xue, J., Wang, J., Ye, J.S., Cui, H., Sheu, F.S., and Zhang, Q.,** 2005: Gold-Cluster Sensors Formed Electrochemically at Boron-Doped-Diamond Electrodes: Detection of Dopamine in the Presence of Ascorbic Acid and Thiols, *Advanced Functional Materials*, **15,** 639-647.

[135] **Chen, S.M. and W. Y. Chzo, W.Y.,** 2006: Simultaneous voltammetric detection of dopamine and ascorbic acid using didodecyldimethylammonium bromide (DDAB) film-modified electrodes**,** *Journal of Electroanalytical Chemistry*, **587,** 226-234.

[136] **Lee, K-M., Chen, P-Y., Hsu, C-Y., Huang, J-H., Ho, WH., Chen, H-C., Ho, K-C.,** 2009: A high-performance counter electrode based on poly(3,4-alkylenedioxythiophene) for dye-sensitized solar cells, *Journal of Power Sources*, **188**, 313–318.

[137] **Johnsson, B.,** 1991: Immobilization of proteins to a carboxymethyldextran-modified gold surface for biospecific interaction analysis in surface plasmon resonance sensors, *Analytical Biochemistry*, **198**, 268-277.

[138] **Girija, T.C.,** 2006: Sangaranarayanan M.V.: Investigation of polyaniline-coated stainless steel electrodes for electrochemical supercapacitors, *Synthetic Metals*,**156**, 244-250.

CURRICULUM VITAE

Candidate's full name: Fatma Gül GÜLER

Place and date of birth: Fatih/ İSTANBUL, TÜRKİYE, 12.01.1986

Permanent Address: Ali Rıza Gürcan Cad., Gözde Amaç Sitesi, A-3 Blok Daire:11 Merter/İSTANBUL

Universities and Colleges attended: Bachelor's degree: Eskisehir Osmangazi University, Chemistry (2004-2008)

Publications:

- **Guler, F.G.,** Sarac, A.S., 2011: Electrochemical synthesis of Poly[3, 4-Propylenedioxythiophene-co-N-Phenylsulfonyl Pyrrole]: Morphological, electrochemical and spectroscopic characterization. *Express Polymer Letters,* **5(6)** 493-505.